2014

Stratigraphy, depositional environments, and petroleum potential of the Three Forks Formation -- Williston Basin, North Dakota

Richard A. Ashu
University of North Dakota

STRATIGRAPHY, DEPOSITIONAL ENVIRONMENTS, AND PETROLEUM POTENTIAL OF THE THREE FORKS FORMATION – WILLISTON BASIN, NORTH DAKOTA

By

Richard A. Ashu
Bachelor of Science, University of Buea, 2005
Master of Science, Vrije Universiteit, 2008
Master of Science, New Mexico Highlands University, 2010

A Dissertation

Submitted to the Graduate Faculty

of the

University of North Dakota

In partial fulfillment of the requirements

for the degree of

Doctor of Philosophy

Grand Forks, North Dakota
May
2014

ProQuest LLC.
789 East Eisenhower Parkway
P.O. Box 1346
Ann Arbor, MI 48106 - 1346

This dissertation, submitted by Richard Ashu in partial fulfillment of the requirements for the Degree of Doctor of Philosophy from the University of North Dakota, has been read by the Faculty Advisory Committee under whom the work has been done, and is hereby approved.

_____
DR. RICHARD D. LEFEVER

_____
DR. PHILIP J. GERLA

_____
DR. JOSEPH HARTMAN

_____
DR. WILLIAM D. GOSNOLD

_____
DR. TURK RHEN

This dissertation is being submitted by the appointed advisory committee as having met all of the requirements of the Graduate School at the University of North Dakota and is hereby approved.

_____
Wayne Swisher
Dean of the Graduate School

_____

Title	Stratigraphy, Depositional Environments, and Petroleum Potential of the Three Forks Formation - Williston Basin, North Dakota.
Department	Geology
Degree	Doctor of Philosophy

In presenting this dissertation in partial fulfillment of the requirements for a graduate degree from the University of North Dakota, I agree that the library of this University shall make it freely available for inspection. I further agree that permission for extensive copying for scholarly purposes may be granted by the professor who supervised my dissertation work or, in his absence, by the Chairperson of the department or the dean of the Graduate School. It is understood that any copying or publication or other use of this dissertation or part thereof for financial gain shall not be allowed without my written permission. It is also understood that due recognition shall be given to me and to the University of North Dakota in any scholarly use which may be made of any material in my Dissertation.

Richard Ashu
May 7, 2014

TABLE OF CONTENT

LIST OF FIGURES

Figure Page

LIST OF TABLES

ACKNOWLEDGMENTS

This research project would not have been possible without support from the Harold Ham School of Geology and Geological Engineering, and the College of Engineering and Mines of the University of North Dakota. The author wishes to express his gratitude to his advisor, Dr. Richard LeFever who was abundantly helpful and offered invaluable assistance, support, and guidance. I thank Dr. Steve Benson and Dr. Nick Lentz for their technical and financial support during this work. I wish to express my sincere gratitude to the members of the supervisory committee, Dr. Joseph Hartman, Dr. Philip Gerla, Dr. William Gosnold, and Dr. Turk Rhen without whose knowledge and assistance this study would not have been successful.

ABSTRACT

The hydrocarbon potential of the Three Forks Formation in North Dakota is poorly known due to limited stratigraphic, geochemical, and petrophysical data. This study presents a methodology and results of a reservoir characterization study of the stratigraphy, lithofacies distribution, petroleum potential, and paleo-environments of the Three Forks Formation in North Dakota as a potential for hydrocarbon exploration with the principal objective to evaluate the Three Forks Formation's potential for future developments. The detailed lithology is computed by employing a probabilistic interpretation approach calibrated with lab results and five major lithofacies of the Three Forks Formation in North Dakota, which display a variety of diagenetic characteristics including dolomitization and precipitation of hematite, are identified and presented. These facies correlate well with electrofacies predicted by employing principal component analysis and clustering techniques to selected lithology-sensitive logs. Hydrocarbon source rock analysis, including type and quantity of kerogen, and thermal maturity on all five facies using Rock-Eval 6 pyrolysis and LECO TOC shows that these facies have poor to fair petroleum potential and contain immature Type II and Type III kerogens. In addition, samples from three lithofacies are analyzed by thin section and SEM petrography, plus combined bulk and clay XRD analyses and key aspects controlling the porosity and permeability of this formation are revealed by focusing on the detailed mineralogy, rock type, diagenetic mineral distribution plus overall reservoir quality and the fluid sensitive-

ity. Results show that the Three Forks mineralogy is dominated by dolomite, along with substantial hematite, monocrystalline quartz and mica flakes with trace feldspar, calcite, and pyrite. EDX spectra show that the element distribution is influenced by the lithotype composition, mainly Ca, Mg, and Fe with additional Si, Al, and K. Three stages of the dolomitization process are identified and discussed. Clays mainly consist of illite together with minor chlorite, and kaolinite and are associated with the scattered clasts of quartz and feldspars. The reservoir quality is controlled by intercrystalline, rare micro-vuggy, plus microporosity types that result from diagenetic and depositional events. Six members of the Three Forks are identified and log-derived porosities, water saturations, and net-to-gross values for each Member calculated and areas with high reservoir quality and potential pay zones highlighted. Also, core data are quantitatively compared with results from the Archie, Simandoux, Modified Simandoux, Indonesia, and Dual-Water models. A proposed depositional model is constructed based on detailed core examination and petrographical analysis and sufficient evidence is provided to show that the Three Forks Formation is of peritidal to sabkha-like origin. A proposed hypothesis is that dolomitization commenced soon after deposition and was pervasive that no original carbonate texture is detectable.

SECTION I

RESEARCH BACKGROUND

CHAPTER 1

INTRODUCTION

This study focuses on the sedimentary structures, depositional environments, and petroleum potential of the Upper Devonian rocks of the Three Forks Formation in North Dakota (Fig. 1-1). Very few detailed studies of the stratigraphy, depositional environments or diagenesis of the Three Forks have been undertaken in recent years. The Three Forks Formation extends approximately 764 km (475 miles) north-south and 480 km (300 miles) east-west across the Williston Basin Province of North Dakota, South Dakota, Montana, Saskatchewan, and Manitoba, as defined in Anna et al. (2010).

Because of its predominantly dolomite composition, the Three Forks is classified as a carbonate reservoir and has become an industry priority over the past decade. The duties of the modern geologist usually involve making use of proper reservoir descriptions to plan the optimum exploitation by correctly targeting new wells. Assessing the reservoir's paleoenvironments and providing detailed well-to-well correlation of lithofacies is vital in building an extensive understanding of the likely reservoir geometry as well as a detailed three dimensional picture of the stratigraphy (Akbar et al., 1995).

The sources of such data include visual core description and analysis and well logs. Whereas well logs provide indirect information about mineralogy, lithology, porosity and fluid content, core analysis provides both quantitative and semi-quantitative data on the

texture, sedimentary structures, pore, and grain size distributions, permeability, facies distribution, and depositional environments, of a reservoir formation. Furthermore, a vital component in evaluating the petroleum potential or overall performance of a hydrocarbon reservoir is the study of its sedimentary series (Serra and Abbott, 1982). Also, the properties of a reservoir, as expressed by its sedimentary attributes (from core samples) can be used to correlate and predict the reservoir quality of uncored wells.

The term *sedimentary facies* is used to identify a mass of sedimentary rock that can be defined and distinguished from others in terms of its descriptive or interpretive characteristics (Selley, 1978). Facies that describe the sum of all lithologic features such as texture, color, stratification, components, grain size, sedimentary structures, or bedding characteristics are referred to as lithofacies. The identification of individual lithofacies within a reservoir has major contributions for petroleum reservoir characterization.

Because of the uncertainties and constraints associated with core-scale data especially in fine-grained sediments like those of the Three Forks, the dependence on well logs (or in combination) to deliver information on depositional environments and subsequent diagenetic changes has become an integrated part of reservoir characterization and management (Hsien-Cheng et al., 2002; Serra and Abbott, 1982). Facies based on the petrophysical responses of well logs of a formation interval penetrated by a well are defined as "electrofacies.” Thus electrofacies can be delimited exclusively on the basis of log responses without reliance on cores, cuttings, or outcrops data (Zimmerle, 1995).

It is uncommon for wells that penetrate the Three Forks to have core across the reservoir. This is probably because the portion of the Three Forks that is recovered is probable a part of the 'Bakken- Upper Three Forks system', which is considered to be a more productive zone than the rest of the Three Forks Formation. This creates a major challenge in detailed interpretation of the lithofacies within a specific area at the core-scale. The use of methods that apply artificial intelligence in predicting lithofacies from logs is necessary in such a situation. Therefore, establishing a sophisticated correlation between identified electrofacies and core data is a vital step if geological information needs to be extracted from well-logs alone (Bucheb and Evans, 1994).

Hydrocarbon prospectivity in the Williston Basin is dependent on the availability of oil and/or gas-prone rock units that may have generated and expelled hydrocarbons or contain commercial accumulations. However, little is known of the thermal maturity of the upper Devonian Three Forks Formation even though such information is crucial for predicting the type of hydrocarbons that may have been generated or whether or not the hydrocarbon in the Three Forks Formation is indigenous or might have migrated from the Bakken Formation that lies above or from the Birdbear Formation underneath.

Devonian rocks only occur in the subsurface of the State of North Dakota and consist predominantly of marine carbonates, evaporites, and shales. The presence of anhydrite in the Three Forks only adds to the complexity in interpreting the depositional environments. Traditionally, the nodular habit of anhydrite which is commonly associated with finely crystalline dolomitic rocks and laminated sediments (with or without dark "organic" films) have been interpreted as signatures for tidal-flat (shallow-water) sedimentary

environments in older sequences (Dean, et al., 1975). However, commonly used indicators such as laminated anhydrites may form in both sabkha like depositional paleoenvironments and deep water settings (Butler, 1969; Davies and Ludlum, 1973).

A combination of Dunham's (1962), Folk's (1959) and of Gregg and Sibley (1986) classification schemes are used to interpret carbonate fabrics and dolomite textures accordingly while the Wentworth (1922) scale is used to describe sand-sized grains. Anhydrites are classified according to Meikles et al. (1969) with bedding shape modifiers from Campbell (1979). Close-up photomicrographs are provided to stress: (1) preserved primary and secondary pore types, (2) cements, (3) sedimentary structures, (4) fractures, and (5) pore plugging hematite.

In evaluating the petroleum potential of the Three Forks, critical information and data on the prospectivity in terms of key diagenetic processes that operate within the Three Forks are derived from thin section analysis, X-ray diffraction (XRD), scanning electron microscopy (SEM), and petrophysical analysis. The amount and character of the organic matter (OM) present or might have existed, given the proper conditions, to generate oil/gas is also examined. The petrophysical characteristics such as porosity, permeability, grain density, and fluid saturations are also examined using examples from five wells. Understanding these aspects provides a basis for evaluating the resource potential of the Three Forks in North Dakota.

1.1 Regional Setting and Study Area

The geologically defined Williston Basin is a structural-sedimentary intracratonic oval-shaped depression that occupies the western ramp shelf of the North American craton. Prominent structural features of the Williston Basin include the Cedar Creek anticline, Billings anticline, Little Knife, and Nesson Anticlines. A part of the Northern Great Plains of United States and Canada, the Williston Basin consists of Paleozoic carbonates interbedded with evaporites and detrital clastics, and Mesozoic to Cenozoic clastic sediments with a total thickness of approximately 4880 m (16,000 ft) (Borchert et al., 1990).

Six main depositional sequences, punctuated by major unconformities during the Middle Ordovician, Devonian, Mississippian, Pennsylvanian, and early Tertiary have been identified within the Phanerozoic rocks of North America (Sloss, 1984). These are from bottom to top, the *Sauk, Tippecanoe, Kaskaskia, Absaroka, Zuni,* and *Tejas.* The Upper Kaskaskia (Mississippian and uppermost Devonian) is the major source of petroleum in the Williston Basin and exhibits a range of depositional environments from very shallow marine to hypersaline (Borchert et al., 1990).

The Three Forks Formation covers approximately seventy five percent of the western subsurface of the State of North Dakota and attains a maximum thickness of 82 m (270 ft). The composition of the Three Forks Formation is mostly variations of greenish-grey, grayish-orange and grayish red silty to sandy dolomite, ferroan and non-ferroan dolo-mudstones, altering amounts of anhydrite, and minor amounts of other detrital compo-nents. The well-defined depocenter covers Mountrail, Dunn, and Eastern McKenzie

counties (LeFever, 2004) and thins outwards from the basin centre.

The detailed lithology study on the Three Forks Formation is derived from cores and logs from the following counties: (1) Ward County, (2) McKenzie County, (3) Williams County, (4) Divide County, and (5) Mount rail County (Fig. 1-1). These areas are chosen because of the availability of core sections and a high concentration of log information within this region. Because the number of well logs used in this research cover a vast area of the Three Forks in North Dakota, the results are not biased by the chosen counties.

1.2 Statement of the Problem

The Three Forks Formation is one of the most unpredictable petroleum systems within the Williston Basin consisting of a combination of carbonates, clays, organics and detrital material; of poor to moderate reservoir quality, and reflecting its depositional and post-depositional fabric. This investigation is undertaken because of the need for detailed study of the upper Devonian rocks in the Williston Basin in North Dakota as relatively little work has been published on the facies characteristics, hydrocarbon quality and quantity, and origin of the petroleum resources of the Three Forks in particular.

In addition, the Three Forks Formation presents exploration challenges, associated with its complex stratigraphy and an overall poor understanding of its depositional environments. This study therefore intends to describe these features and highlight factors that make this formation a "challenging environment" by outlining field and laboratory techniques that should in general provide insight into whether or not:

1. Source rocks do exist and if they are responsible for petroleum accumulations?

2. The Three Forks Formation will generate oil or gas?
3. What are the expected yields?
4. Can the petroleum potential be predicted?

1.3 Aims and Objectives

This dissertation focuses on the sedimentary succession of the Upper Devonian rocks of the Williston Basin in North Dakota and aims to discuss the sedimentary and depositional evolution of the predominantly carbonate Three Forks Formation by characterizing the lithofacies in order to interpret the evolution and hydrocarbon potential of the formation.

Obviously, the basic question once petroleum has been discovered is to estimate how much of it exists and how much can be extracted. According to the USGS estimates, the Bakken - Three Forks system may contain some of the largest unexplored oil accumulations in the United State (Gaswirth and Marra, 2014) and presumably, the Three Forks Formation consists of over ninety percent recoverable oil (Beitsch, 2010)i.e. the amount of hydrocarbon likely to be recovered during production although its stratigraphic sequences, depositional environment, and most importantly source rock characteristics have not been a major target. Hence, this research deals with some of these initial questions by implementing the following objectives:

1. Compute the lithology of the Three Forks, identify and describe five of its lithofacies through visual core description, and to compare these lithofacies with predicted electrofacies,
2. Identify the sedimentary features of the different members in a depositional framework and reconstruct their environments of deposition.

3. Provide insight into the diagenetic characteristics and reservoir quality of these facies, and
4. Compute the petroleum potential of the Three Forks by looking at its geochemical characteristics and performing a petrophysical evaluation.

In order to meet these objectives, subsurface information is gathered from well logs through a petrophysical analysis, detailed core description, geochemical analysis, and petrographical investigations, so as to characterize the stratigraphic geometry, depositional environments, and petroleum potential of the Three Forks in North Dakota. The results of this study can be extended to other parts of the Williston Basin as part of the reservoir characterization and prediction process.

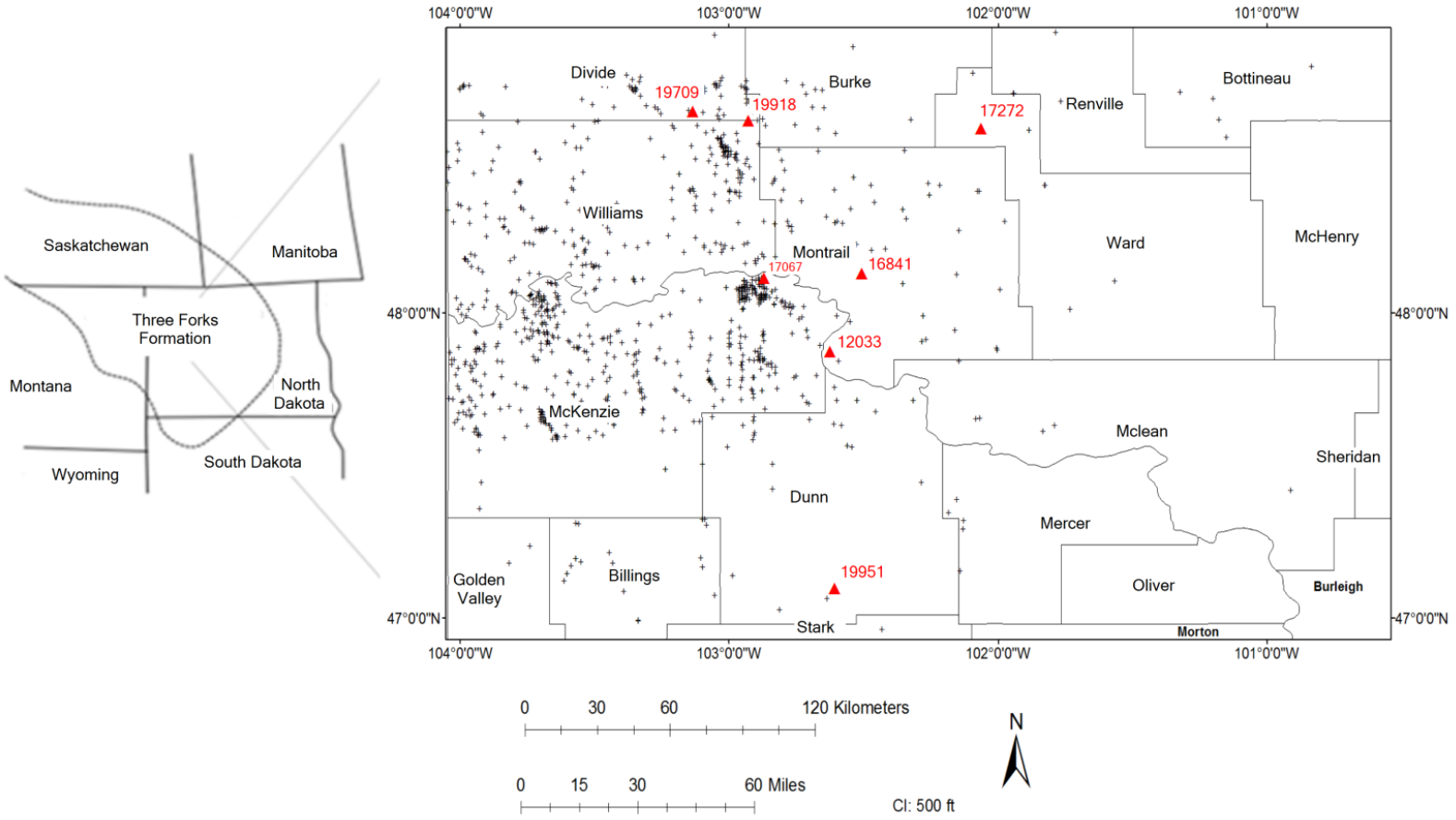

Figure 1-1: Map Showing the Extent of the Three Forks Formation and the Distribution of Wells Used in this Study. Triangles Indicate Wells Used for Stratigraphic Modeling and Core Description.

CHAPTER 2

LITTERATURE REVIEW

The geological characterization of the Three Forks Formation may be traced back to 1893 when Peale expressed difficulties in defining exactly the boundaries between Paleozoic rocks in Montana and as a result, he separated the Devonian rocks into the Three Forks shales, overlying the Jefferson Formation and underlying the Madison Limestone in the vicinity of Three Forks, Montana. The arenaceous upper part of the Three Forks has been considered by some workers as a separate formation, but its thinness and non-resistant nature in outcrops made it more reasonable to be considered a member of the Three Forks (Benson, 1966, p. 2594; Baillie, 1953). LeFever and others (2011) reclassified this upper sandy portion as the Pronghorn Member of the Bakken Formation.

Berry (1943) and Sandberg (1961) provided detailed descriptions of Devonian rocks within the Williston basin as consisting predominantly of marine carbonates, evaporites, and clastic sediments (sandstones and shale beds). The Birdbear and Three Forks Formations have a combined thickness of about 104 m (340 ft) around the south end and eastside of the Nesson anticline, deposited in shallow waters during Late Devonian time in an arcuate belt (Sandberg, 1961). By Mid-Devonian time, the Williston basin had been covered by clastic sediments resulting from marine transgression, south-eastwards from

northern Alberta over an unevenly eroded surface. The regression phase was accompanied by the precipitation of anhydrite and halite at the centre of the basin.

The analysis of shaly formations presents a major challenge especially with the absence of core analysis data or dealing with little information on clay types and distribution. The presence of clays affects both porosity and resistivity logs in terms of conductivity (Asquith and Krygowski, 2004). Various theoretical models have been proposed to model the fluid-solid interaction in reservoir rocks for the purposes of lithology prediction and fluid exploitation. However, most of these theories have drawbacks and can only be applied under certain conditions with some requiring specific parametric quantities that are not easily procurable.

Hilchie (1982) showed that clays tend to have different effects on logs depending on whether they are effective (montmorillonite and illite) or non effective (kaolinite and chlorite). However, the influence of both types of clays on the density log is exclusively dependent on the clay density. With the gamma ray device, the presence of radioactive minerals other than clays causes the calculated clay volumes to be overestimated.

The 1970s saw a recast in our understanding of the deposition and early diagenesis of carbonate rocks from an approach based essentially on grain textures to one grounded on sedimentary structures and early diagenetic features, thanks to comprehensive studies of modern shallow marine carbonate environments; see for example Demicco and Hardie (1994), Kinsman (1966), Butler (1970), Kendall and Skipwith (1969), Hardie (1977a), and Enos and Moore (1983). The fundamental concept of this approach is grounded on

the c*omparative sedimentology* method of Ginsburg (1974) in which paleo-sedimentary environments are decoded by means of comparisons with modern analogs. Demicco and Hardie (1994) emphasized the need of a concrete understanding of shallow marine carbonates at the individual sedimentary structure scale in order to accurately reconstruct the large scale accumulation history of carbonate deposits.

The pattern of shallow marine carbonates buildup is remarkably similar through time with the host sediments produced in situ in shallow water settings (Wilson, 1975). These buildups occur in all tectonic-basin settings and exist as a succession of depositional environments from the landward edges to the distal depths (Demicco and Hardie, 1994). To avoid confusions in terminology, this study sticks to the descriptive definition of facies by Moore (1949): “a sedimentary facies is defined as any areally restricted part of a designated stratigraphic unit which exhibits characters significantly different from those of other parts of the unit." Selley (1970) modified this definition by including five defining parameters: geometry, lithology, paleontology, sedimentary structures, and paleo-current pattern. The goals of lithofacies identification are to improve our understanding of the paleo-depositional environments.

Lithofacies prediction from well logs has been quite successful in the literature (Hsien-Cheng et al., 2002; Saggaf and Nebrija, 2003; Qi and Carr, 2006). With the success in developing shale petroleum systems in the Williston Basin during last decades, increasing detailed research from geologic and engineering perspectives are necessary to support shale and carbonate production. On the basis of physical characteristics, chemical and biogenic features, Slatt et al., (2009) presented the importance of lithofacies identification

in reservoir characterization by integrating visual core description, petrography, and mineralogy. The usefulness and effects of lithofacies on TOC prediction, petrophysical analysis, completion strategies, and porosity measurement is also stressed.

SECTION II

THEORETICAL CONSIDERATIONS

CHAPTER 3

PETROPHYSICAL PARAMETERS

The aim of this chapter is to introduce the basic petrophysical parameters and laboratory measurements that are investigated in this study. Petrophysical parameters can be derived from well logs as well as laboratory measurements on core samples. Results obtained from laboratory analysis are used to calibrate log measurements. The principal objective is to facilitate the understanding of the most important physical controls of a reservoirs; porosity and permeability, and how they become modified by post-depositional changes (diagenesis). Other aspects that are required in assessing the quality of a reservoir such as fluid saturations and pore-size distribution are also presented.

3.1 Hydrocarbon Reservoir Properties

A petroleum reservoir is a subsurface pool of hydrocarbons contained in porous or fractured rock formations. A reservoir rock is therefore a rock with sufficient porosity to contain accumulations of hydrocarbons. Most reservoirs are in sandstones and carbonates (limestone, dolomite) although metamorphic and igneous rocks are known to be reservoirs under exceptional conditions. Fluid within a reservoir can be divided into three broad groups; (1) aqueous solutions with dissolved salts, (2)liquid hydrocarbons, and (3) gases (hydrocarbon and non-hydrocarbon).The distribution of these constituents within a reservoir is controlled by factors such as; (1) the petrophysical properties of the forma-

tion, (2) the physical, chemical properties of the fluids themselves, and (3) thermodynamic conditions of the reservoir. Porosity and permeability determine the capacity to accumulate and transmit petroleum.

3.1.1 Shale Volume (Vsh) Indicators

Shale incorporates the bulk volumes of silt, dry clay, and chemically bound waters. A shale indicator is simply any well log or log combination whose response equation(s) can integrate a shale fraction term. A major mistake in clay volume estimation arises from the assumption that shales are composed of 100 percent clay. Usually, shales constitute 50 to 70 % clay, 25 to 45 % silt and clay-sized quartz, and 5 % other minerals which may include feldspars and carbonates. Normally, the total gamma-ray count or the neutron-density log separation is not affected by the non-clay mineral fraction in shale. The principal cause of non-linearity between weight percent clay and GR is the unequal distribution of non-magnetic heavy minerals in sedimentary rocks (Ellis and Singer, 2007).

3.1.2 Porosity

Porosity is a measure of the potential storage volume for hydrocarbons and water in a formation. Schmoker et al. (1985) showed that porosity in carbonate reservoirs ranges from 1 to 35%, with an average of 10% in dolomite reservoirs and 12% in limestone reservoirs in the United States. Porosity is defined as the ratio of pore volume to bulk volume expressed either as a fraction or percentage.

$$\text{Porosity} = \frac{\text{Pore volume}}{\text{Bulk volume}} = \frac{\text{Bulk volume} - \text{Mineral volume}}{\text{Bulk volume}} \ldots (1)$$

Several types of porosity can be described depending on the time of pore development or the degree of connectivity. Morphologically, porosity can be classified into three types:

1. Catenary- where the pore opens to more than one throat passage
2. Cul-de-sac- where the pore opens to only one throat passage
3. Closed pore- where there is no connection with other pores.

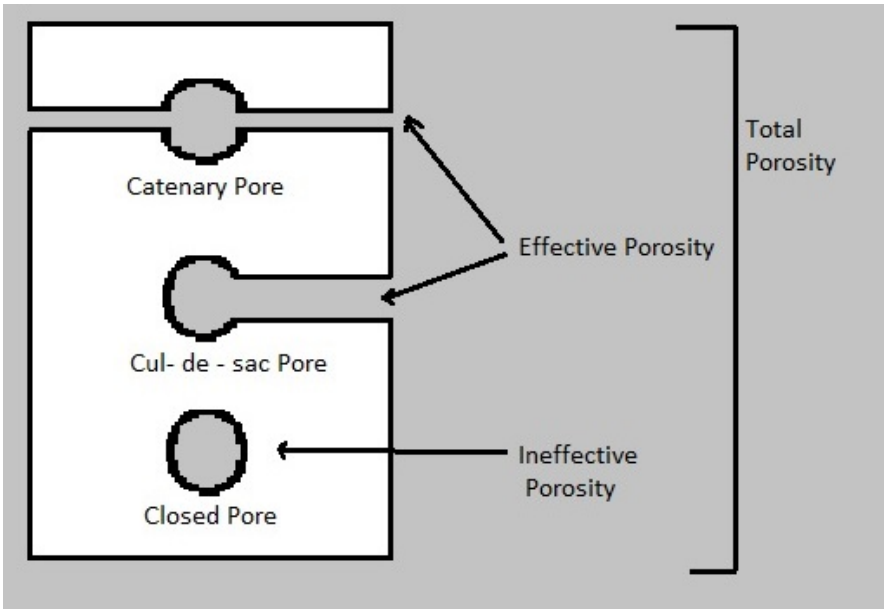

Figure 3-1: Porosity Types that May Exist in a Formation.

Porosity may also be describes in terms of total or effective porosity. The total porosity (ϕ_t) defines the ratio of total pore volume and includes fluids associated with shale even though these fluids cannot usually be produced. By quantifying and subtracting the contribution of the shale to the total porosity, the effective porosity (ϕ_e) can be calculated. Thus, the effective porosity defines the ratio of the interconnected pore spaces to the total bulk volume of the rock sample and provides a more accurate approximation of the

reservoir's potential (Fig. 3-1). Catenary and Cul-de-sac pores constitute the effective porosity and denote the fractional porosity available for fluid flow. Morphological type (3) does not permit flow of any kind and is said to be ineffective. The productivity of a reservoir is therefore controlled by such parameters as: (1) the size and geometry of pores, (2) the diameter and tortuosity of the connecting pore-throats.

3.1.2.1 Controls and Evolution of Porosity

Porosity can also be classified as primary or secondary, according to the time of formation with reference to sedimentation.

Primary Porosity

This refers to porosity formed at time of sediment deposition and can occur as either interparticle or intraparticle pores. Interparticle porosity is easily lost in soft sediments and carbonate sands through compaction and cementation respectively although commonly retained in siliciclastic sands. Intra particle porosity consists of pores usually within carbonate grains and is often Cul-de-sac pores.

Secondary Porosity

This is porosity which results from pores that developed after sediment deposition. This may be facilitated by processes such as dissolution, hydrofracturing and tectonic processes. Secondary porosity can thus be broken down into vuggy and fracture types. Figure 3-2 is a schematic representation of the main factors that control the porosity of carbonate reservoirs after sediment deposition.

Diagenetic processes occurring near the surface decrease and/or rearrange porosity. Such

processes include meteoric diagenesis, leaching, compaction, clay coating, bioturbation, and dolomitization. In addition, burial history, temperature, duration and depth of burial, are critical factors affecting the rate of porosity loss (Moore, 2001).

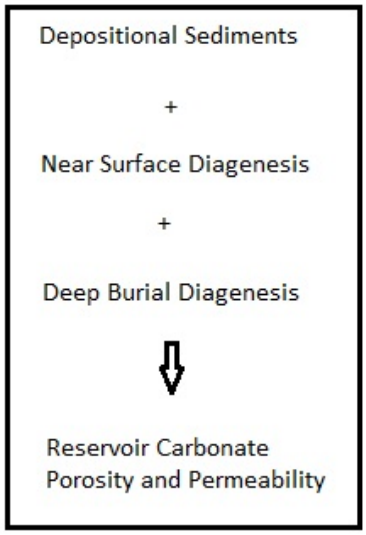

Figure 3-2: Factors Controlling Porosity and Permeability in Carbonate Reservoirs.

3.1.2.2 Porosity Measurements

An estimate of porosity can be achieved using four techniques:

1. Well logs: depending on lithology, the Sonic, Neutron, or Density logs can be used.
2. Seismics: through change in acoustic impedence as density decreases with increasing porosity.
3. Visual inspection of core slabs, using a low-power petrographical microscope. Visible porosity in thin section can be measured by point counting the visible pores or by using image analysis software to calculate pore space.
4. Direct measurements on core samples by means of laboratory measurements.

Carbonate rocks are compressible with porosity decreasing with increasing effective stress. For quality purposes, only porosity measurements at in-situ stress conditions are considered, which for the Three Forks Formation is about 4,000 psi.

Intergranular porosity is the most common porosity type in sedimentary rocks and does not depend on grain size but is largely controlled by the degree of grain sorting. Porosity is affected by grain packing, degree of sorting, and grain shape. Cubic packing (47.6% porosity) is the most open arrangement of grains while rhombohedral packing (25.96% porosity) is the closest arrangement for idealized, spherical grains. If sorting is poor, the porosity of a cubic - packed sample is reduced from about 48% to about 13% (Fig. 3-3).

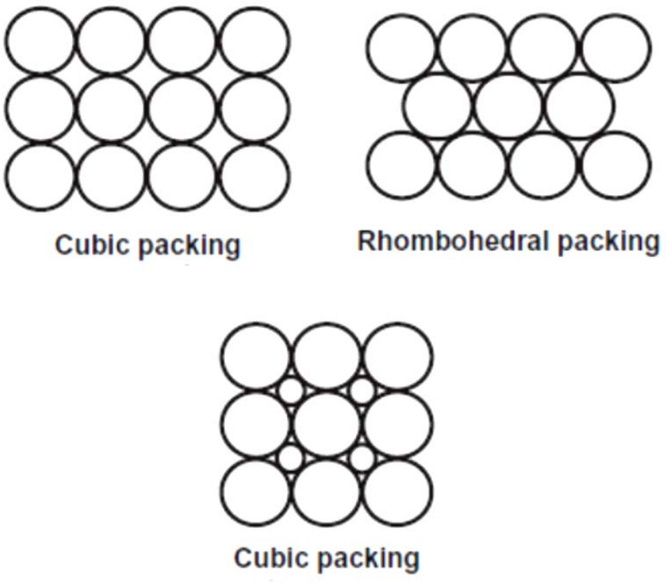

Figure 3-3: The Importance of Packing and Sorting to Porosity. Cubic (47% porosity), rhombohedral (26% porosity) packing and the importance of sorting. The introduction of smaller but uniform grain size reduces the original porosity from 47.6% to 12.5%.

3.1.3 Permeability

Another important rock property is permeability which relates to the rate at which fluids within a formation can be recovered through connecting pore spaces of reservoir rock. The type of cementing material between grains, size of pore openings, degree of pore connectivity are some of the major controls of permeability. Permeability is expressed by Darcy's Law shown below:

$$k = \frac{Q\mu}{A}\left(\frac{L}{\Delta P}\right) \ldots (2)$$

Where,

> Q = flow per unit time (cm/s), k = permeability (cm^2), μ = fluid viscosity (cp), (ΔP) = change in pressure (psi), L = length of rock (cm) the potential drop across a horizontal sample, and A is the cross-sectional area of the sample (cm^2).

Air or brine can be used as a fluid to determine the permeability of a rock sample. During this process, if a high flow rates is kept constant, the results from air and brine permeability are alike. However, at low flow rates, air permeability is always greater than liquid permeability. This is because gas molecules do not stick to the pore walls and exhibited some finite velocity (slippage) at grain surfaces at a given pressure differential while liquids have zero velocity at grain surfaces. This is referred to as the "Klinkenberg effect" and is critical in low-permeability rocks. The Klinkenberg correction, is therefore a method to correct gas permeability measured at low mean flowing pressure to an approximate liquid permeability (Monicard, 1980; Engler, 2003).

3.1.3.1 Types of Permeability

Permeability can be described as absolute, effective, or relative. Absolute permeability denotes measurement conducted when a single fluid, or phase, is present in the rock. Effective permeability is preferentially of a particular fluid when other immiscible fluids are present in the reservoir. Relative permeability is the ratio of effective permeability of a particular fluid at a particular saturation to absolute permeability of that fluid at total saturation. Thus the effective or relative permeabilities most accurately describe fluid flow in reservoirs since more than one fluid is usually present.

3.1.3.2 Measuring Permeability

Several methods can be used to measure the permeability of a formation. In this study, permeability is determined mainly from core analysis as this method provides the most accurate and values. Permeability may be classified as fair, between 1 to 10mD; Good from 10 to 100mD; very good from 100 to 1000mD (Garven, 1986).

3.1.4 Fluid Saturation

Water saturation (Sw) is defined as that fraction of the pore volume, filled with water such that the sum of water and hydrocarbon saturations are one and is usually calculated from the resistivity of the formation (Rt). Because clays have different electrical conductivity properties, measured *Rt* in shaly formations becomes strongly affected by the type and distribution of clays present. Several attempts to correct the clay conductivity problem by modifying Archie's original equation have been well documented; see for example Clavier et al., 1984; Worthington, 1985; Woodhouse, 1998. To correct the *Rt-Sw*

obtained in shaly zones identified by the previous *Vcl* analysis; advanced interpretation is performed using five models. These are: the *Archie Total*, *Simandoux, Modified Simandoux, Indonesia and Dual Water models.* Their predicted *Sw* are calculated, compared, and presented in chapter 10.

3.1.5 Reservoir Characterization

Mapping the important properties in the vertical and horizontal dimensions of the Three Forks Formation is a critical part of the formation evaluation process. In this study, the vertical dimensions are divided into gross and net pay and represented using isopach maps. The main criteria used are the porosity-permeability distribution within the reservoir and the degree of water saturation. The continuity of these parameters is largely controlled by variations in the depositional environments and post-depositional fabrics of the reservoir.

3.1.6 Diagenesis

Diagenesis includes all relatively low-pressure, low-temperature alteration processes (mainly chemical), by which changes in sediments are brought about after deposition but before their final lithification. Due to their solubility, carbonates can be readily modified by diagenetic processes such as dissolution of minerals which increases porosity. Selective dissolution is responsible for the creation of fenestrae and stylolite textures.

CHAPTER 4

WIRELINE LOGS

Wireline tools measure the geological properties of subsurface rocks. Traditionally, a combination of both nuclear (radiation-based) and nonnuclear (non-radiation-based) tools are used to investigate the geological formations surrounding the borehole. The results are presented as logs and interpreted for such parameters as: formation water saturation, porosity, permeability and other rock characteristics. Below are some of the different log types that have been used in this research. A summary of the basic tools that are used in this study is given in Table 4-1.

Table 4-1: Summary of the Basic Tools that Provide Information on Formation Fluid Content, Porosity, and Lithology.

Formation Fluid Content Indicators	Porosity-Lithology Indicators
1. Induction 2. Laterolog 3. Micro-focused and 4. microresistivity devices	1. Acoustic (sonic) 2. Density 3. Neutron 4. Natural gamma ray

4.1 Resistivity Logs

Electrical resistivity is a key geophysical method employed in both surface and subsurface geophysics and is well known among geophysical methods for exploration, devel-

opment and definition of identified targets. While most parts of a rock are basically insulators, the fluids within the pore are conductors. In contrast, hydrocarbon fluids are virtually infinitely resistive. This idea can be used to differentiate porous formations containing salty water with an overall low resistivity from very low porosity formations containing hydrocarbons with very high resistivity. Therefore, high resistivity values probably signify a hydrocarbon bearing formation.

Working Principles: The formation resistivity is measured in ohm-m and expressed on a logarithmic scale (e.g. 0.2 to 2000 ohm-m) as a resistivity log. The success of such logs therefore relies on their ability to delineate non-conducting hydrocarbons from all conducting formation waters. Other tools like the induction and propagation resistivity logs make use of the conductivity properties of clays and a few other minerals such as pyrite, but presented as ohm-m.

4.1.1 Types of Resistivity Logs

As many as 17 types of resistivity logs can be documented, which differ primarily in how far into the rocks they measure the resistivity. Below are the resistivity logs employed in this study:

1. Array Induction Tool (AIT) - It measures five depths of investigation.
2. Dual Induction Log (DIL) - Consist of deep and medium depths of investigation.
3. Dual Laterolog (DLL) - Consist of deep and medium depths of investigation.

4.2 Natural Gamma Ray (GR) Log

The GR log records the naturally occurring radiation of rocks found in the formation. The

gamma ray emission results from the disintegration due to Potassium, Uranium, and Thorium. This tool does not emit any radiation but uses a radioactive sensor that measures the strength of the received gamma rays which depend on: 1) the source emitting gamma rays, 2) the concentration of the source material within the formation, 3) the distance between the source and the tool detector. The standard GR tool has limited depth of investigation and vertical resolution of approximately 10 inches.

4.2.1.1 Gamma Ray Environmental Corrections

Gamma ray measurements are affected by borehole size, mud weight (often containing barite) and eccentricity. These effects decrease the GR count rate as the mud "shields" some gamma rays before reaching the tool. Similarly a tool centered in the borehole receives less GR counts than an eccentered tool (misaligned to the borehole/formation interface) up against the borehole wall. In intervals that suffer from caving, there is more drilling mud between the formation and the gamma ray detector to attenuate the gamma rays produced by the formation.

Since the counts are underestimated, environmental corrections must be applied to log readings before any quantitative analysis if the density of the drilling fluid and bit size are known.

4.3 The Caliper Log

The caliper log provides continuous recording of borehole diameter versus depth and is generally run together with the gamma ray log. Its main application in this research is to locate caved zones, tight spots and the recognition of permeable zones (mud cake). The

caliper tool works by pressing pads against the borehole wall as a means of registering the borehole size and identifying caving or dissolution/washout by salt.

4.4 Porosity Logs

The nuclear tools of interest to this research use either sources of gamma rays or neutrons and are important in determining important hydrocarbon characteristics such as porosity, composition, and whether or not oil or water is present.

4.4.1 The Formation Density Log

The formation density log measures the bulk density of the formation and is used to derive a value for the total porosity, the detection of gas-bearing formations, the recognition of evaporates and to evaluate shaly-sand reservoirs and complex lithologies. The formation density tools are induced radiation tools. The depth of investigation of the logging tool is about 13 cm (5 in).

The vertical resolution is about 26 cm (10 in). The main use of the formation density log is to determine porosity. The formation density log was employed for the identification of minerals and in combination with the neutron log to identifying lithologies. The density tool works by emitting gamma rays while a detector detects scattered returning gamma rays whose density is proportional to the density of formation (mineral and fluids). A combination of neutron and density readings is thus required for accurate porosity assessment.

Effects of Shale and Gas on the Density Porosity Model

When clays are present in the formation matrix, the measured neutron porosity is greater

than the actual formation porosity due to the presence of hydrogen within the clay structure which is interpreted as part of the porosity. If the pores are filled with gas rather than oil or water, the measured porosity is lower than the true porosity because gas contains less hydrogen concentration than in oil or water. The hydrocarbon effect on density logs is much smaller compared with the acoustic log. Oil does not significantly affect density porosity but gas does (gas effect). As a result the tool provides the best indication of porosity in liquid-filled holes.

4.4.2 The Neutron Log

The neutron log measures the hydrogen atoms concentration in a formation by bombarding the formation with high energy neutrons which undergo scattering in the formation, losing energy and producing high energy gamma rays. These scattering reactions occur most efficiently with hydrogen atoms. The resulting low energy neutrons or gamma rays can be detected, and their count rate is related to the amount of hydrogen atoms in the formation. Therefore, in clean formations where the porosity is filled with water or oil, the neutron log measures liquid-filled porosity.

Working principle

The neutron tool consist of a source that emits neutrons that collide with larger atomic nuclei with little energy loss but lose energy in collisions with H atoms, which are of roughly same mass as neutrons themselves. The neutron tool response is therefore controlled by the concentration of hydrogen atoms in the formation, providing a good measure of formation porosity if liquid-filled (oil or water) pore spaces contain hydrogen. The neutron-density log combination is used to determine porosity and lithology.

The neutron log response is inversely proportional to porosity so that low-measurement values correspond to high porosities, and high-measurements correspond to low porosities. The reason for this is because in formations with a large amount of hydrogen atoms, the neutrons are slowed down and absorbed very quickly and in a short distance resulting in a low count rate in high porosity rocks. Conversely, when only a small amount of hydrogen atoms is present, the neutrons are slowed down and absorbed more slowly and travel further through the rock resulting in a higher count rate in low porosity rocks.

The compensated neutron logs used in this research have the advantage of sidewall neutron logs being less affected by borehole irregularities. Since the neutron measurements were recorded in apparent limestone units, the apparent porosity is equal to true porosity hence, no corrections were applied. The vertical resolution of neutron tools falls between 25 to 50 cm (10 to 20 in) depending the source-detector spacing. The true bed resolution (the thinnest bed for which the true neutron porosity in that bed is measured) is approximately three times the vertical resolution i.e. 91 to 122 cm (36 to 48 in).

4.4.3 Acoustic (sonic) Log

The sonic log is a display of the travel time of acoustic (elastic) waves through the formation and in some cases displays the velocity. Some of the main uses of such data are to support and calibrate seismic data, determine the formation porosity, for stratigraphic correlation, identification of lithologies, facies recognition, and identification of source rocks.

Borehole Compensated Sonic (BHC) Tool

This research utilizes the BHC tool because of its ability to compensate automatically for

tool misalignment or changes in the borehole size. Calibration is done inside the borehole opposite beds of pure and known lithology, such as anhydrite (50 μs/ft.), salt (67 μs/ft.), or inside the casing (57 μs/ft.). The depth of penetration is small (2.5 to 25 cm; 1 to 10 ft) with larger wavelengths giving larger penetrations.

Effect of Shale and Hydrocarbon on the Sonic Derived Porosity

The density of shales is quite variable (depending on the degree of compaction) and so is its effect on the sonic derived porosity. High density shales (ancient compact shales), tend to decrease the transit times and hence give slightly lower sonic derived porosities than young, low density shales. Exactly the opposite is the case for ancient compact shales with high densities, which give lower transit times and smaller porosities. The presence of gas (low density), increases the travel time and hence, decreases the apparent density of a formation thereby overestimated the formation porosity.

Also, the interval transit time of the sonic waves (Δt) increases when hydrocarbons are present. This is known as the *hydrocarbon effect* and if not corrected, the calculated porosity from the sonic log will be too high. The effect of shales on the sonic porosity is not as great as the effect of gas. Hilchie (1978) proposed the following empirical rectifications for the hydrocarbon effect:

$$\phi = \phi_{sonic} \times 0.7 \text{ (gas) and } \phi = \phi_{sonic} \times 0.9 \text{ (oil)}$$

CHAPTER 5

MATERIALS AND METHODS

The data for this study are obtained mainly from well logs and core samples. Core samples provide descriptive, semi-quantitative and quantitative data which are used to supplement log derived values. This chapter provides key information on the techniques and methods that are used to collect, process, and present the data that are applied to the subsequent chapters.

The study employs the following techniques to accomplish its goals:

1. Core description and lithostratigraphic modeling for facies identification using multivariate analysis of wells logs. A detailed description of the subsurface lithology is achieved by integrating data from visual core analysis with geophysical modeling using the Interactive Petrophysics software and ArcGIS program.
2. A detailed petrographical analysis that involves the use of thin sections, X-ray diffraction (XRD) and scanning electron microscopy (SEM) of core samples.
3. Petrophysical and analysis of well logs and core samples to determine the relationships between porosity (ϕ), permeability (K), and water saturation (Sw).
4. Geochemical analysis is used to determine the TOC content and type of kerogen, which is necessary for a definitive conclusion on source potential.

5.1 Log Analysis

5.1.1 Filtrate Salinity and Density

In the absence of mud filtrate salinity or mud filtrate density information, they are calculated from the *Rmf* or in the case of oil-based mud they are calculated from *Rw* using the equations below (IP, 2011).

$$\text{Sal} = \log\left(\frac{3.562 - \log(Rmf\ 75 - 0.0123)}{0.955}\right) .. (3)$$

$$\rho_{\text{mf}} = 1.0 + 7 \text{ x } Sal \text{ x} 10^{-7} - (Temp - 80)^2 \text{x } 10^{-6} \ldots .. (4)$$

Where,

Sal = salinity (ppm) and ρ_{mf} = mud filtrate density (gm/cc), *Temp* = formation temperature (°F), *Rmf75* = Rmf converted to 75°F.

5.1.2 Formation Temperature (T_2):

$$T_2 = \frac{D(BHT - T_1)}{TD} + T_1 \ldots . (5)$$

Where,

T_2 = Formation temperature (°F), *D* = Log Depth (ft), *BHT* = Bottom hole temperature (°F), *TD* = Total depth, T_1 = Surface Temperature (°F).

5.1.3 Determination of Clay Volume (Vcl):

The determination of the amount of clay present in a formation is a necessary step in calculating formation porosity and fluid content. The presence of clays, if not accounted for, will normally cause the calculation of a neutron or acoustic derived porosity to be optimistic (overestimated). Similarly, the porosity calculated from the density device will

be optimistic, except when the clay density is greater than the clean matrix density. If the shale density is greater than the clean matrix density, the calculated porosity will be underestimated (Kamel and Mabrouk, 2003).

The clay volume may be calculated from the gamma ray log, the neutron log, the resistivity log, or a combination of logs. The gamma ray log had been corrected before the Vcl is determined. The following methods and equations are applied for the determination of Vcl:

5.1.3.1 The Gamma Ray Log

Gamma Ray Environmental Corrections Example:

For a GR_{log} = 32 API, hole size (dhole) = 12 inches, mud weight (Wmud) = 9.2 lbs/gal and tool diameter is $3^3/_8$" and centered.

- Calculate t = Wmud x [2.54 (dhole) - 2.54 (dsonde)] / [8.345 x 2] => **t = 12 g/cm^2**
- Follow the red line on the x-axis (Fig. 5-1) to project up at t = 12 g/cm^2 to $3^3/_8$" tool centered line to read Correction factor of approx. = 1.20.

  GR_{corr} = 1.2 x GR_{log} = **38.4** API

The shale volume (Vsh) is determined from:

$$\text{VshGr} = \text{GRI} = \frac{(Gr - Gr_{clean})}{(Gr_{shale} - Gr_{clean})} \dots (6)$$

Where,

Gr = gamma ray log, Gr_{clean} = gamma ray minimum, Gr_{shale} = gamma ray maximum, *GRI*= gamma ray index.

The *Vsh* is corrected for clay volume (*Vcl*) using the Larionov's correction for older

rocks:

$$VclGr = 0.333\ (2^{2\ \mathrm{x}\ GRI} - 1) \ldots (7)$$

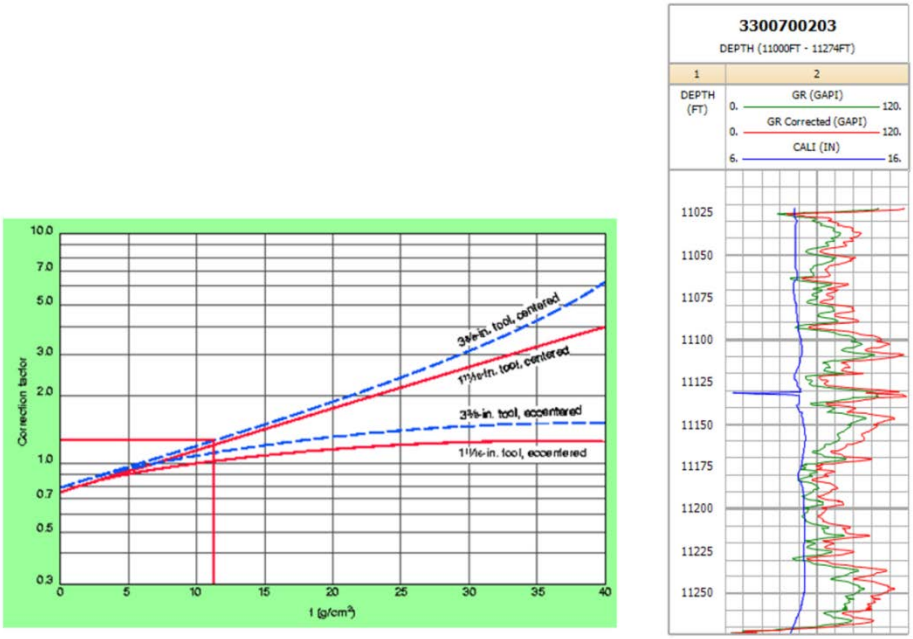

Figure 5-1: Procedure for Establishing a Correct Gamma Ray Reading. (A) Gamma Ray borehole and mud weight corrections, modified from petrolog.net. (B) Example of a corrected gamma ray log for borehole effects and mud weight for an eccentered, non barite open hole.

5.1.3.2 The Neutron Log

$$\mathrm{VclNeu} = \sqrt{\frac{\phi_{\mathrm{Neu}}}{\phi_{\mathrm{NeuClay}}}} \mathrm{x} \frac{\phi_{\mathrm{Neu}} - \phi_{\mathrm{NeuClean}}}{\phi_{\mathrm{NeuClay}} - \phi_{\mathrm{NeuClean}}} \ldots (8)$$

Where,

ϕ_{Neu} = log reading; $\phi_{NeuClean}$ = log value in a clean, zero clay zone (in limestone porosity units); $\phi_{NeuClay}$ = log value in a 100% clay zone.

5.1.3.3 The Resistivity Log

$$VclRes = \frac{R_{clay}}{Rt} \text{x} \frac{(\text{R}_{\text{clean}} - \text{Rt})}{(\text{R}_{\text{clean}} - \text{R}_{\text{clay}})} \ldots (9)$$

Where,

R_{clean} = resistivity in a clean zone; R_{clay}, log value in a 100% clay zone; Rt = true formation resistivity.

For *Rt* greater than 2 x *Rclay* then

$$VclRes = 0.5 \text{ x } (2 \text{ x VclRes})^{0.67 \text{ x } (\text{VclRes } +1)} \ldots (10)$$

5.1.3.4 Neutron-Density (ND) Crossplot[1]

$$\text{VclND} = \frac{(\text{Dencl}_2 - \text{Dencl}_1)}{(\text{Dencl}_2 - \text{Dencl}_1)} \text{x} \frac{(\text{Neu} - \text{NeuCl}_1)}{(\text{Neu}_{\text{clay}} - \text{NeuCl}_1)} - \frac{(\text{Den} - \text{Dencl}_1)}{(\text{Den}_{\text{clay}} - \text{Dencl}_1)} \text{x} \frac{(\text{NeuCl}_2 - \text{NeuCl}_1)}{(\text{NeuCl}_2 - \text{NeuCl}_1)} \ldots (11)$$

5.1.3.5 Sonic-Density (SD) Crossplot[2]

$$\text{VclSD} = \frac{(\text{Dencl}_2 - \text{Dencl}_1)}{(\text{Dencl}_2 - \text{Dencl}_1)} \text{x} \frac{(\text{Son} - \text{SonCl}_1)}{(\text{Son}_{\text{clay}} - \text{SonCl}_1)} - \frac{(\text{Den} - \text{Dencl}_1)}{(\text{Den}_{\text{clay}} - \text{Dencl}_1)} \text{x} \frac{(\text{SonCl}_2 - \text{SonCl}_1)}{(\text{SonCl}_2 - \text{SonCl}_1)} \ldots (12)$$

5.1.3.6 Neutron-Sonic (NS) Crossplot[3]

$$\text{VclNS} = \frac{(\text{Neucl}_2 - \text{Neucl}_1)}{(\text{Neucl}_2 - \text{Neucl}_1)} \text{x} \frac{(\text{Son} - \text{SonCl}_1)}{(\text{Son}_{\text{clay}} - \text{SonCl}_1)} - \frac{(\text{Neu} - \text{Neucl}_1)}{(\text{Neu}_{\text{clay}} - \text{Neucl}_1)} \text{x} \frac{(\text{SonCl}_2 - \text{SonCl}_1)}{(\text{SonCl}_2 - \text{SonCl}_1)} \ldots (13)$$

Where,

[1]Neu and Den are the neutron and density log readings; $DenCl_1$, $NeuCl_1$ and $DenCl_2$, *NeuCl2* are the density/neutron values for the two ends of the clean line on a neu-den crossplot.

[2]Son = sonic log reading; $DenCl_1$ & $SonCl_1$ and $DenCl_2$ & $SonCl_2$ are the density/sonic values for the two ends of the clean line on a *son*-den crossplot.

[3]$NeuCl_1$, $SonCl_1$ and $NeuCl_2$, $SonCl_2$ are the neutron and sonic values for the two ends of the clean line on a *neu*-son crossplot.

5.1.4 Values Used for Determination of Vcl

The wet clay properties are obtained from crossplots of double clay indicators. For example, the wet clay density is selected from the shale point, which is chosen towards the bottom right hand edge of the density-neutron-gamma ray crossplot (Fig. 5-2). On this plot, shales and gypsum would trend toward the east and northeast while light hydrocarbons and gas trend toward the northwest. Conversely, sonic values in clay zones are derived from the sonic /density gamma ray crossplot. The gamma ray response varies greatly throughout the Three Forks Formation from top to bottom. Since estimating the volume of shale from the gamma ray log involves the use of GRmin and GRmax (Eq. 6), proper zonation that reflects changes in depositional environments or reservoir rock properties is required to calculate the petrophysical properties correctly.

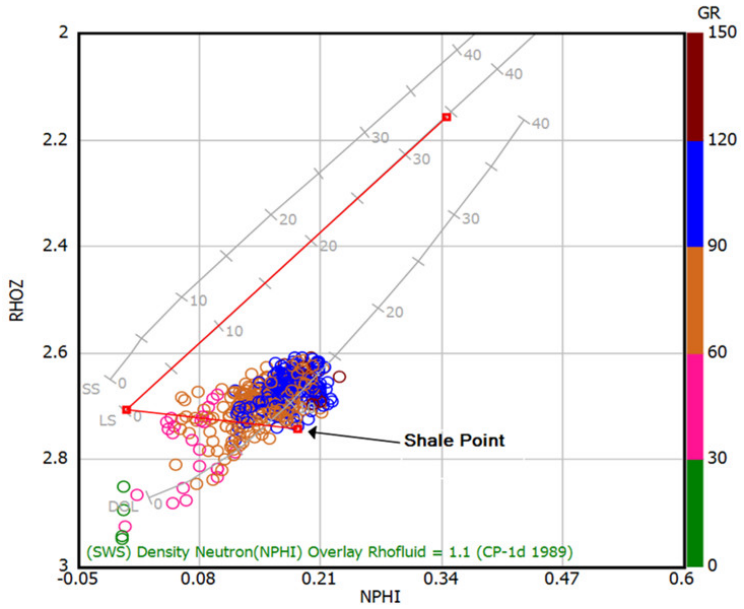

Figure 5-2: Example of the Neutron-Density-Gamma Ray Crossplot, Used for the Determination of the Wet Clay Density (Well 19709).

During clay volume analysis, the acceptable *Vcl* is calculated as the minimum shale

response of all single and/or double shale indicators. This is a common practice as this calculated *Vcl* provides the best approximation of clay content at any particular level (Poupon and Gaymard, 1970). Also, by using multiple clay indicators, a plausible evaluation of clay is obtained since each indicator may give a different value of clay volume.

5.1.5 Porosity (ϕ) Calculation

Indirect measurements of porosity can be obtained from nuclear measurements (density and neutron logs), sonic log, or measurements of the magnetic resonance of formation nuclei (NMR log). The density, neutron or sonic logs when used separately, will produce different values in response to lithology variations but in combinations of two or three at a time, a more accurate porosity can be estimated and the lithology easily deduced.

5.1.5.1 Sonic Porosity Models

Expressions that relate velocity to porosity and to pore-fluid compressibility are often used for inferring porosity from well logs, as well as in-situ indicators of pore fluid type within the formation. The Wyllie et al. (1956) time average equation is widely used to evaluate porosity in terms of velocity or Δt, written as:

$$\phi = \frac{\Delta t - \Delta t_{matrix} - Vcl * \left(\Delta t_{clay} - \Delta t_{matrix}\right)}{\left(\Delta t_{fluid} - \Delta t_{matrix}\right) * Cp} \ldots (14)$$

Where,

> Δt is the transit time in the formation of interest, Δt_{ma} is that through 100% of the rock matrix, Δt_{fluid} is that through 100% of the pore fluid, Δt_{clay} = Sonic clay value, and Cp = Compaction factor.

5.1.5.2 Density-Neutron Crossplot: Accurate Porosity Determination

Crossplots are graphical relationships of two or more measurements (one measurement displayed along the x-axis and the other displayed along the y-axis) to determine formation lithology and accurate porosity. Since both the density and neutron porosities had been measured in limestone units, the density vs. neutron crossplot was the most suitable for the Three Forks Formation as opposed to the sonic vs. density crossplot; widely used in the interpretation of shaly sands.

The ND Porosity (ϕ) Model - Corrected for Vcl Content and ρ_{hyden}:

The true porosity of the formation is derived from a crossplot of Eqs. 15 and 16.

$$\phi_{Neu} = \frac{\phi_{neu} - VclXNeu_{cl} + Neu_{Matrix} + Exfact + Neu_{sal}}{Sxo + (1 - Sxo)\ X\ Neu_{HyHI}} \ldots (15)$$

$$\phi_{Den} = \frac{\rho_{ma} - \rho_b - Vcl\ X\ (\rho_{ma} - \rho_{cl})}{\rho_{ma} - \rho_{fl}\ X\ Sxo - X\ \rho_{HyAp}\ X\ (1 - Sxo)} \ldots (16)$$

Where,

Vcl = Wet clay volume, Neu_{Cl}= Neutron wet clay value, Neu_{matrix} = Neutron matrix correction, *Exfact* = Neutron excavation factor, Neu_{Sal} = Neutron formation salinity correction, *Sxo* = Water saturation in flush zone, Neu_{HyHI} = Neutron hydrocarbon apparent hydrogen index; ρ_{ma} = Matrix density, ρ_b = bulk density, ρ_{cl} = wet clay density, ρ_{fl} = Filtrate density, ρ_{Hyap} = Apparent hydrocarbon density.

5.1.6 Formation Water Resistivity (Rw):

The formation water resistivity was obtained from the North Dakota Catalog of Water Chemistries and corrected for formation temperature using Arp's empirical formula:

$$Rw_2 = Rw_1 \frac{(T_1 - 6.77)}{(T_2 + 6.77)} \ldots\ldots (17)$$

Where,

$Rw_1 and\ Rw_2$ are the formation water resistivity at temperatures T_1 and T_2.
Results from Arp's equation are compared with Pickett plots to obtain a value for the cementation factor *m* (Archie's equation, Eq. 18) (Bateman, 1985).

5.1.7 Water Saturation (Sw) Determination:

Determination of *Sw* from resistivity logs using the Archie equation (Eq.18) is the most widely used open hole method to evaluate *Sw* for most operational purposes (Woodhouse, 1998). This equation is most applicable when the *Vcl* is less than 10% (clean sands) and is dependent on the accuracy of six inputs: porosity, *a, m, Rw*, and *Rt*; readily available from well logs while *n* is from core laboratory electrical measurements (usually assumed to have a value of 2). Because of the high *Vcl* content in the Three Forks, modified techniques that attempt to correct this problem are used separately and results compared. Such modified techniques or models include:

5.1.7.1 The Archie Total Porosity Model

The Archie Total Porosity Model (Eq. 18) provides a good estimate of *Swt* in shaly sands especially where *Rw* is low as in the Three Forks Formation where *Rw* is close to 0.02 Ohm·m. Since the Archie Effective Porosity Model (Eq. 19) considers formation water as the only electrically conductive component, its results are expected to be pessimistic in the shaly zones. For this reason, the Archie Effective Porosity is not considered in this study.

$$Sw_T = \sqrt[n]{\frac{a \text{ x } Rw}{Rt \text{ x } \phi^{\text{m}}}} \ldots (18)$$

$$Sw_e = \left(\frac{Sw_T - Sw_b}{1 - Sw_b}\right) \ldots (19)$$

5.1.7.2 The Indonesia Model

The Indonesia Model (Eq. 20) is based on readily available standard log analysis parameters and applied herein as a total porosity model because of its ability to predict 100% *Sw* in shaly sands.

$$\frac{1}{Rt} = S_w^n \left(\left(\frac{Vcl^{(2-Vcl)}}{Rcl}\right) + \left(\frac{\sqrt{\Phi_e^m}}{Rw}\right)^{1/2} \right)^2 \ldots (20)$$

5.1.7.3 The Simandoux and Modified Simandoux Models

The Simandoux and Modified Simandoux Models (Eqs.21/22) take into account the distribution of all three forms of clays in the determination of *Sw* in shaly sands. The purpose of having 1-Vcl in the denominator in Eq. 22 is to decrease the calculated *Sw* computed from Eq. 21 (Woodhouse and Warner, 2005).

$$\frac{1}{Rt} = \frac{\phi^m \text{ x } \text{Sw}^\text{n}}{a \text{ x } \text{Rw}} + \frac{Vcl \text{ x } \text{Sw}}{\text{Rcl}} \ldots (21)$$

$$\frac{1}{Rt} = \frac{\phi^m \text{ x } \text{Sw}^\text{n}}{a \text{ x } \text{Rw x } (1 - \text{Vcl})} + \frac{Vcl \text{ x } \text{Sw}}{\text{Rcl}} \ldots (22)$$

5.1.7.4 The Best et al.'s Dual-Water equation Model

This model (Eq. 23) was employed because of its ability to predict *Swt* independently from special core analysis (SCAL) data.

$$\frac{1}{Rt} = \frac{\phi_T^m \text{ x } \mathrm{Sw_T^n}}{a}\left(\frac{1}{Rw} + \frac{Sw_b}{Sw_T}\left(\frac{1}{Rw_b} - \frac{1}{Rw}\right)\right) \ldots (23)$$

Because the value for the normalized cation-exchange capacity *Qvn* in the Normalized Waxman-Smits model is identical to Sw_b from Eq. 23 when the models have the same exponents (Woodhouse and Warner, 2005) and the lack of SCAL data on clay conductivity *BQv*, both the original and normalized Waxman-Smits-Thomas Models are not considered in this study.

5.1.7.5 Derivation of "m"

The true formation resistivity (Rt) with 100% water is represented by *R0*. The ratio *Rt/Ro* is defined as the Resistivity index (RI) and a log-log plot of *Sw* versus *RI* yields a straight line whose slope provides a value for the Archie saturation exponent "n". In the absence of SCAL data, the value for the Archie cementation factor "m*"* is deduced, from a crossplot of resistivity and porosity (Fig. 5-3). This value leans towards 1.6 and 1.8. Equivalent values between 1.6 and 2 are considered for the parameter "*n"* where appropriate.

5.1.8 Hydrocarbon Saturation (Sh):

Sh=1-Sw……(24)

In equations 18 through 23,

ϕ = porosity, *m* = Cementation factor, *n* = Saturation exponent, *a* = Tortuosity factor, *Vcl* = Wet clay volume, *Swe* = Effective water saturation, *Swt* = Total water saturation, *Swb* = Bound water saturation where the bound-water resistivity (*Rwb*) is the value of $R_t\Phi_t^m$ in

the clay, *Rw* = Formation water resistivity, *Rt* = True formation resistivity, *Rcl* = Resistivity of the clay and *T* = Formation temperature (°C).

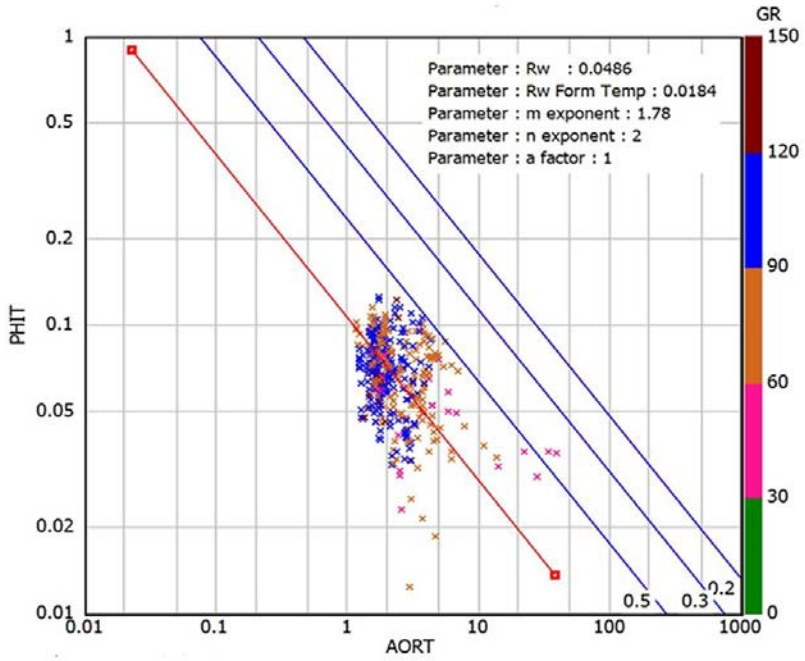

Figure 5-3: Crossplot of resistivity and Porosity for Determination of the Archie Cementation Factor "m" and the Saturation Exponent "n".

5.2 Routine Core Analysis

Results from conventional core analysis on more than 900 core plugs are used to calibrate and validate results. Core analysis showed that the grain densities within the Three Forks Formation vary rapidly within wells and across fields. Grain densities from five wells covering an average of 46 m (150 ft) below the Bakken Formation, and sampled on a foot-by- foot to 0.5 ft scale, range from 2.73 gm/cc to 2.95 gm/cc with a mean value of 2.79 gm/cc. Hence, a variable grain density (2.73 to 3.0 gm/cc) is used to calculate porosities with the neutron-density porosity model. Routine core analysis also provided ground truth data on porosity; air and Klinkenberg permeabilities and fluid saturations.

5.3 Core Description

Cores were described at the Wilson M. Laird Core and Sample Library of the North Dakota Geological Survey and three major stratification types are observed in the Three Forks Formation: (1) layers with internal cross-stratification, (2) layers with no internal cross-stratification between layer boundaries, and (3) layers of alternating shale and carbonates with or without anhydrite. A summary of the distinctive primary and secondary sedimentary features recognized within each Member is presented.

5.4 Multivariate Analysis

Two main multivariate analysis techniques are used in this study. These are the principal component analysis (PCA) and cluster analysis (Reyment et al., 1999). These calculations are performed in the statistical prediction module of the IP software.

5.4.1 Principal Component Analysis (PCA)

This is a technique used to reduce multidimensional data sets to lower dimensions for analysis. PCA has the ability to combine multiple logs into a single log without losing information, identify patterns in data, and expressing the data in such a way as to highlight their similarities and differences. Consider a two dimensional scatter plot of the data from the formation density and neutron logs as presented as Figure 5-4. The PCs are the eigenvectors of this cloud, computed to locate the major axes in order of importance. Given that the data points are equally weighted, if the shape of this cloud of data points was ellipsoidal, the first PC (PC1) represents the largest variability and is aligned according to the direction of maximum length of the ellipsoid. The second PC (PC2) is the

second longest axis but in a perpendicular direction and no correlation exist between PC1

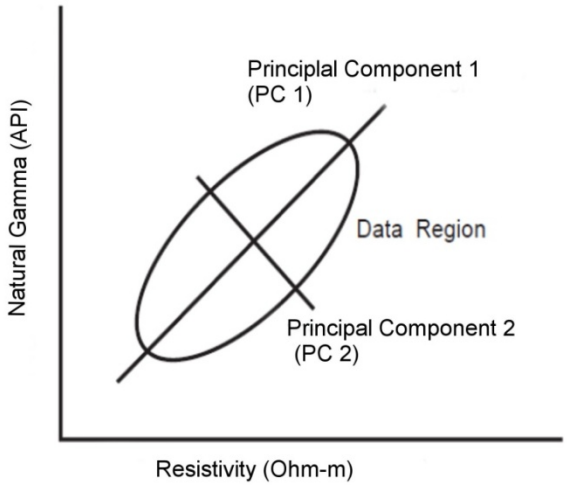

Figure 5-4: Principal Components of a Two Dimensional (Variable) System.

and PC2. Similarly, if nlog responses from a sequence of zones are plotted as points in a space, they form a cloud in n-dimensions which can be described by a set of axes defined by PC1, PC2….PCn. Thus, their use eliminates the redundancy between original logs.

The process of PCA can be summarized by the following steps:

1. First, the logs are standardized. This is done by calculating the mean and standard deviation of each log over the selected depth interval. (all subsequent calculations and plots are in Standard Deviation (SD) units).
2. The correlation matrix is calculated using the standardized data. The correlation matrix, as opposed to the covariance matrix, is used so as to reduce the effects of the different geophysical measurement units.
3. The order and orientation of the principal components are determined from the eigenvalues and eigenvectors of the correlation matrix. The square root of the eigenvalues indicates the length, and thus the order, of the component axes.

4. The percent of the total variation accounted for by each principal component is calculated based on the relative size of the eigenvalues. The relative size of the eigenvector elements indicate the degree to which each geophysical log contributes to the variation described by that component.
5. In order to better understand the underlying geologic factors controlling the components, "score" values are calculated using the eigenvectors and original log traces. The calculation of the scores, performed at each depth increment, produces new "principal component score logs," in units of standard deviation. These new, and uncorrelated, logs represent the combined loading of the component by each of the original logs.

5.4.2 Cluster Analysis

Cluster analysis is a technique that is used to find similarities between data according to their characteristics and grouping similar data objects into clusters. The goal is that objects that are related are placed in the same group based on a common similarity in such a way that they are different and become separated from unrelated groups. The greater the homogeneity within a cluster the greater the difference between groups and hence, the more distinct the clustering (Haldiki et al., 2002). Clusters are defined in such a ways that the boundaries are imprecise and are controlled by the nature of data and the desired outcome. The procedure involves two steps:

5.4.2.1 Log Segmentation

Log segmentation is achieved through K-mean clustering which works by associating each cluster with a centroid and assigning each data point to the cluster with the closest

centroid or mean value (Fig. 5-5). K-mean clustering is used to zone the data (PCs) by

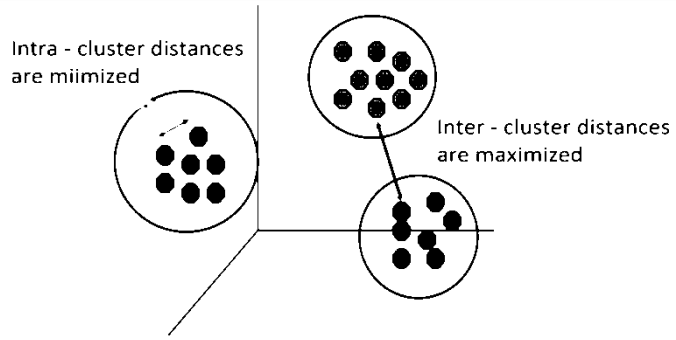

Figure 5-5: Technique of K-mean Clustering Algorithm.

minimizing the within-zone sums of squares of the difference between the data point and the zone mean value. Thus, the average value for a particular zone is taken as the representative value for that zone.

5.4.2.2 Cluster Consolidation

Hierarchical clustering technique is applied to enable zones (clusters) to be grouped based on their measured similarity. Hierarchical clustering works by computing the distances between all clusters and then merging the two closest zones together.

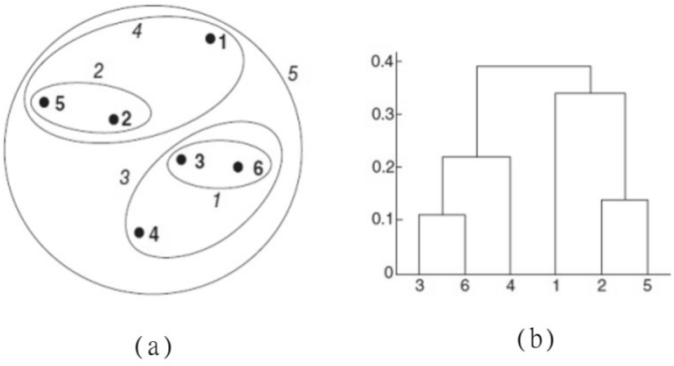

Figure 5-6: An Example of a Complete Link Clustering of Six Points. (a) Linked clusters, (b) a representative dendrogram.

The new cluster distance to all other clusters is then recomputed and the two closest clusters merged again. This process continues until only one cluster is left. Such a consolidation is achieved by building a binary tree of successively merged groups of points. The set of nested clusters is presented as a dendrogram (Fig. 5-6).

5.5 X-Ray Diffractometry (XRD), Thin-Section Microscopy, Scanning Electron Microscopy (SEM), TOC and Rock-Eval Pyrolysis

Laboratory investigations on selected samples by means of XRD, thin-section microscopy, and SEM techniques were performed by AGAT Laboratories, Calgary. In addition to qualitative mineral identification, XRD is routinely used for quantification of mineralogical data in geological samples by fingerprinting approach (Bish and Post, 1989; Moore and Reynolds, 1997). Small portions of each sample were analyzed for bulk and clay XRD. The details on this technique are given in Appendix 1and the results are listed in Table 8-1.Investigations on the generative potential and thermal maturity of the Three Forks using TOC and Rock-Eval were done by the Petromarkers, Inc. laboratories in Texas, United States. The time-signal curves, produced during pyrolysis are presented as Appendix 2.

Many dolomite-rock classification schemes have been generated over the past decades in an attempt to categorize the shapes and textures that result from nucleation and growth of dolomite crystals. These include Friedman (1959/1965), Gregg and Sibley (1987), Zenger (1981), Randazzo and Zachos (1984), and Shukla and Friedman (1983). The usefulness of crystal morphology and their relationship have been well applied by (Gregg and Sibley, 1987) who recognized the importance of crystal-boundary shapes in characteriz-

ing the different mechanisms of crystal growth.

The descriptions of compositional and diagenetic characteristics of the Three Forks Formation are based on optical microscopy on 6 thin sections. Thin sections are analyzed following standard petrographical procedures (Appx. 3) and examined petrographically. The petrographical data summary, including framework mineralogy, diagenetic minerals and cements, textures, plus thin section porosity is provided in Table 8-2. Representative thin section photomicrographs with descriptions, illustrating general and specific features of the samples are also provided.

The use of SEM to study the nature of the pore structures and authigenic cements in reservoir rocks has been widely documented (Hardy and Tucker, 1998; Ruan and Ward, 2002). The methods used in this study are given in Appendix 3. Representative SEM photomicrographs with descriptions, illustrating general and specific features of the Three Forks are provided in chapter 9. Energy Dispersive X-ray (EDX) analysis is also carried out to get the elemental composition of the samples.

Abbreviations, units, terminology and interpretations used for TOC/Rock Eval have been thoroughly discussed by Espitalie et al. (1977), Peters (1986), Katz (1983), Langford and Blanc-Valleron (1990) and Hunt (1996). Standard definitions for Rock-Eval data include:

1. The hydrocarbons already present in the rock sample are represented as S1 and corresponds to the total free hydrocarbons (oil and gas) that evolve without cracking of the heavy hydrocarbons. This is reported in terms of how many milligrams of free hydrocarbons can be thermally distilled out of one gram of the sample.

2. The second peak, identified as S2 and expressed as milligrams of hydrocarbons per gram of rock corresponds to the fraction of original kerogen capable of generating hydrocarbons that have not yet been converted to oil and (or) gas from the thermal breakdown of kerogen (Tissot and Welte, 1978). Thus, S2 indicates the potential amount of hydrocarbons that the source rock might still produce if thermal maturation continues.
3. The S3 peak represents CO_2, generated during the process due to thermal cracking of the kerogen expressed in milligrams per gram of rock.
4. Tmax, the temperature at which the maximum hydrocarbon is generated (for the S2 peak).
5. The hydrogen index (HI) represents the ratio of hydrogen to TOC and is equivalent to the total hydrogen in the kerogen expressed as (S2/TOC) x 100.
6. The oxygen index (OI) is the ratio of CO2 to TOC and is equivalent to the total oxygen content in the kerogen expressed as (S3/TOC) x l00.
7. The Production index (PI) is the ratio of the amount of oil already generated or contained in a sample to potential hydrocarbons and is expressed as S1/ (S1 + S2).

SECTION III

RESULTS AND INTERPRETATIONS

CHAPTER 6

STRATIGRAPHY

A total of 725 wells are selected for project, and were used to create isopach maps of the various members. Of the 725 wells, 32 are selected for petrophysical evaluation, creating a data base of 160 conventional logs with each log suite consisting of the gamma ray (Gr), formation density (RHOB), neutron porosity (PHIN), sonic (ΔT), and resistivity (Rt) logs. Cores from seven wells that go through the Three Forks were described (Appx. 4).

The Ordovician to Pennsylvanian stratigraphy in the study area is shown in Figure 6-1. The type section of the Three Forks Formation is originally described from the outcrop north of the Gallatin River in Gallatin County, Montana by Sandberg and Hammond (1958). Within the subsurface in North Dakota, the standard subsurface section of the Three Forks Formation is placed between the depths of 10,076 ft and 10,310 ft of the Mobil Birdbear well No. 1 in Dunn County. Lithologically, the Three Forks Formation consists of different colors of laminated to bedded carbonates, separated by dark grey to grey-brown, wavy to discontinuous seams of shale, and various forms of anhydrite. Within the studied wells, the distinction between the Pronghorn and the overlying lower Bakken is usually a sharp (erosive) unconformable contact (Fig. 6-2A/B), while the contact between the Pronghorn and the underlying Three Forks may be a sharp and dis-

conformable surface or transitional which is difficult to identify (Fig. 6-2C).

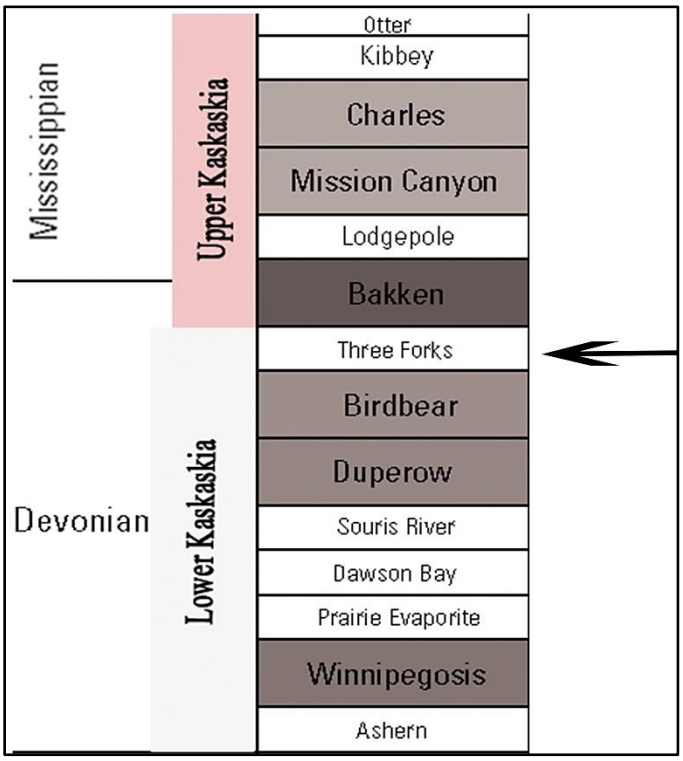

Figure 6-1: Partial Stratigraphic Column of North Dakota Showing the Stratigraphic Position of The Three Forks (Modified from Anna et al., 2010).

Where the Pronghorn is absent, the Three Forks makes a conformable contact with the Bakken Formation. The lower contact with the Birdbear Formation is conformable and is taken at the base of the reddish brown dolomitic mudstones of the lower Three Forks Formation. The Three Forks Formation has previously been included in several classification schemes and subdivided into a number of informal units or members (LeFever, 2011).

In this study, the Three Forks Formation is subdivided into six members (from bottom to top) based on their gamma ray-resistivity log response. These members can be traced

across most of the basin, similar to those observed by Christopher (1961) in southeastern Saskatchewan, all of which may or may not be present within a given well section in North Dakota. A reference log for the Three Forks is shown in Figure 6-3 with the corresponding core photographs presented as Figure 6-5.

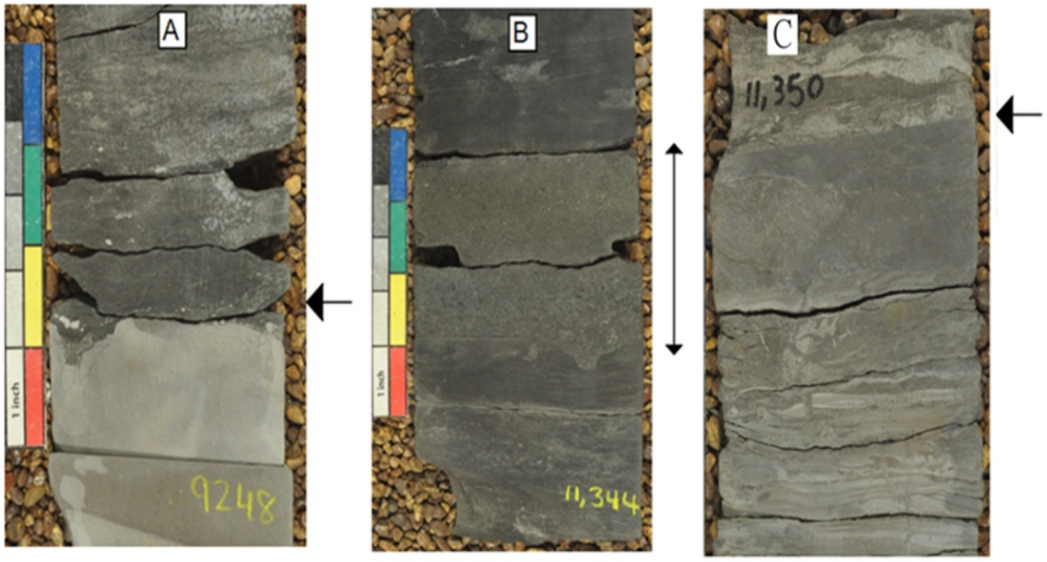

Figure 6-2: Disconformity Surfaces in the Bakken-Three Forks System. (A) contact between the Pronghorn (below) and lower Bakken Formation in a proximal setting, well 19951, (B) distal setting well 19918; and (C) the Pronghorn (above) and the Three Forks in well 19918.

6.1 Core Description and Lithofacies Identification

A stratum or layer is a body of rock different from those above and below by variations in physical properties and/or composition with boundaries between adjacent layers recognizable as either sharp or gradational (Pettijohn et al., 1987). Strata could be laminated (<10 mm) or bedded (>10 mm) with commonly used modifiers such as thinly bedded or thick beds still in use. Stratification is a key feature of all sedimentary rocks. The habit of these strata boundaries and the diagnostic features of the material in between

are the bases for core description. Core descriptions provide a summary of major features seen within individual sections with emphasis on sedimentary structures.

6.1.1 Three Forks Silt

The Three Forks silt is defined to include Member 5 and the rest of the upper Three Forks which consist of Member 6 and the Pronghorn Member of the Bakken Formation where present (Fig. 6-3). The reason for grouping these strata is the fact that only a few cores examined have Member 5, Member 6, or the Pronghorn Member. In other words, members 5 and 6 are rare in core. Also, the strata between the lower Bakken and Member 4 of the Three Forks are thin compared to the rest of the Three Forks. Thus, grouping them together makes it easier for mapping purposes (Fig. 6-4).

The upper Three Forks consists mainly of silty, light grey brown dolomite and slightly limy shale that constitute Member 6 and may include a portion of slightly burrowed dolomitic siltstone that marks the start of the Pronghorn Member. The complete Pronghorn as defined by LeFever (2011) includes rocks between the unconformity at the top of Member 5 and the lower Bakken shale and constitute, from bottom to top, a burrowed basal sandstone, a medium brown dolomitic mudstone with hummocky cross-stratification, a brachiopod bearing lime mudstone, and dark grey limestone.

Member 6 consists of dolomite; light brown to tan, grayish brown; may be sucrosic, some microcrystalline to cryptocrystalline, very silty in part, friable to firm with poor visible porosity and disseminated pyrite. Member 6 is commonly interbedded in part with bluish-green shale. Member 5 forms the first marker bed (bench) of the Three Forks as observed

on the gamma ray log and is the thinnest Member of the Three Forks with an average thickness between 4 m (13 ft). Three lithologies commonly occur in cores of this Member: (1) a well sorted mixture of very fine to fine-grained tan and light to dark grey dolo-

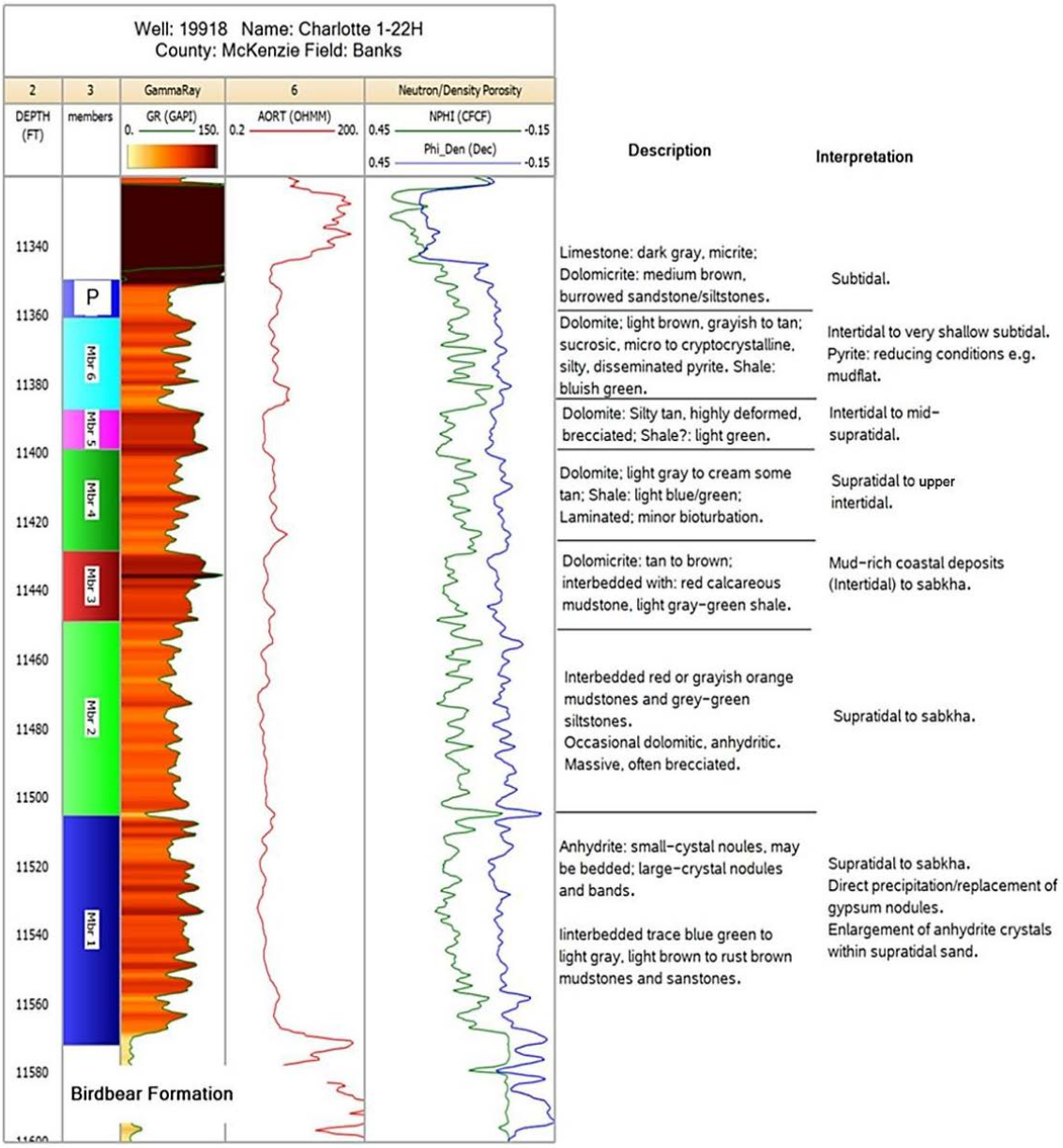

Figure 6-3: Typical Well Log Responses for the Three Forks Formation. Six members (from bottom to top) and the Pronghorn Member of the Bakken (P) with corresponding depositional environments.

mitic siltstone; (2) a poorly sorted to brecciated (Fig. 6-5), silty to sandy, greenish-grey to pale yellowish grey dolomite; and (3) highly deformed grey-green shale and tan colored dolomitic mudstone from top to bottom. Together, these sediments represent a change in depositional environments from shallow intertidal to supratidal.

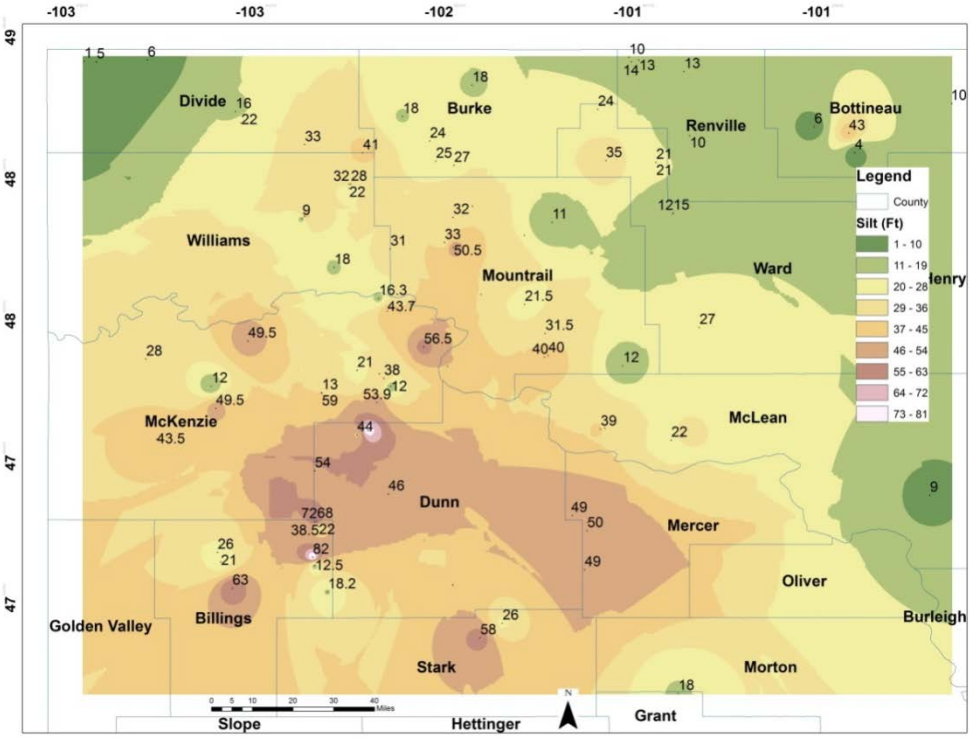

Figure 6-4: Isopach Map of the Silt Portion of the Three Forks Formation. The silt portion includes the strata between Member 4 and the lower Bakken Member.

6.1.2 Member 4

Lithologically Member 4 is very similar to Member 5, consisting of slightly deformed, brecciated in parts, intercalated light to dark blue/green shales and light grey to cream (some tan) dolo-mudstones at the top that continues with periodic occurrences of even to wavy laminations and terminates with moderately deformed and brecciated sediments at its base. Like Member 5, Member 4 is dominated by microcrystalline to cryptocrystalline

textures with poor visible porosity.

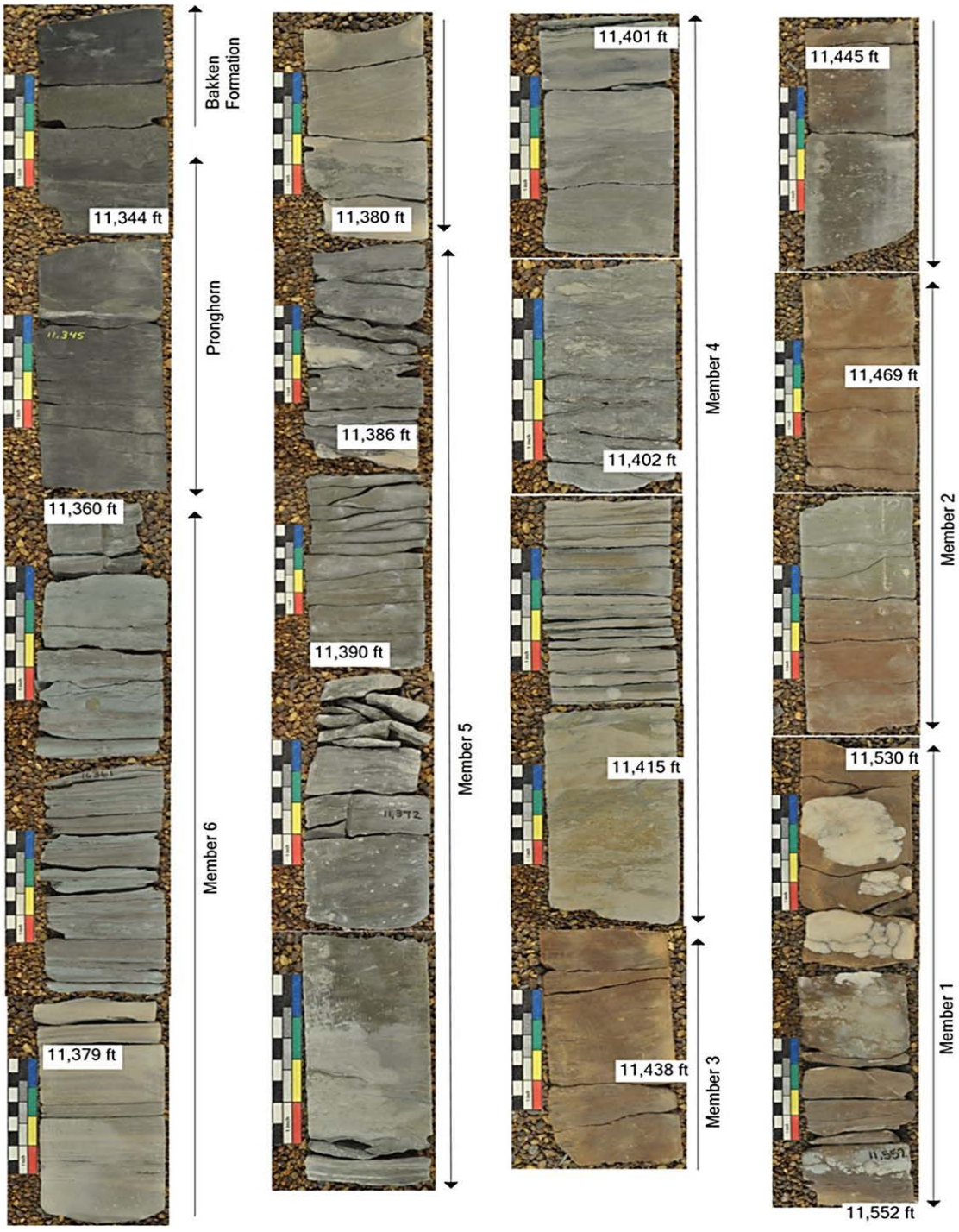

Figure 6-5: Slabbed Core of the Three Forks Formation in the Charlotte 1-22H Well Showing All Members. Stratigraphic depth increases from left to right and from top to bottom.

Member 4 sits on the second marker bed (second bench) of the Three Forks Formation and is present in all cores examined. Its thickness varies slightly throughout the studied sections ranging from about 6 m (20 ft) to 18 m (60 ft) (Fig. 6-6). Recognizable sedimentary structures include cross-laminations: flaser bedding, parallel lamination, climbing ripples, soft-sediment deformation and minor burrowing. The lower contact between Member 4 and Member 3 is conformable throughout the study area although it appears as a sharp contact on logs.

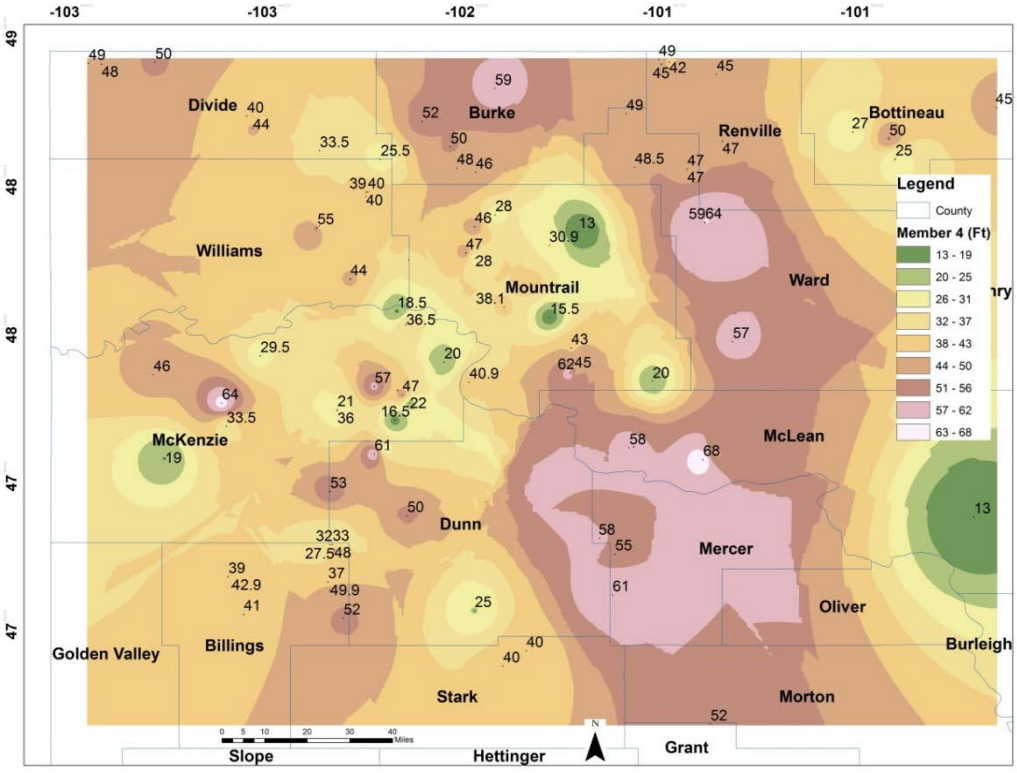

Figure 6-6: Isopach Map of Member 4 of the Three Forks Formation.

6.1.3 Member 3

The thickness of this Member ranges from 6 to 9 m (20 to 30 ft) as shown in Figure 6-4. Since its contacts with Member 4 above and Member 2 below are both gradational, the

lithology of Member 3 falls between dark grey-green, slightly deformed and brecciated (in part) dolomite rich shales; interbedded with tan to brown dolomite, weakly oxidized moderate yellow to light brown silty to sandy calcareous mudstone and light grey-green shale with very poor visible porosity. These rocks are generally structureless or contain slight, wispy laminae and may be poorly sorted and anhydritic towards Member 2. The isopach map of this Member is shown in Figure 6-7.

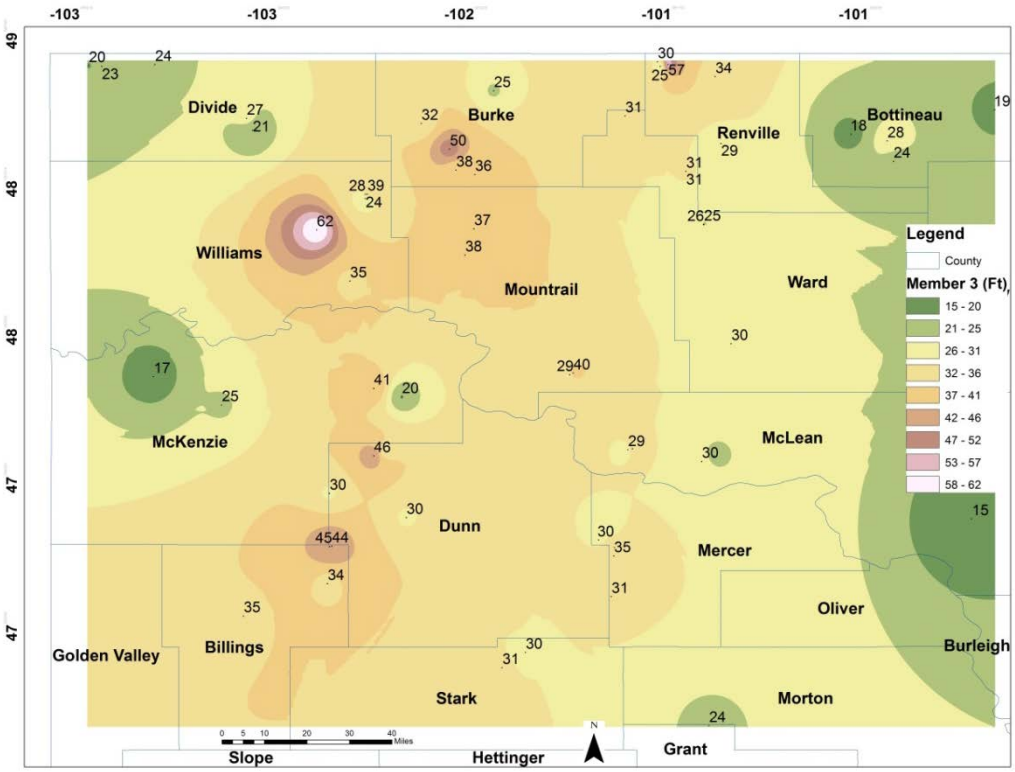

Figure 6-7: Isopach Map of Member 3 of the Three Forks Formation.

6.1.4 Member 2

As mentioned above, the contact between Member 3 and 2 is gradational. Member 2 is third marker bed (third bench) and is the most extensive member with an average thickness of over 15 m (50 ft) (Fig. 6-8).

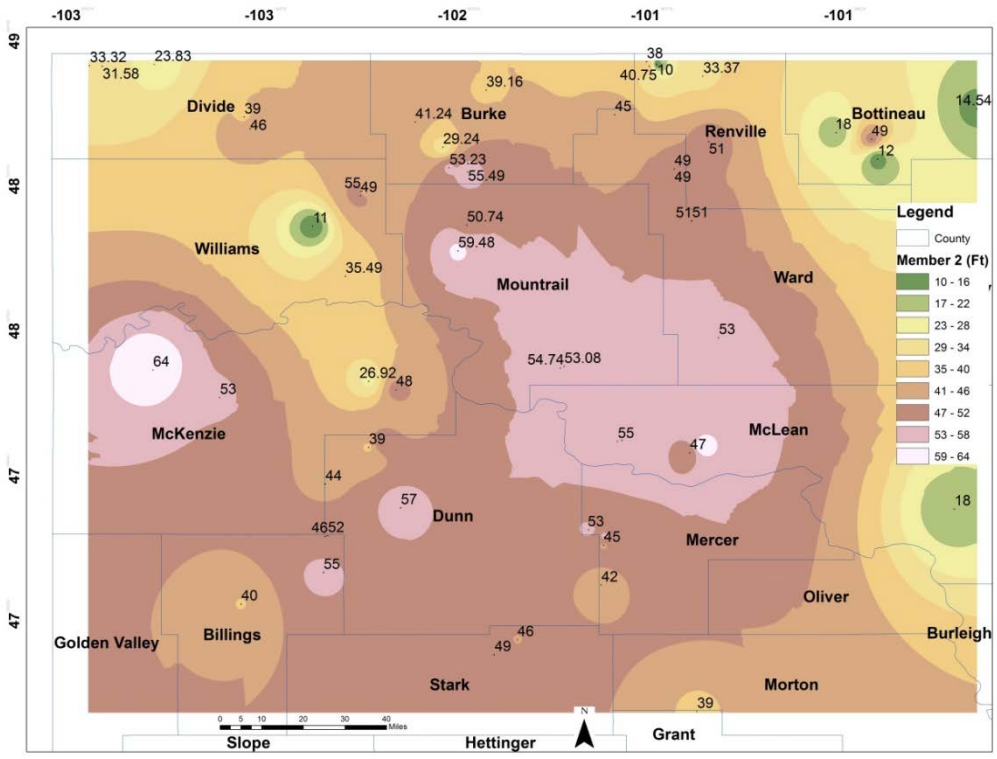

Figure 6-8: Isopach map of Member 2 of the Three Forks Formation.

Member 2 consists predominantly of two lithologies: grey-green shales, occasionally dolomitic; interbedded with oxidized dolo-mudstones whose color varies from grayish orange to dark brown (or red) with sporadic appearances of various forms of anhydrite. Sedimentary structures are scares but minor burrowing and soft sediment deformation is locally observed. Anhydrite may be white to creamy, micro to cryptocrystalline, nodular (chicken-wire), but mostly bedded.

6.1.5 Member 1

Member 1 is commonly represented by a progression from medium tan, rust brown to dark red sandstone beds intermixed with light grey, to trace blue green, light brown mudstones. Generally the sediments are moderately dolomitic and characterized by

deformation and extremely diverse microbreccias of both dolo-mudstones and anhydrite with poor intergranular porosity. The different forms of anhydrite identified include: (1) distorted, nodular, bedded, and nodular mosaic; (2) nodular mosaic or chicken-wire; and massive anhydrite. Some examples of these different structural forms of anhydrite present in Member 1 and Member 2, and the brecciated nature of these sediments are shown (Fig. 6-9). Primary sedimentary structures are less obvious as in Member 2 probably due to the high degree of deformation. These breccias are interpreted as polygenetic, formed either by erosion and redeposition of irregular fragments of earlier formed dolomite during weak synsedimentary processes or a direct response to stress such as tectonic, physical deformation, neomorphism, or dolomitization (Wanless, 1977). The isopach map of Member 1 is presented as Figure 6-10.

Based on information gathered from core description, lithofacies are defined to be meaningful, predictable, and capable using their distinguishing characteristics. Five main lithofacies from top to bottom have been recognized in the Three Forks Formation at the core-scale (Fig. 6-11). The following discussion describes these different facies and representative samples of each facies are selected for thin section analysis, XRD, SEM, and Rock-Eval. Locations where samples were taken are shown in the Figure 7-5.

6.1.6 Lithofacies 1: Silty Dolomite

The rocks belonging to this lithofacies consists mainly of very fine to fined grained beds and very thin, siltstone laminations of dolo-mudstone. The color is a mixture of light to dark grey intermixed with very pale orange to grayish yellow lime mud (Fig. 6-11A). Disseminated pyrite and bedding-plane partings (probably enlarged by stress relief) are

common but stylolites occur less frequently. The typical bed thickness is 1.5 cm to 6 cm

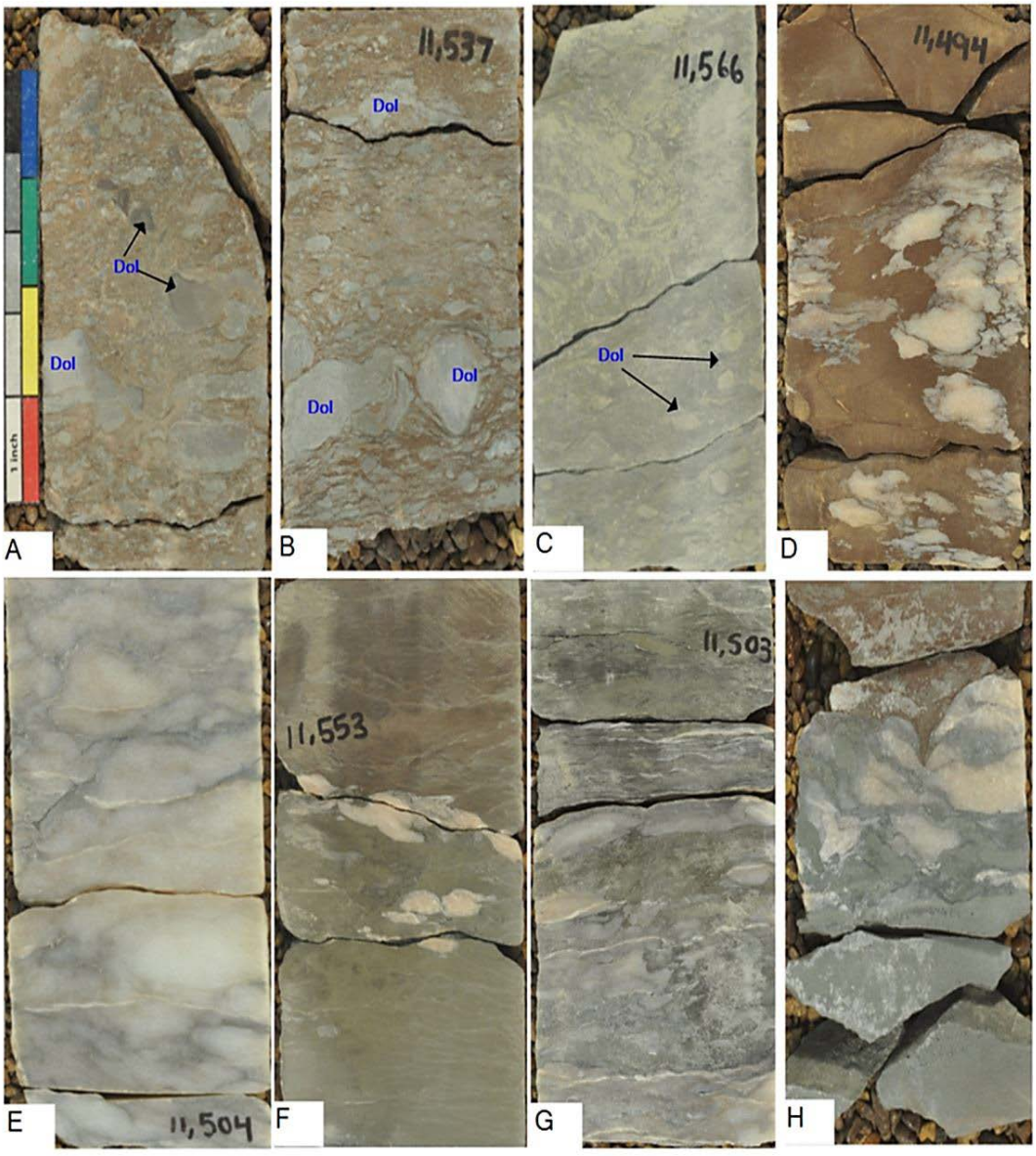

Figure 6-9: Slabbed Core Photographs of Breccia and Anhydrite Occurrence in Member 1 and Member 2 from Well 19918. (A) Large brecciated dolomite fragments; and (B) subangular to rounded, poorly sorted and deformed dolomite fragments surrounded by a finely recrystallized iron-rich matrix; (C) irregularly shaped dolomite fragments in a greenish shale matrix; (D) chicken-wire or nodular mosaic anhydrite; (E) massive anhydrite; (F) distorted nodular anhydrite; (G) distorted bedded nodular anhydrites; (H) distorted nodular mosaic anhydrite, generated by a replacement of an earlier gypsum crystal and addition of sulphate from pore waters causing expansion of the sabkha sediments and the formation of folds.

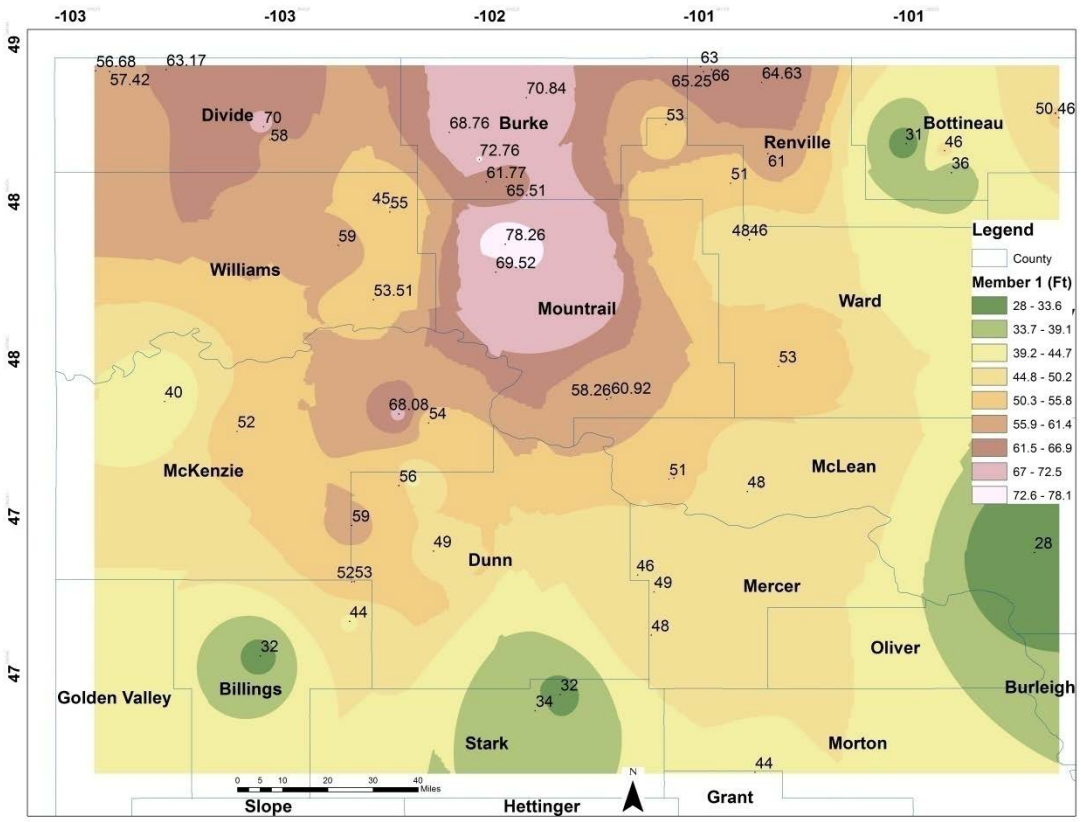

Figure 6-10: Isopach Map of Member 1 of the Three Forks Formation

(0.5 in to 2 in) while laminations are only a few millimeters thick. This facies may be massive or slightly cross-laminated and may display evidence of slight bioturbation.

6.1.7 Lithofacies 2: Intraclastic Blue-grey Dolomite

This lithofacies is recognized as the grayish-blue green to pale yellowish grey colored silty to sandy dolomite of the Three Forks Formation (Fig. 6-11B). The main characteristics are the mottled, intraclastic to lightly brecciated textures. Intraclasts usually include irregularly-shaped sand-sized grains of dolomitic composition (in the top and middle members) and anhydrite (mostly in the lower members). Locally, syneresis or sub-aqueous shrinkage cracks and minor desiccation cracks are present.

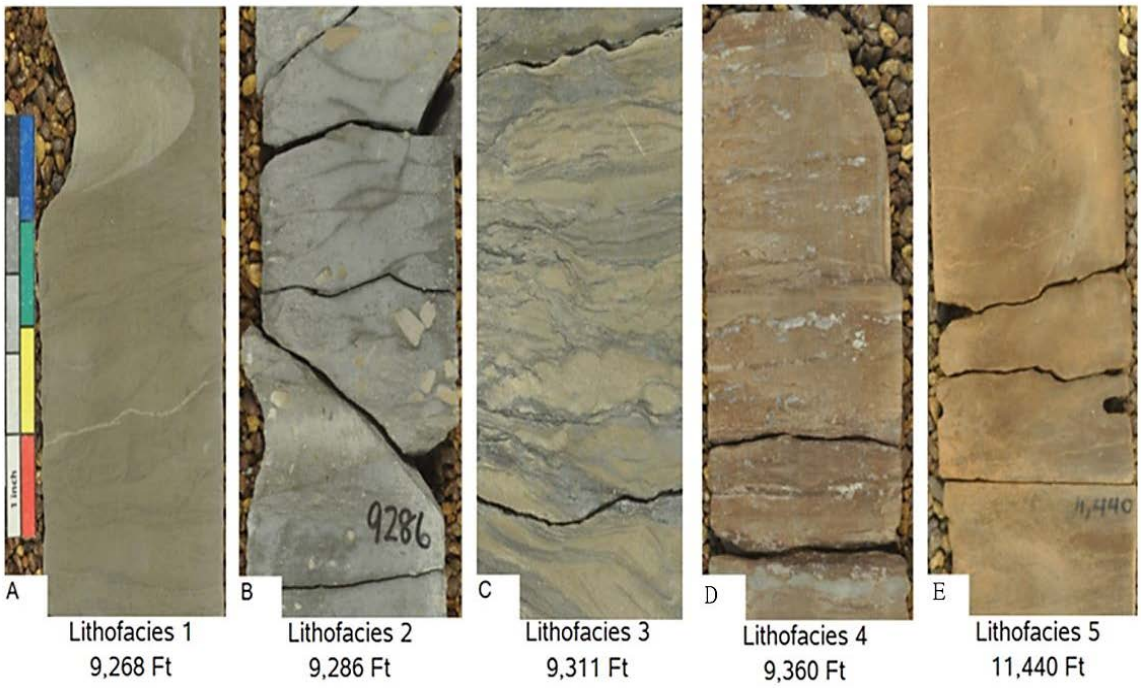

Figure 6-11: Identified Lithofacies in the Three Forks Formation. Samples from Lithofacies 1 to Lithofacies 4 are selected from well 19951 while Lithofacies 5 is from well 19918.

Overall, this lithofacies appears blocky with less obvious sedimentary structures such as cross-lamination and interbedding. Similar to Lithofacies 1, pyrite crystals are disseminated locally with microcrystalline, micro-sucrosic in part with trace intercrystalline porosity.

6.1.8 Lithofacies 3: Boudinage Dolomicrite

This lithofacies consists of interlaminated, interbedded dark grayish-green shale and light tan to olive grey silty dolomite with a typical asymmetric boudinage structure (Fig. 6-11C). These cylinder-like structures of strongly deformed or disrupted layers develop as a response to bulk extension along the enveloping surfaces or layer-normal compression (Mandala et al., 2000). Similar to Berwick's (2008) Facies C, brecciation and intense soft

sediment deformation makes identification of primary and secondary structures very difficult. Breccias are subangular to irregular with sizes between 2 cm (0.79 in) and 6 cm (2.36 in). This facies is the most extensive and is present in all studied cores and in all members.

6.1.9 Lithofacies 4: Highly Oxidized Dolo-mudstone

This lithofacies consists mainly of highly oxidized dark brown to medium tan silty to sandy dolomitic mudstone. This lithofacies is mostly occurs in the lower members and often associated with bedded or nodular anhydrite. Overall, this lithofacies is less deformed with a massive appearance in hand specimen. Anhydrite nodules within this facies range between 0.2-10.0 cm (0.079 - 3.9 in) in diameter (Fig. 6-11D).

6.1.10 Lithofacies 5: Slightly Oxidized Dolo-mudstone

This lithofacies consists of fine to very fine weakly oxidized moderate yellow to light brown siltstone. Even though this facies is quite similar to lithofacies 4, it is mostly massive and interbedded with green shales or claystones (Fig. 6-11E) is common. This facies was not observed in all cores studied.

CHAPTER 7

LITHO-STRATIGRAPHIC MODELLING

The fine grained lithologies of the Three Forks Formation make it difficult to interpret the primary and secondary depositional features by simple observation. As a result, different aspect of the lithology such as rock type, porosity, and grain density are identified by resorting to petrophysical modeling. The Three Forks Formation can well be characterized with four basic logs: gamma ray, formation density, neutron, and sonic logs. Since each log measures a different physical property, when used in combination or in tandem they provide a much better understanding of both pore volume and mineral composition.

As a rule, shales are distinguishable from dolomites by their higher gamma ray values. In monomineralic rocks such as pure limestones, the porosity logs should provide comparable results and the two porosity traces of the density and neutron log for example should represent a common reading. However, the presence of varied proportions of shale and dolomite in the Three Forks induce much higher neutron porosity than the density porosity (Fig. 6-3). Using these concepts, a generalized pattern of the variation in lithologies within the Three Forks is achievable. Therefore, detailed analysis is blotted out by compositional variation within the formation, affecting log readings. Some of these variations can be resolved by applying cross-plotting techniques.

Figure 7-1 summarizes the frequency neutron-density and sonic-density porosity

crossplots of the Three Forks Formation. The reference lines represent theoretical compositions of pure dolomite (DOL), limestone (LS) and sandstone (SS) over a range of porosity. Therefore, for a given set of porosity coordinates, the rock composition can be interpreted with reference to its mineralogy and pore volume by interpolating between these references. The nature of the frequency distribution of Three Forks general indicate a wide range of carbonates (dolomite and limestone) with very little of quartz (sandstone) although the precise composition at any specific zone still remains uncertain. Because of this disadvantage of double porosity crossplots, all three porosity logs are usually combined for more explicit evaluation.

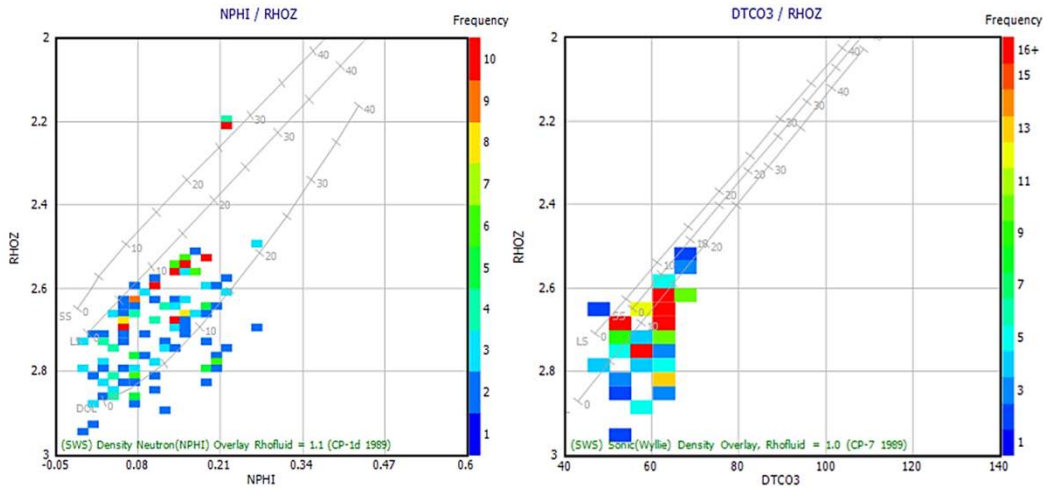

Figure 7-1: Frequency Crossplots for the Three Forks Formation Based on 32 Wells. (Left) Density-neutron (Right) density-sonic.

By combining the density, neutron and sonic logs, the complex lithology of a formation can be decoded with limited uncertainty. A *litho-porosity* or M-N crossplot is traditionally used to present this information in 2-dimensions. To obtain an M-N crossplot, the

slope (M) of the sonic-density crossplot is plotted against the slope (N) of the neutron-density crossplot with each rock mineral represented by a unique point (independent of porosity) which depends exclusively on the matrix and fluid characteristics of the rock at any specific level. Consequently, the M–N crossplot of log data symbolizes a continuous map of the rock characteristics of the formation. It is concluded from Figure 7-2, that the lithology of the Three Forks Formation is mainly within the compositional triangle of calcite-dolomite-anhydrite with shales.

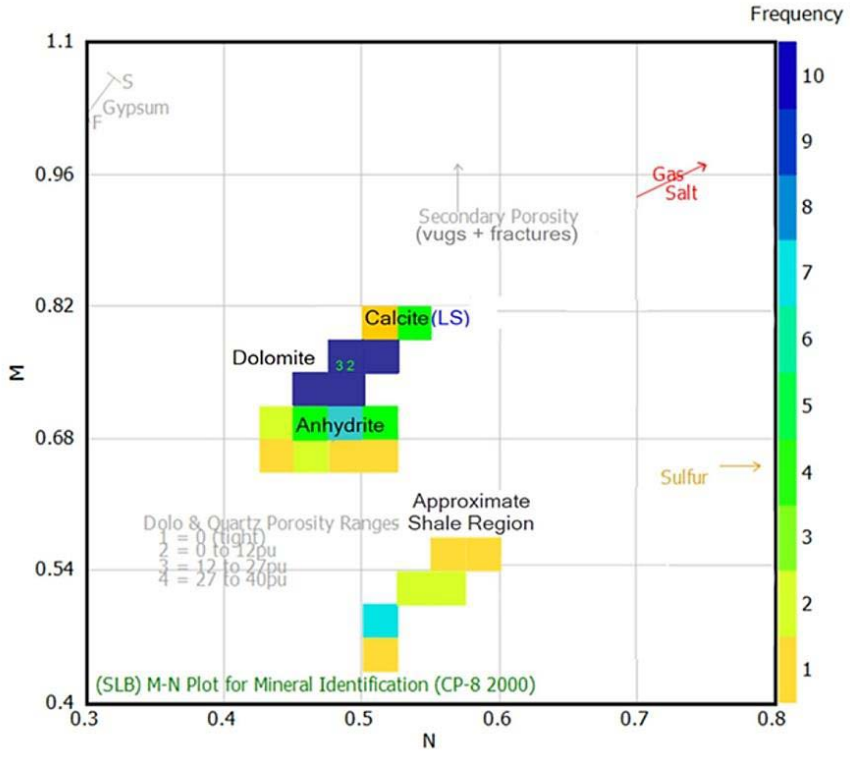

Figure 7-2: M-N Crossplot for the Three Forks Formation Based on 32 Wells.

By duplicating the above process and applying a *probabilistic interpretation* technique, the mineralogy in the multiple reservoir zones of the Three Forks Formation can be resolved. A mineral model is built to describe the main minerals and fluids at any particu-

lar zone of the formation and expressed in vertical profiles of variation. Calibrated with results from XRD and routine core analysis, the main elements included in the models for reservoir rocks of the Three Forks include: porosity, resistivity, and gamma ray logs, calcite, dolomite, anhydrite, clays, quartz, oil, and water. Also, a single mineral model does not sufficiently describe all zones in a well therefore several models are adjusted to give the best possible reconstruction for the depth interval to which it applies. Finally the system of equations is solved to find the most probable result for each layer in the well and presented.

7.1 Statistical Application of Litho-Stratigraphic Modeling

A systematic analysis can be made of patterns and interrelationships of log data by using statistical methods (Bornemann et al., 1982). The set of log measurements at any level in a well constitutes a description of the rock properties at that point. Thus, a well log represents an array of response to these properties. The results acquired from core analysis are based on a small sample size that is considered representative of the formation as a whole. Electrofacies however, will provide bulk information on variations within the formation by representing a series of contiguous zones where log values are basically constant or where change in log values is negligible.

As a consequence, how well separate electrofacies are distinguished depends on our ability to identify these zone boundaries. This is usually achieved by performing some form of multivariate statistical analysis. In addition, electrofacies prediction is used to build a relationship between common logs and lithofacies recognized from core descriptions. This integration thus permits the prediction of lithofacies in uncored wells having

the same set of logs. The following approach is implemented to improve the quality, efficiency and ease interpretation of derived electrofacies:

1. Logs are environmentally corrected for the effects of borehole size, temperature and mud salinity,
2. The logs are depth-matched to core depths,
3. To reduce the error associated with tool calibration and malfunction, each log is normalized for each principal component (PC). The normalized data are then condensed by PCA,
4. The main PCs are segmented (zoned) and consolidated using cluster analysis.

7.2 Model Implementation

Results of the combined PCA for wells 17067, 16841 and 12033 belonging to 'set 1' are given in Table7-1. Results for well 15591(reference well) are also provided. Notice that the first two principal components account for about and 77% of the total variability in both cases. A c*luster randomness plot* (Fig. 7-3A) is used to decide at which level adding another cluster gives more information or noise. The higher the value the more structured the data. The resulting dendrogram illustrating the clustered hierarchies for set 1 is shown in Fig. 7-3B. Finally, the electrofacies for these wells are correlated and presented in Figure 7-4.

7.3 Model Validation

The objective for electrofacies determination is to build a quantitative relationship between common logs and lithofacies recognized by core data which can subsequently improve our understanding of log-facies from wells without core information. The Three

Forks is subdivided into four major electrofacies which have well defined log characteristics.

Table 7-1: Summary of PCA Conducted on Wells 17067, 16841, 12033, and the Reference Well (19951).

Input Curves: RT, GR, DT, NPHI, RHOZ			
Well:		**17067, 16841, 12033**	**19951**
Output Curves	**Names**	**% Variability**	
1st	PC1	50.18	57.37
2nd	PC2	26.09	19.37
3rd	PC3	15.16	9.99
4th	PC4	8.57	8.38
5th	PC5	0	4.89

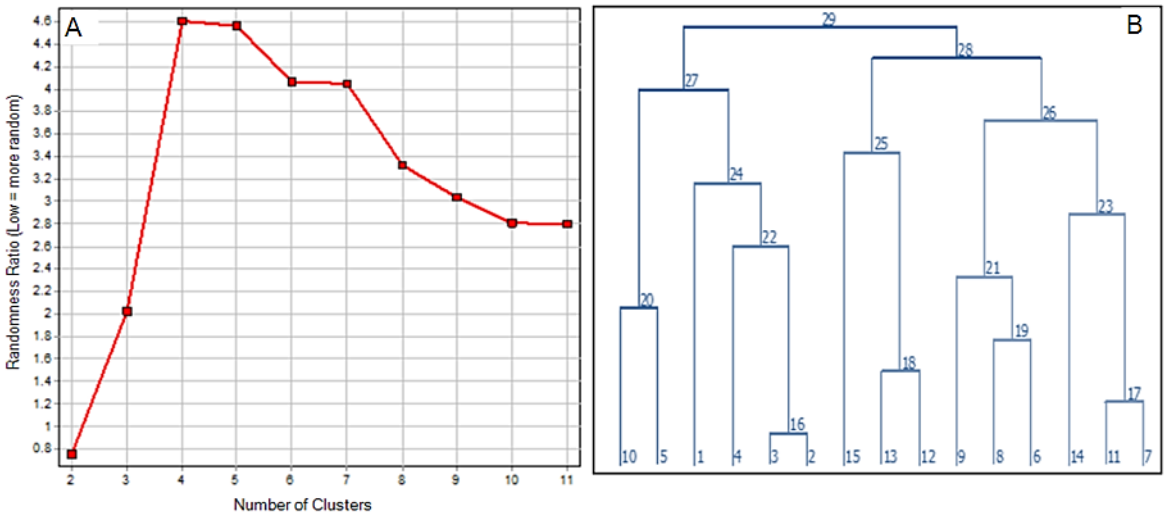

Figure 7-3: Techniques for Litho-stratigraphic Model Validation and Interpretation. (A) Cluster randomness plot for set 1, showing the optimum number of clusters for electrofacies identification, (B) resulting dendrogram for set 1.

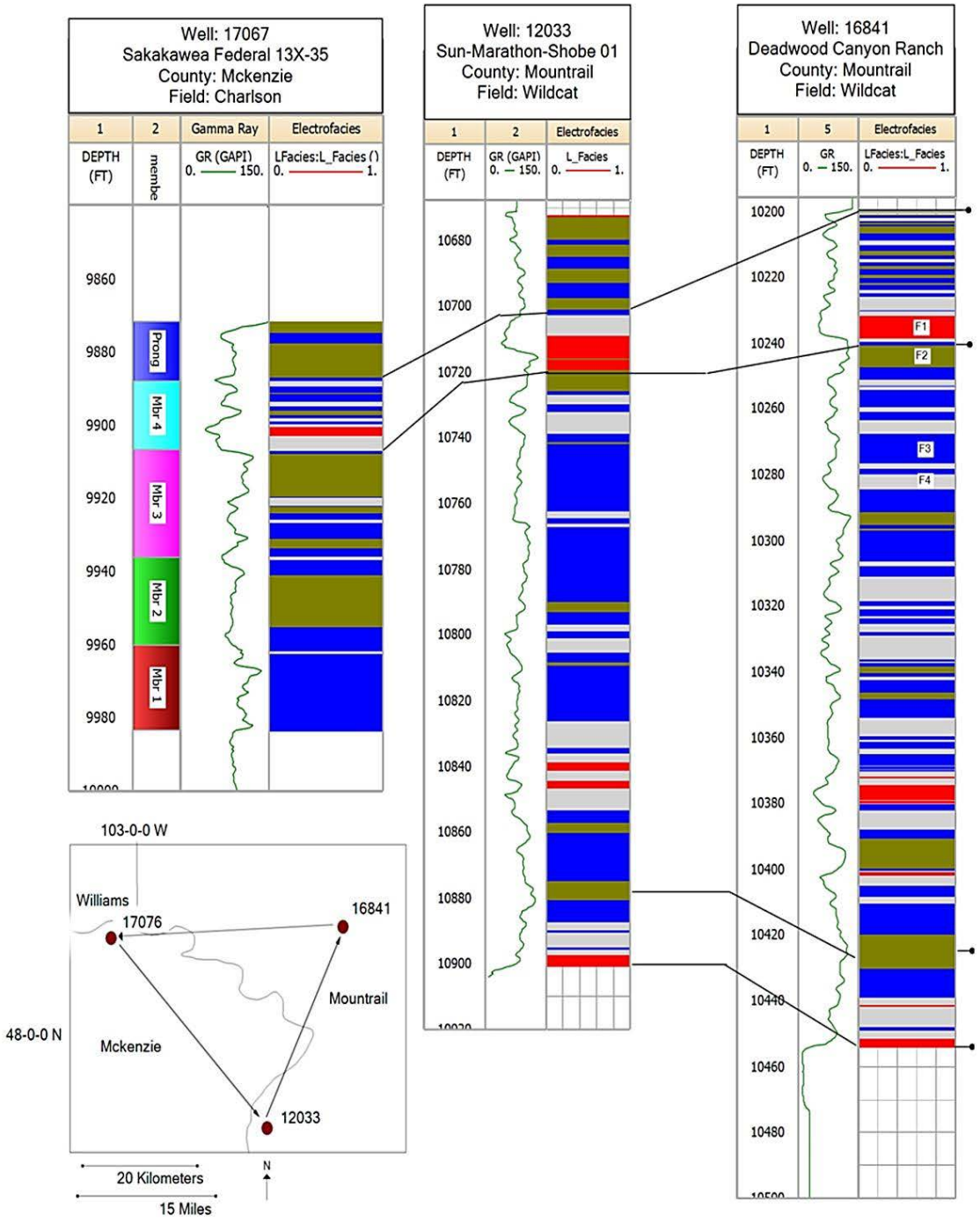

Figure 7-4: Vertical Stacking Pattern and Lateral Correlation of Electrofacies For Wells in Set 1. F1 to F4 are hypothetical facies that can be traced across fields as demonstrated by a few lines. Bottom left, areal distribution of wells within the study area.

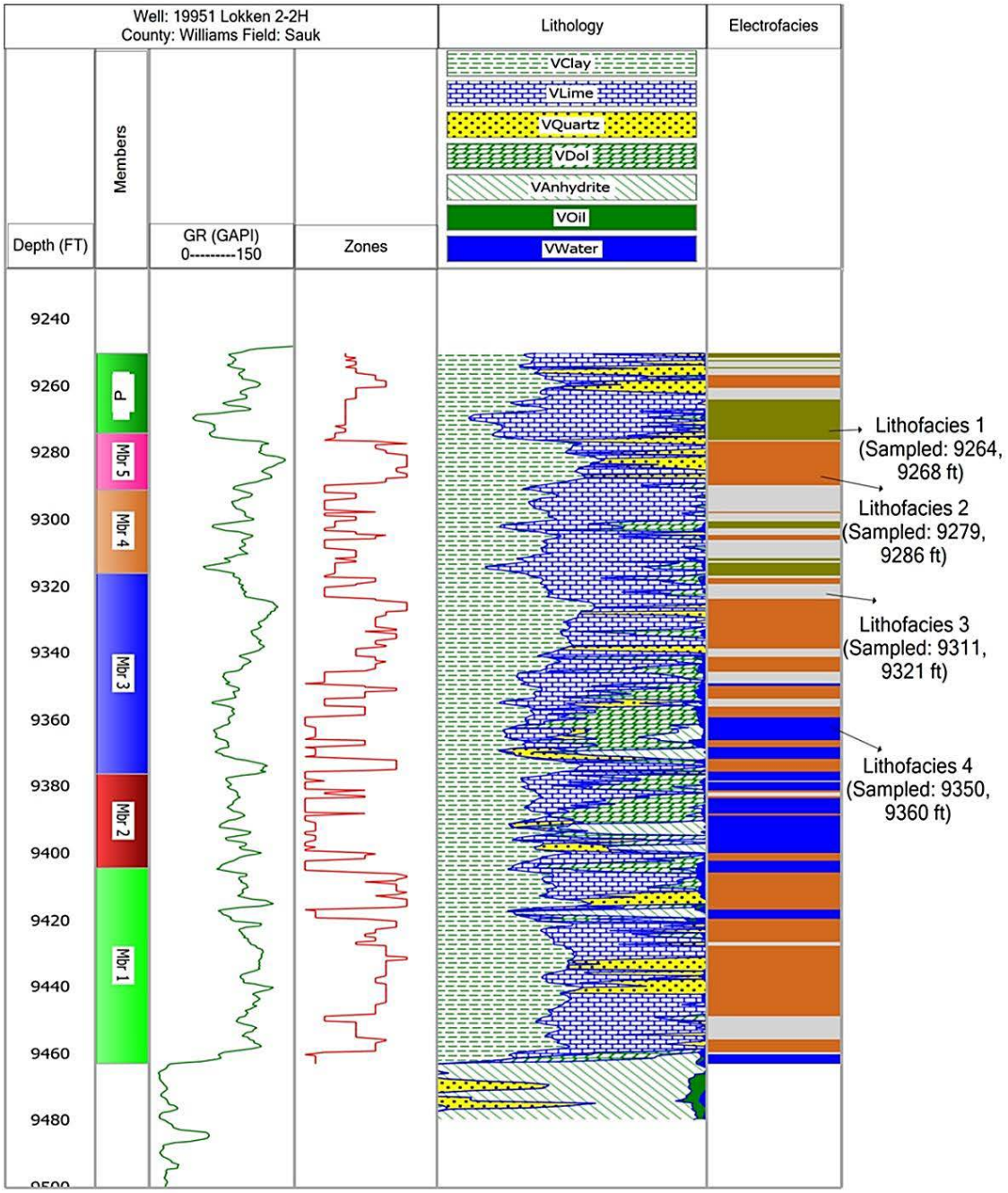

Figure 7-5: Stratigraphic Gamma-Ray and Facies Interpretation of Well 19951 (Sauk Field) Using Statistical Calibration between Log Data and Core Analysis. Sampled depths indicate cored intervals where samples were collected for petrographical and geochemical analyses. The calibration allows facies to be mapped across the Sauk, Wildcat and Charlson fields.

To validate these results, electrofacies are derived for the reference well (19951) following the same approach and compared with results from core description. Figure 7-5 displays the zoned curve for the reference well in track 4, the lithology in track 5 and a perfect match between log-derived facies and core lithofacies in track 6 which strongly validates this procedure.

CHAPTER 8

PETROLOGY

In hand specimens, all samples selected for thin section and SEM petrography, plus combined bulk and clay XRD analysis are classified as silty/sandy dolo-mudstone since they contain minor amounts of coarse silt to very fine lower size sand grains, scattered throughout the samples.

8.1 The Bulk and Clay XRD Results

Results of the combined bulk and clay XRD analysis are presented asTable8-1 while the average percentages of the combined mineralogy are presented as Figure 8-1. The non-clay portions of the samples are dominated by dolomite (56% to 60%) CaMg $(CO_3)_2$ along with lesser quartz (14% to 16%) SiO_2 with minor amounts of potassium feldspar (2% to 3%) $KAlSi_3O_8$ and plagioclase feldspar (1% to 2%) Na $(AlSi_3O_8)$ – Ca $(Al_2Si_2O_8)$, calcite (1% to 2%) $(CaCO_3)$, hematite (trace to 1%) Fe_2O_3, plus trace siderite $(FeCO_3)$.

8.1.1 Type of Clay Mineral

The results of the combined bulk and clay XRD analysis also show that the clay portion consists of illite (14% to 15%) $KAl_2(OH)_2AlSi_3(O,OH)_{10}$, together with chlorite (2% to 4%) $(Mg,Fe)_5Al(AlSi_3)O_{10}(OH)_9$ and kaolinite (3%) $Al_4Si_4O_{10}(OH)_8$. The clay fraction (< 3 μm fraction that best represent finer matrix clays) ranges from 4.85% to 8.73% of the

total weight volume of the samples (Tab. 8-1) and consists of (76% to 86%) clay minerals. The minerals illite, chlorite, and kaolinite occur in all facies in examined. In addition, clay fraction XRD results suggest that Illite is the most abundant clay mineral (50% to 54%), plus lesser amounts of chlorite (10% to 25%) and kaolinite (10% to 12%). The predominant non-clay minerals in the clay fraction are dolomite (6% to 12%), quartz (4% to 8%), siderite (1% to 3%), potassium feldspar (1% to 2%) and plagioclase feldspar (1%), plus hematite (1%; except in facies 1).

The results of the XRD studies include detailed evaluations of the clay minerals and the quantification of the whole rock matrix components. The mineral phases identifiable in the Three Forks include dolomite, clays, quartz, K-feldspar, plagioclase, calcite, hematite, and siderite in other of abundance. A summary of the average bulk and clay mineralogy of all samples is presented as Table 8-1.

The silicates (quartz, K-feldspar, plagioclase, hematite) are of detrital origin while clay minerals are formed as a result of weathering and hydrothermal alteration. Kaolinite is present in all samples and can be directly precipitated from fluids (Buatier et al., 2012). It generally occurs as filling of the pores. However, together with chlorite and illite, theses clay minerals are interpreted as terrigenous weathered or diagenetic products of plagioclase and K-feldspar.

8.2 Thin Section Analysis and Interpretation

Thin section analysis provides qualitative information on the composition, fabric and diagenetic features of geologic samples and is therefore used to evaluate field observa-

tions (core description). To describe grain sizes for the sand grains in the sample, the

Table 8-1: Summary of XRD Analysis.

										← Clays →			
Facies ID	**Type of Analysis**	**Wt. %**	**Qtz**	**Plag**	**K-Feld**	**Cal**	**Dol**	**Hem**	**Sider**	**Kaol**	**Chl**	**Ill**	**Total Clay**
1 Top Member	Bulk Fraction:	91.27	16	2	2	1	65	1	0	2	1	10	13
	Clay Fraction:	8.73	8	1	1	0	12	0	2	12	10	54	76
	Bulk and Clay:	100	15	2	2	1	60	1	TR	3	2	14	19
3 Middle Member	Bulk Fraction:	93.50	17	1	2	1	61	0	0	3	3	12	18
	Clay Fraction:	6.50	8	1	2	0	7	1	3	12	16	50	78
	Bulk and Clay:	100	16	1	2	1	58	TR	TR	3	4	15	22
4 Bottom Member	Bulk Fraction:	95.15	15	2	3	2	58	1	0	3	3	13	19
	Clay Fraction:	4.85	4	1	1	0	6	1	1	10	25	51	86
	Bulk and Clay:	100	14	2	3	2	56	1	TR	3	4	15	22

XRD LEGEND

Bulk Fraction – greater than 3 microns size fraction, Clay Fraction – less than 3 micron size fraction. Bulk and Clay – mathematical recalculation including the bulk and clay fraction representing the whole sample. Total Clay – sum of the clay minerals (may include authigenic and matrix clays plus clays in rock fragments). Musc –Muscovite, Dol – Dolomite, Plag - Plagioclase Feldspar, Hem –Hematite, Ill – Illite, Qtz – Quartz, Kaol – Kaolinite, Sider – Siderite, K-feld - Potassic Feldspar, Cal – Calcite, Tr - Trace; detectable, but not measurable (0 – 1%).

Wentworth (1922) scale is used. In this context of textures rather than composition, the Wentworth scale (Appx.5) classifies all grains with average diameters greater than 2 mm as gravel, those with average diameters between 2 mm and 1/16 mm (62 μm) as sand, and those finer than 62 μm as mud. In this study, the dolomite crystal size is classified by the following size criteria for carbonate authigenic constituents. The carbonate crystal size

ranges are as follows: very fine (4 to 16 µm), fine (16 to 62 µm), medium (62 to 250 µm), coarse (250 to 1000 µm) and very coarse (1000 to 4000 µm). The size of the inter-crystalline pores depends on the crystal size of the host dolomite.

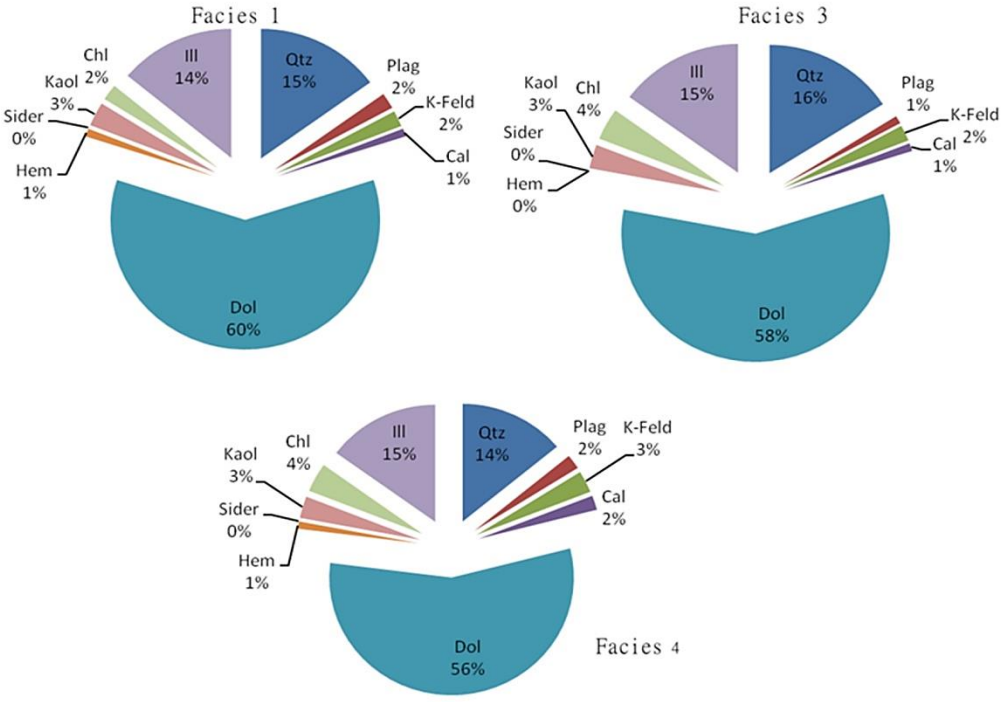

Figure 8-1: Average Percentages of Combined Bulk and Clay Mineralogy of Facies 1(top), 3 (middle) and 4 (bottom) of the Three Forks.

8.2.1 Sample Description

Detailed description of all samples is discussed together in the following sections. Compositionally, the samples consist of dolomite (40% to 57%) and hematite (10% to 37%) along with clays and organics (16% to 20%) and minor to lesser fine silt to very fine upper grained (average: coarse silt to very fine lower) monocrystalline quartz (5% to 11%) with mica flakes (2% to 3%). Trace amounts of feldspar, calcite and pyrite are also

noted (Tab. 8-2). The discrepancy in the amount of clays detected by XRD (Tab. 8-1) and point-counting results (Tab. 8-2) is due to the clays being present in the matrix. Muscovite and biotite flakes and mica in all types of lithoclasts are recorded as illite in a XRD.

Table 8-2: Thin Section Petrographical Summary of 3 Dolomitic samples from Facies 1,3, and 4 of the Three Forks Formation.

Facies ID		**1**	**3**	**4**
Mineralogy	Calcite, Feldspar, Pyrite	TR	TR	TR
	Dolomite	54	57	40
	Quartz	10	11	5
	Mica	3	2	2
	Hematite	13	10	37
	Clay+organic Matter	20	20	16
Total Rock Volume (%)		**100**	**100**	**100**
Detrital Grains	Quartz	10	11	5
	Feldspar	TR	TR	TR
	Mica	3	2	2
	Total	13	13	7
Matrix	Clay and Organics	20	20	16
	Total	20	20	16
Pore Filling Cement	Calcite	TR	TR	TR
	3rd/Euhedral dolomite	1	1	3
	2nd/Subhedral dolomite	35	26	29
	1st/Anhedral dolomite	10	13	TR
	Fe-Dolomite	8	17	8
	Hematite	13	10	37
	Total	67	67	77
Replacement	Pyrite	TR	TR	TR
Total Rock Volume (%)		**100**	**100**	**100**
Crystal Texture (Matrix)		Anh	Anh	-
Crystal Texture (Cement)		Anh-Euh	Anh-Euh	Anh-Euh
Original Texture		Mudstone	Mudstone	Mudstone
Porosity	Intercrystalline	2	2	TR
	Micro-vuggy	1	-	-
	Total TS Porosity (%)	3	2	TR
Reservoir Quality		P-M	P-M	P

Legend: Euh – Euhedral, Anh – Anhedral, G-Good, M-Moderate, P-Poor, TR-Trace.

Additionally XRD analysis does not differentiate between detrital clays, authigenic clays

and clays derived from disintegrated rock fragments that may be accumulated in the clay fraction of the XRD samples. The amounts of quartz detected by XRD (Tab. 8-1) are different than their respective point-counted values (Tab. 8-2). Furthermore, the dolomite content in XRD is higher than in thin section. These could be a product of heterogeneous distribution; non-crystalline carbonaceous debris skews percentage, plus possible micro-dolomite in the detrital matrix.

The provenance and diagenetic history of sedimentary rocks and dolomite in particular can readily be recognized if the textures (as defined by the crystal shape, size, orientation, and packing) that develop as a result of the dynamics of nucleation and growth are well~~s~~ understood (Friedman, 1965; Gregg and Sibley, 1984). The most common form of dolomitization involves the replacement of shallow-water limestones by supersaturated solutions with respect to Mg^{2+} ions. Dolomite is a metastable mineral (Ahr, 1998). With continued influx of the dolomitising solution, early formed dolomite crystals can be partially or completely replaced by later more stable crystal phases during burial and metamorphism. As dolomite cement forms overgrowths on the earlier formed dolomite crystals, it becomes difficult to trace its depositional conditions. The end result is in a series of distinctive textures that form in a sequential manner with progressive degrees of dolomitization, consisting of matrix-selective replacement, over-dolomitization (precipitation of dolomite cement on earlier formed dolomite), formation of vugs and molds, emplacement of calcium sulphate (in the case of seawater dolomitization), and in the case of advanced burial, formation of saddle dolomite (Machel, 2004).

The descriptive classification system of Gregg and Sibley (1987) is used to interpret

dolomite textures because of its genetic implications and because it only requires information on crystal size distribution and shape of the crystal boundary. Crystal size distributions are classified as 'unimodal' or 'polymodal', while crystal shapes are classified as 'planar-e' (euhedral), 'planar-s' (subhedral), and 'nonplanar-a' (anhedral) (Fig. 8-2). As mentioned above, dolomite crystal sizes are controlled by the available nucleation sites and the rates of crystal growth. A unimodal size distributions usually indicated a single nucleation event on a unimodal substrate while polymodal sizes can originate from multiple nucleation events on a unimodal or polymodal substrate or as a result of differential nucleation on an originally polymodal substrate. Also, early-formed dolomites tend to be more finely crystalline than burial-stage dolomites (Bahremandi et al., 2013).

Usually, the first stage of dolomitization involves selective matrix replacement by heterogeneous nucleation, a process by which $CaCO_3$ acts as substrate on which dolomite nuclei are formed and may continue to grow (Walton, 1969; Berner, 1980, p. 95). Matrix replacement is promoted by factors such as: (a) the matrix consists of thermodynamically metastable carbonates (aragonite and/or high-Mg-calcite), which have higher solubilities than low-Mg-calcite; (b) the matrix has much smaller grain sizes and, thus, a large number of available active sites for nucleation and (c) the matrix has a higher permeability than the larger, more massive particles or cements (Gregg and Sibley, 1987). As these nuclei continue to grow, they form a loose mesh of microscopic crystals that ultimately coalesce to an interconnected mosaic. At low supersaturation and/or temperatures, this produces faceted crystals and planar interfaces. At high supersaturations, or above a "critical roughening temperature," growth occurs by random addition of atoms

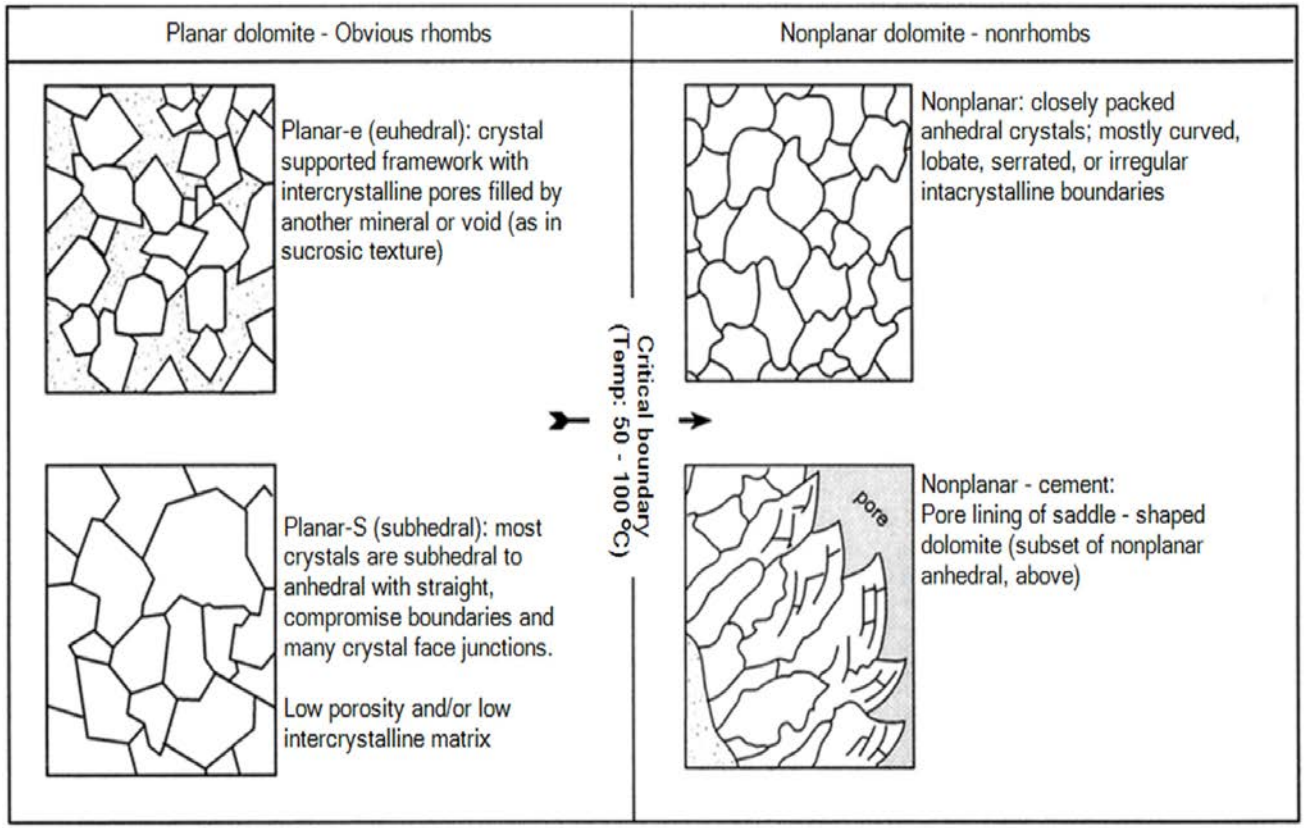

Figure 8-2: Common Dolomite Textures Stressing the Effect of Temperature on the Style of Dolomite Development. Modified from Gregg and Sibley, 1984; Gregg and Sibley, 1987.

to the crystal surface and non-planar fabrics are favored. Calculation of this critical roughening temperature requires knowledge of the enthalpy of fusion and the enthalpy of dissolution, neither of which is known for dolomite (Lewis 1975; Weeks and Gilmer 1979; Human et al. 1981; Jetten et al. 1984). However, the critical roughening temperature for dolomite has been estimated to lie between 50 and 100 °C (Gregg and Sibley 1984, 1986).

As mentioned above dolomite is the major mineralogical component in these samples. Original or precursor textures could not be identified by the white card technique (Folks, 1987) because pervasive dolomitization and recrystallization have totally obliterated the original depositional texture. Nonetheless, minor amounts of dolo-micrite are observed associated with the scattered clasts (Figs. 8-3 to 8-5). Following these guidelines, three main stages of dolomitization observed in these samples. These stages are:

8.2.1.1 Dolomite Type 1 (Very Fine Crystalline Dolomite)

The first stage or dolomite type 1 (labeled Dol 1 on Figs.) is classified as very fine to fine crystalline (< 62.5μm) generally anhedral dolomite consisting of tightly to loosely interlocked crystals embedded in matrix material. This dolomite 1 has replaced the matrix of the original rock. Intercrystalline porosity occurs in poor amounts in dolomite type 1.

8.2.1.2 Dolomite Type 2 (medium crystalline dolomite)

The second stage of dolomitization (labeled Dol 2 on Figures) which replaces earlier stage of dolomite and most abundant (range between 26% and 35%). is a late stage phase (2^{nd} generation dolomite) is generally better formed subhedral to euhedral dolomite

rhombs (> 62.5μm or medium crystalline) that cement the larger intercrystalline pores. Overall, the second dolomite consisting of a mosaic of interlocking rhombohedral crystals (Figs. 8-3 to 8-5; 8-6, 8-8, 8-9) that are highly pervasive and replace all calcareous fabric types (cements, allochem and orthochem) equally.

Also, this dolomite occasionally presents a sugary texture (sucrosic) that may have resulted to a certain degree from the bulk volume shrinkage that accompanies calcite replacement by dolomite or from the dissolution of residual calcite during the final stages of dolomitization (Selley, 2000). This late stage dolomite in general is present throughout and is well formed, larger and probably precipitates at a slower rate and later in time than the first stage dolomite. The intercrystalline porosity in these samples is mostly formed within this dolomite.

In places, these dolomite rhombs have clay inclusions, which suggest that the clay was incorporated in the crystals at the time of their precipitation. Most of the coarsely crystalline dolomites have straight boundaries. The fabric could be described as planar subhedral. However, the medium and fine crystalline dolomites have fewer straight boundaries and the fabric is non-planar anhedral.

8.2.1.3 Dolomite Type 3 (coarse crystalline dolomite)

Rare medium to coarsely crystalline euhedral dolomite cements are considered the last stage dolomite cement (i.e. 3rd generation of dolomite cement) and are present mostly in the porous areas (labeled Dol 3 on Figs.) consist of dolomite (1% to 3%) rhombs (often with saddle morphology) that cement the intercrystalline pores (Figs. 8-4, 8-5). A planar

fabric where most of the crystals are euhedral is usually only seen in dolomites which have intercrystalline pore space. Both the 2nd and 3rd generation dolomites are occasionally turquoise stained (due to carbonate staining) indicating some dolomite rich in iron (Figs. 8-3, 8-4)

8.2.1.4 Matrix material

Matrix material (16% to 20%) consists of detrital clays, organic matter, plus dolo-micrite. Clay and organics generally occur as lenses of shale (Fig. 8-4B: L9), elongated clasts (Fig. 8-3B; 8-4A/B) and also arises as compacted into the interstitial pores. Detrital clays locally coat some of the sand grains in the samples (Fig. 8-3B; 8-4C/D). This is also supported by XRD analysis (Tab. 8-1). In addition, dolo-micrite appears along with the clasts (Fig. 8-3D, 8-4B). Later stage dolomite locally replaces the matrix material. Hematite is finely disseminated in the matrix. XRD analysis detects minor amounts of calcite (1% to 2%), which is possibly associated with the matrix as microcrystalline calcite.

8.2.1.5 Other Components

Sand grains are mainly monocrystalline quartz, where the overall grain size ranges from fine silt to very fine upper grained. The subangular to subrounded, poorly sorted monocrystalline quartz is generally inclusion free grain. Mica appears as tiny muscovite (Figs. 8-3A to C, 8-5A, 8-5D) flacks that occur in minor quantities. Some mica flakes were observed slightly compacted between the dolomite or quartz grains. Trace amounts of potassium feldspar (Fig. 8-3B) grains were also observed locally, which are slightly more angular than the quartz. Hematite (iron rich oxidizing product) is a late stage diagenetic

overprint, occurs as micro-blebs, plus replaces the clay matrix as well as the dolomite rhombs (Figs. 8-3A to C, 8-5A to D).

Hematite also occurs as the pore occluding diagenetic mineral. Facies 4 and Facies 1 contain abundant hematite cement (Tab. 8-2). Figures 8-5A to D illustrate ferroan and non-ferroan subhedral and rare euhedral dolomite rhombs, in addition to quartz grains that are surrounded by deep red hematite cement. Hematite mainly derived from the breakdown of unstable iron-bearing heavy minerals and even small amounts of such cement can yield strongly pigmented redbed sediment. Pyrite is the other non-carbonate diagenetic mineral that locally replaces dolomite cement. Finely disseminated pyrite micro-framboids were also observed in detrital clay matrix. Pyrite is present in trace amounts. These three lithofacies are characterized as follows:

8.2.2 Lithofacies 1

This facies has a thin section porosity of 3%. At moderate magnification view, this facies consist of very fine to medium crystalline dolomite rhombs (Fig. 8-3A). Monocrystalline quartz (Qtz) and trace amounts of feldspar grains are the detrital sand grains that are scattered throughout. Overall, the replacement dolomite is dominated by anhedral to subhedral interlocking very fine crystalline dolomite rhombs (Dol 1), with substantial amounts of recrystallized fine crystalline 2nd stage dolomite (Dol 2) and lesser late stage void rimming fine to medium crystalline euhedral rhombs.

The original carbonate texture would have been mudstone. The mineralogy of this sample is dominated by dolomite (54%) with moderate amounts of matrix material (20%),

hematite (13%) and quartz (10%) along with minor muscovite (Mica, 3%), plus trace calcite, feldspar and pyrite. The matrix is comprised of mixture of very fine crystalline carbonate, pyritized organic matter and clays. Moderate hematite (Hem) and trace pyrite are the other non-carbonate diagenetic minerals that substantially occlude pores or replace the dolomite cements. Visible porosity is represented by small size isolated minor intercrystalline (2%; Ixl) and micro-vuggy (1%) pores.

The intercrystalline porosity is mainly obstructed by the precipitation of anhedral to subhedral dolomite rhombs, plus hematite cements. Minor non-effective microporosity occurs in the "matrix" dolomite. Micro-fracturing is common in this facies and may probably be the results of unloading joints (Fig. 8-3A). Figures 8-3B to D are high, very high to extremely high magnification images highlighting pervasive dolomitization (Dol 1 and Dol 2) which appears to have created all the visible small isolated intercrystalline pores (Ixl).

Dolomite rhombs are in places slightly ferroan. Hematite (Hem) as the pore occluding diagenetic cement also occurs. Hematite also occurs as micro-blebs and replaces the clay matrix and the anhedral-subhedral dolomite rhombs. Hematite in sedimentary rocks forms through chemical precipitation, or through chemical replacement of earlier sedimentary rocks. It is also widely accepted that hematite is the final weathering product of pyrite or siderite formed during the last diagenetic step (Goss, 1987). Monocrystalline quartz also occurs as a detrital sand grain, scattered throughout the matrix (Fig.8-3B).

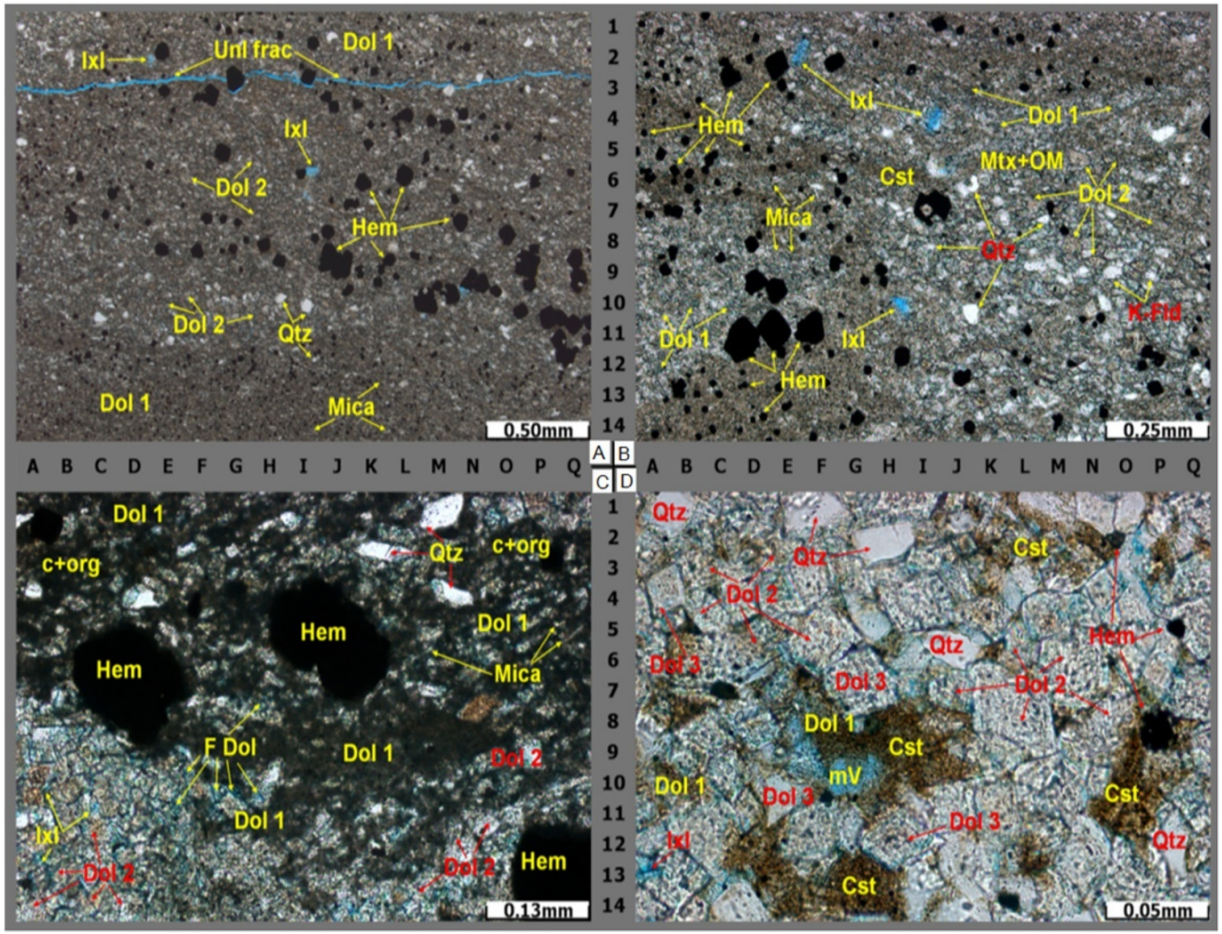

Figure 8-3: Thin Section Photomicrographs of Lithofacies 1. Highlighting: (A) x50ppl, 1st (Dol 1) and 2nd (Dol 2) generation replacement dolomite, associated minerals and unloading fracture (Unl frac) and intercrystalline porosity Ix1, (B) x100ppl, scattered monocrystalline quartz (Qtz), (C) x200ppl Hematite (Hem) occluding pores and as micro-blebs replacing Dol 1 and Dol 2 rhombs, (D) x400ppl, dissolution micro-vugs (mV) and clast rimmed with Dol 3 crystals.

Minor amounts of clasts (Cst; clay and organics generally occur as lenses of shale and elongated clasts) occur as permeability barriers while Figure 8-3C shows the distribution of slightly brownish clay and organics (c+org) which is compacted into the interstitial pores. Scattered distributed muscovite (Mica) along with potassium feldspar (K-Fld) occur as accessory minerals. Note in Figure 8-3D dissolution micro-vugs (mV) rimmed with euhedral dolomite crystals (Dol 3).

8.2.3 Lithofacies 3

At moderate magnification, Facies 3 consist of very fine to medium crystalline dolomite rhombs. Also, monocrystalline quartz and feldspar grains are the detrital sand grains (Fig. 8-4A). The high, very high to extremely high magnification images (Fig. 8-4B to D) highlight the replacement dolomite in this facies, dominated by ferroan (F Dol 1: pale-deep turquoise) and non-ferroan (Dol 1) anhedral to subhedral interlocking anhedral (Dol 1) to subhedral (Dol 2) dolomite rhombs. Similar to Facies 1, pervasive dolomitization must have created all the visible intercrystalline pores. The 3rd generation void rimming euhedral rhombs is locally observed in the porous areas and occludes the intercrystalline pores and limits the interconnectivity (Fig. 8-4C/D; Dol 3).The original carbonate texture would have been mudstone.

Generally, minor amounts of clasts (Cst) occur as lenses of shale and elongated clasts that may act as permeability barriers but occasionally are locally replaced by subhedral dolomite. The distribution of slightly greenish clay plus organics, compacted into the interstitial pores can be seen in the second and third views. Scattered monocrystalline quartz is the detrital sand grain and it is very fine lower in size (on average). Hematite

also occurs as micro-blebs and replaces the clay matrix and the dolomite cement.

The mineralogy of this sample is dominated by dolomite (57%) with moderate amounts of matrix material (20%), quartz (11%) and hematite (10%) along with minor muscovite (Mica, 2%), plus trace calcite, feldspar and pyrite. A major distinguishing characteristic of this facies is the presence of matrix partings (c+org) which are comprised of mixture of very fine crystalline carbonate, pyritized organic matter and clays (Fig. 8-4A). Trace pyrite is the other non-carbonate diagenetic mineral that locally occludes pores or replaces the dolomite cements.

Visible porosity is represented by small isolated minor intercrystalline (2%) pores. The intercrystalline porosity is mainly obstructed by the precipitation of anhedral to subhedral dolomite rhombs and subordinately by hematite cements. Minor non-effective microporosity occurs in the “matrix” dolomite. Also, clay and organics (Cst) generally occur as lenses of shale and elongated clasts (Fig. 8-4A/ B).

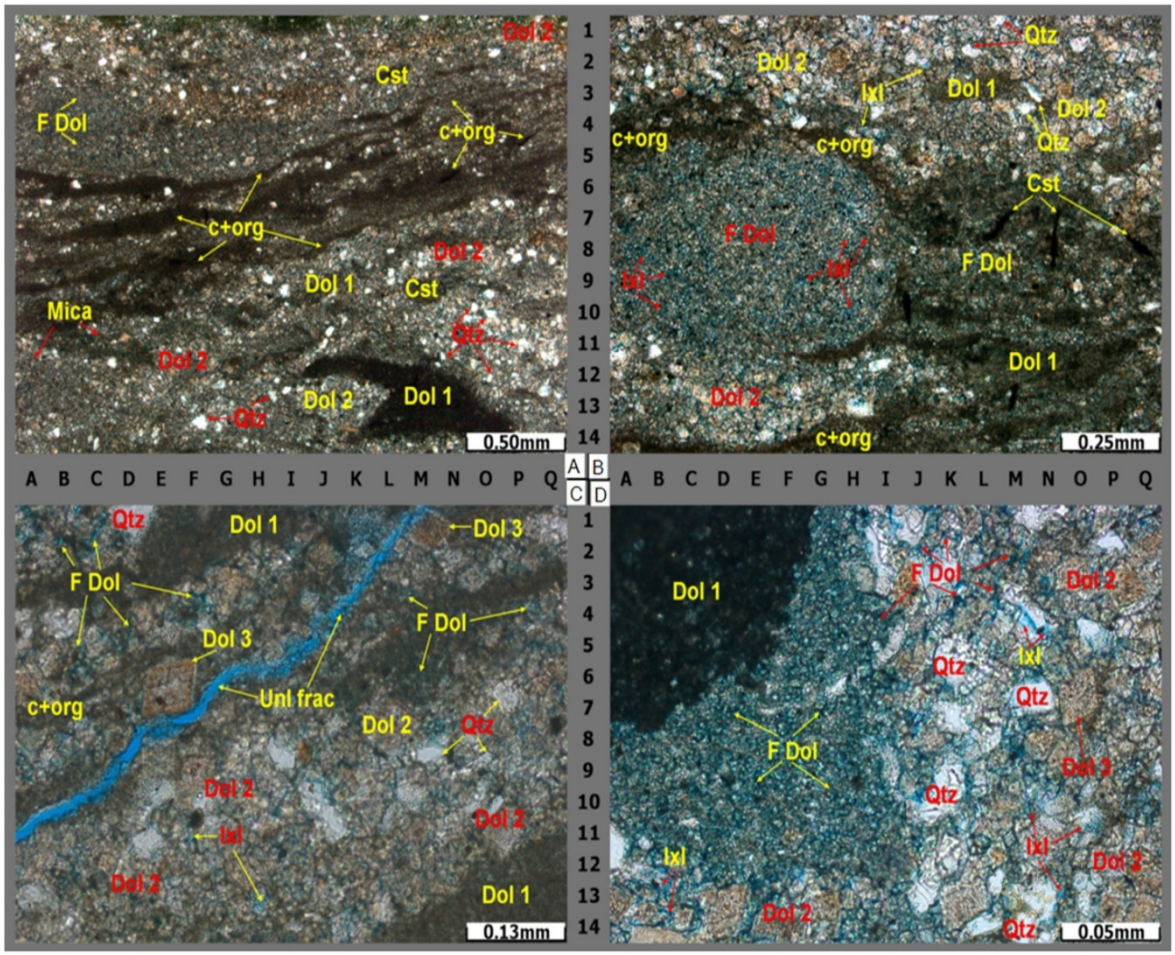

Figure 8-4: Thin Section Photomicrographs of Lithofacies 3. Highlighting: (A) x50ppl, ferroan (F Dol), non-ferroan dolomites, associated minerals, and matrix partings (c+org) (B) x100ppl, anhedral (Dol 1) to subhedral (Dol 2) dolomite, (C) x200ppl, unloading fracture (Unl frac), associated minerals and intercrystalline pores (Ixl), (D) x400ppl, clearly showing the 1st (Dol 1), 2nd (Dol 2), and 3rd (Dol 3) generation dolomites that occludes the intercrystalline pores and limits the interconnectivity.

8.2.4 Lithofacies 4

This facies is characterized by very fine to medium crystalline dolomite rhombs surrounded by deep red hematite cement (Fig. 8-5). Similar to facies 1 and 3, detrital sand grains consist of monocrystalline quartz and trace amounts of feldspar but the replacement dolomite is dominated by ferroan and non-ferroan, subhedral recrystallized 2nd stage dolomite (Fig. 8-5A). This facies also contains more hematite than the others. Mineralogically, this facies is dominated by dolomite (40%) and hematite (37%) cements with moderate amounts of matrix material (16%) and lesser quartz (5%) along with minor muscovite (2%), plus trace calcite, feldspar and pyrite. The original carbonate texture would have been mudstone.

The matrix (c+org) is comprised of mixture of very fine crystalline carbonate, pyritized organic matter and clays. Hematite is the main non-carbonate diagenetic mineral, which completely occludes pores or substantially replaces the dolomite cements. Visible porosity is represented by trace amount of intercrystalline pores. Minor non-effective microporosity occurs in the "matrix" dolomite.

Figures 8-5B to D are extremely high magnification thin section images highlighting the dominant ferroan and non-ferroan subhedral (F Dol and Dol 2) and euhedral (Dol 3) dolomite rhombs as well as quartz (Qtz) grains surrounded by deep red hematite cement. Hematite mainly derived from the breakdown of unstable iron-bearing heavy minerals and even small amounts of such cement can yield strongly pigmented redbed sediment.

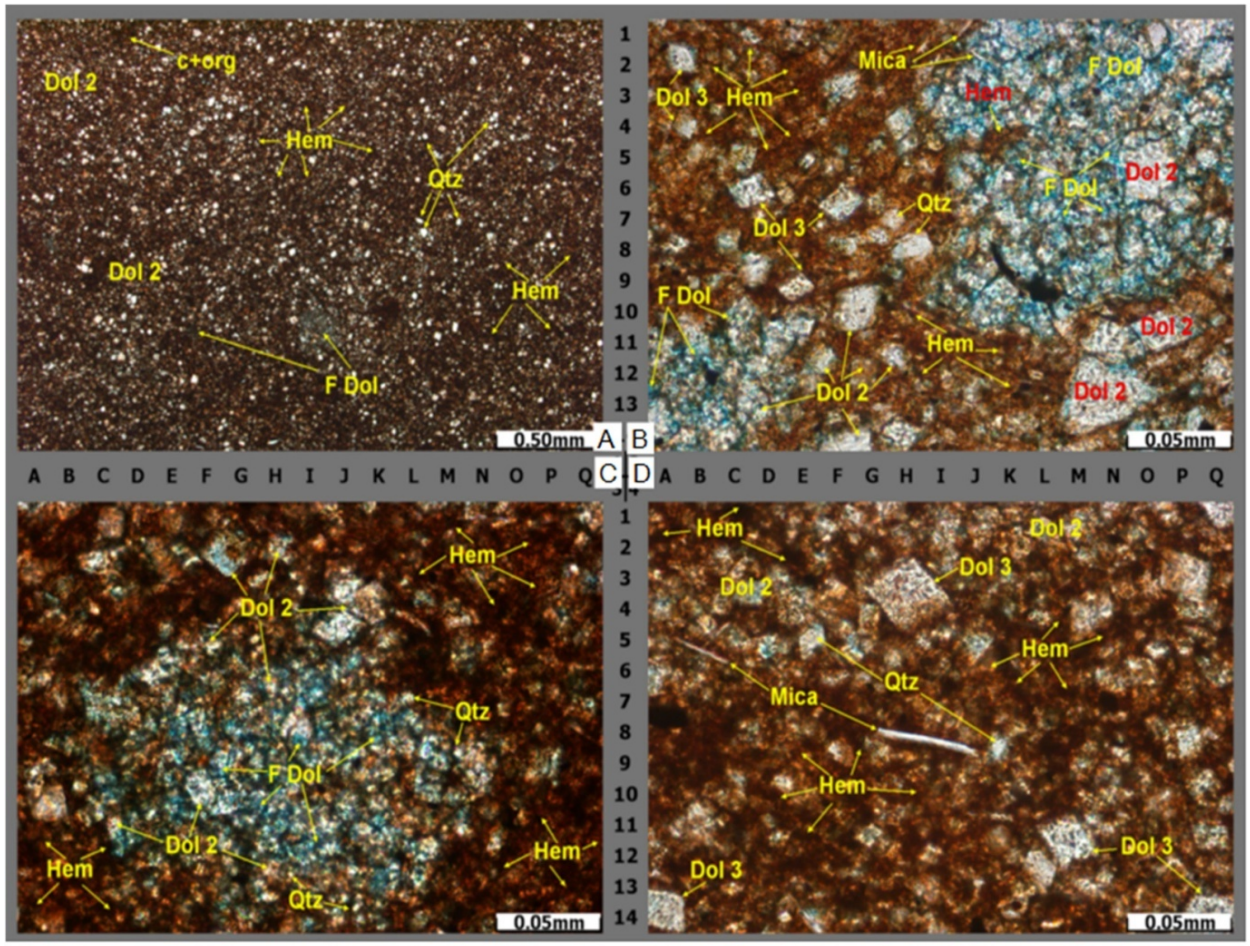

Figure 8-5: Thin Section Photomicrographs of Lithofacies 4. Highlighting: (A) x50ppl, very fine to medium crystalline dolomite rhombs surrounded by deep red hematite cement plus minor amounts of clasts, (B,C,D) x400ppl, ferroan and non-ferroan subhedral (F Dol, Dol 2) and euhedral (Dol 3) dolomite rhombs and monocrystalline quartz.

In addition, minor amounts of clasts generally occur as lenses of shale. In this facies hematite cement appears to have occluded all the intercrystalline pore spaces. Long, thin detrital grains of mica (Figs. 8-5B/D) are also present.

8.3 SEM Analysis and Interpretation

The main purpose of performing an SEM analysis in this study is to obtained three-dimensional data on the occurrence, distribution, abundance, and mode of crystallinity of authigenic hematite in these Three Forks facies. SEM examination of broken fresh rock surfaces of all samples reveals that authigenic hematite is mostly small, round or disc shaped and coarsely crystalline (Figs. 8-6, 8-8, 8-9). The coarser hematite occurs either as irregular platy crystals or as well-developed hexagonal crystals (similar in appearance to kaolinite crystals) and is dark red to black in reflected light.

In SEM, dolomite shows abraded subhedral, rhombic termination. Scattered hematite inclusions within these abraded dolomite rhombs and detrital quartz grains are responsible for the reddish-brown coloration of these facies. The presence of abraded dolomite crystals is strongly suggestive of re-sedimentation (Chilingar et al., 1967). In fact, hematite inclusions within abraded dolomite rhombs are very common. Pervasive dolomitization appears to have created all the visible small intercrystalline pores (Figs. 8-6A: E4, N5; 8-6B: F6, E3; 8-6C: J12; 8-6D: L4; 8-8A/C). The intercrystalline porosity is mainly obstructed by the precipitation of anhedral to subhedral dolomite rhombs and subordinately by hematite cements. Thin section study supports the identification.

The energy dispersive x-ray (EDX) is used to provide elemental identification and

quantitative compositional information. The EDX spectra (Figs.8-7, 8-10) illustrating dolomite and hematite cement shows that the major elements of hematite is primarily iron (Fe) and that of dolomite as (Ca, Mg). Additional elements present in the EDX spectrum (Si, Al, and K) are due to detection of adjacent quartz grains, plus illite and kaolinite clays. In the EDX spectra the peak height of Mg relative to Ca is substantially reduced. This could be partly due to substitution of Fe for Mg in the dolomite lattice and attenuation of Mg in the EDX system. Figure 8-6B: N8 illustrates minute probable detrital illite coating quartz grains. Note in the illite EDX spectrum (Fig. 8-7), the relative peak height of K is more than that of Al.

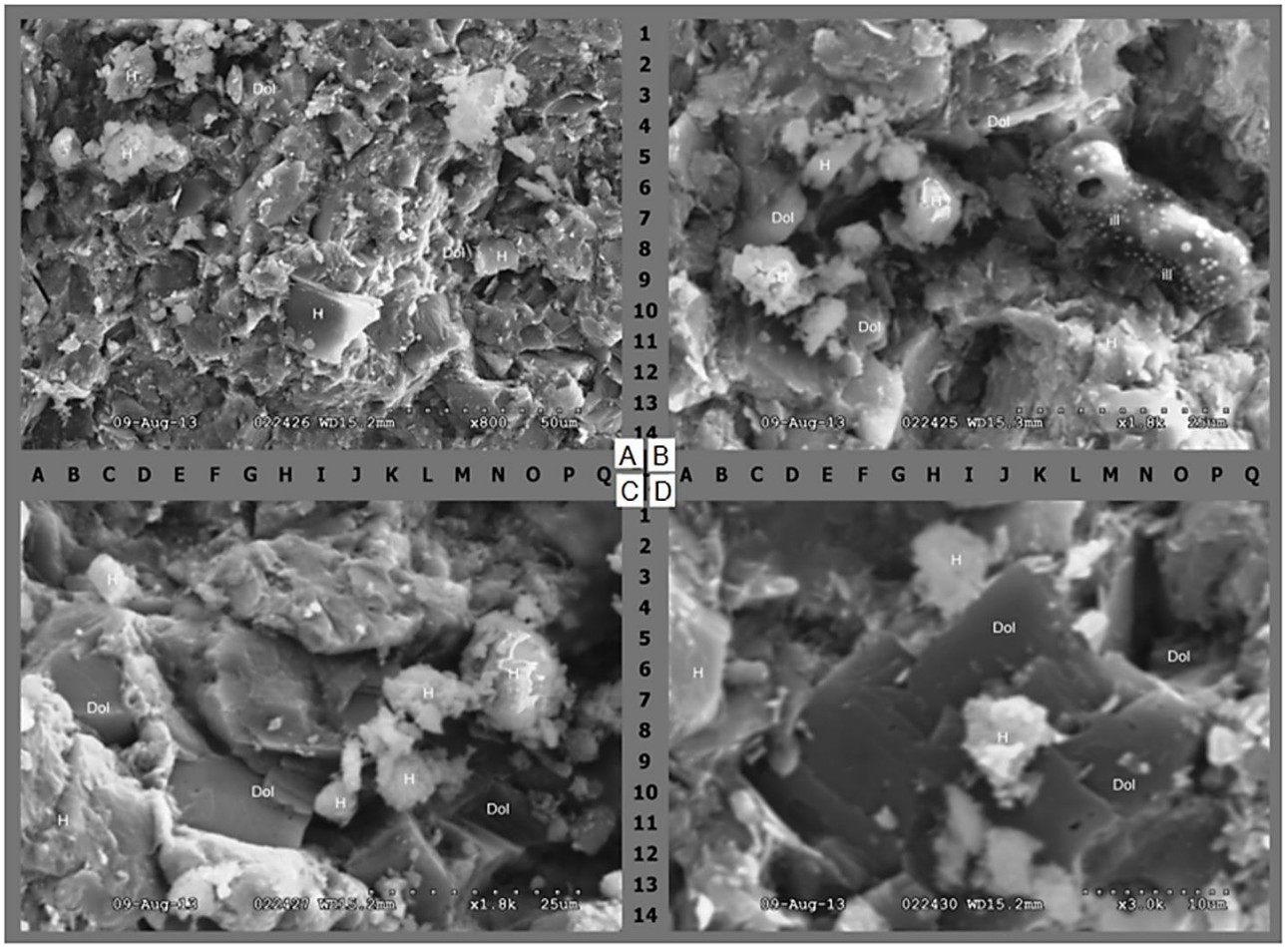

Figure 8-6: SEM Photomicrographs of Lithofacies 1.The distribution of very fine to medium crystalline dolomite rhombs (Dol) and small, round or disc shaped coarsely crystalline hematite cements (H) at: (A) moderate, x800; (B,C) high, x1800; (D) very high, x3000 magnifications. Pervasive dolomitization appears to have created all the visible small intercrystalline pores (A: E4, N5; B: F6, E3; C: J12; D: L3). In B, note minute probable detrital illite coating quartz grain (N6, P9).

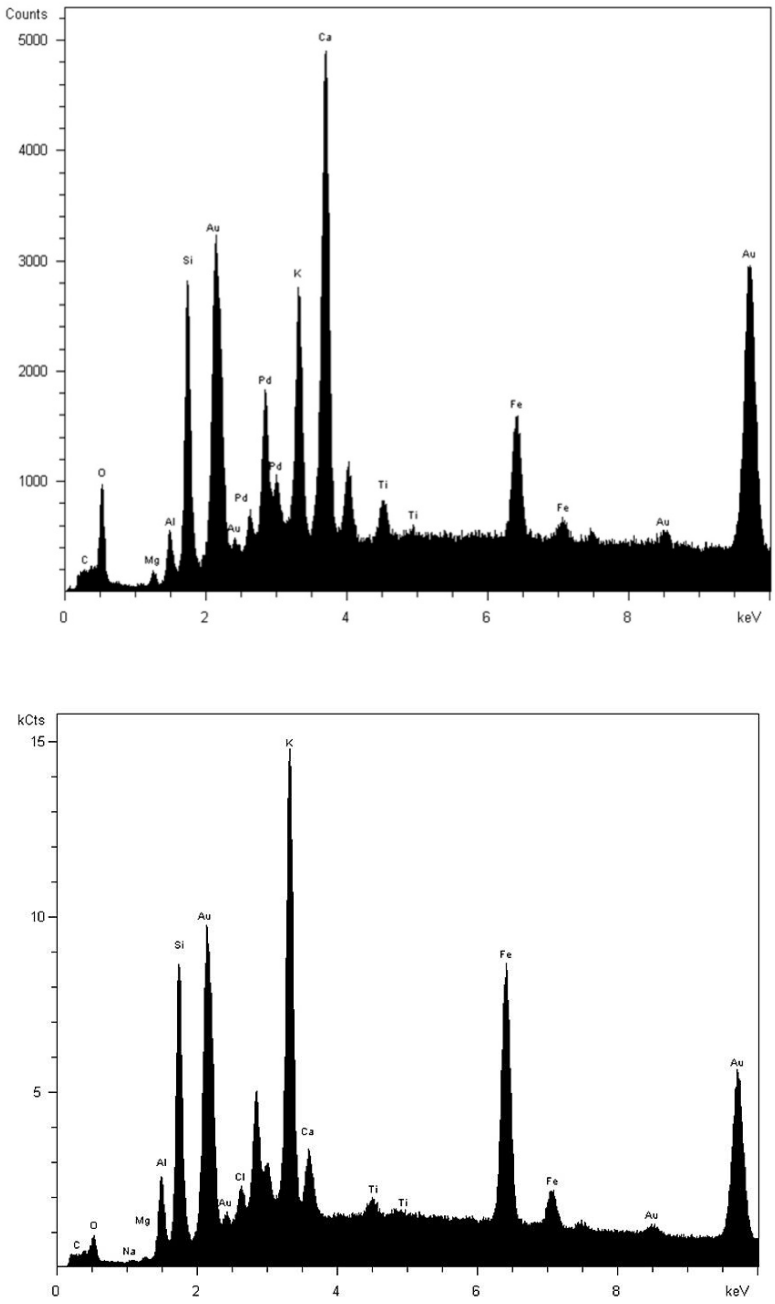

Figure 8-7: EDX Spectra of Lithofacies 1 (above) and Lithofacies 3(below) Illustrating the Major Elements of Dolomite and Hematite Cements in Figures 18-7B and 18-9B, Primarily as Ca and Mg, and Fe Respectively. Additional elements present in the EDX spectrum (Si, Al and K) are due to detection of adjacent quartz grains, plus illite and kaolinite clays.

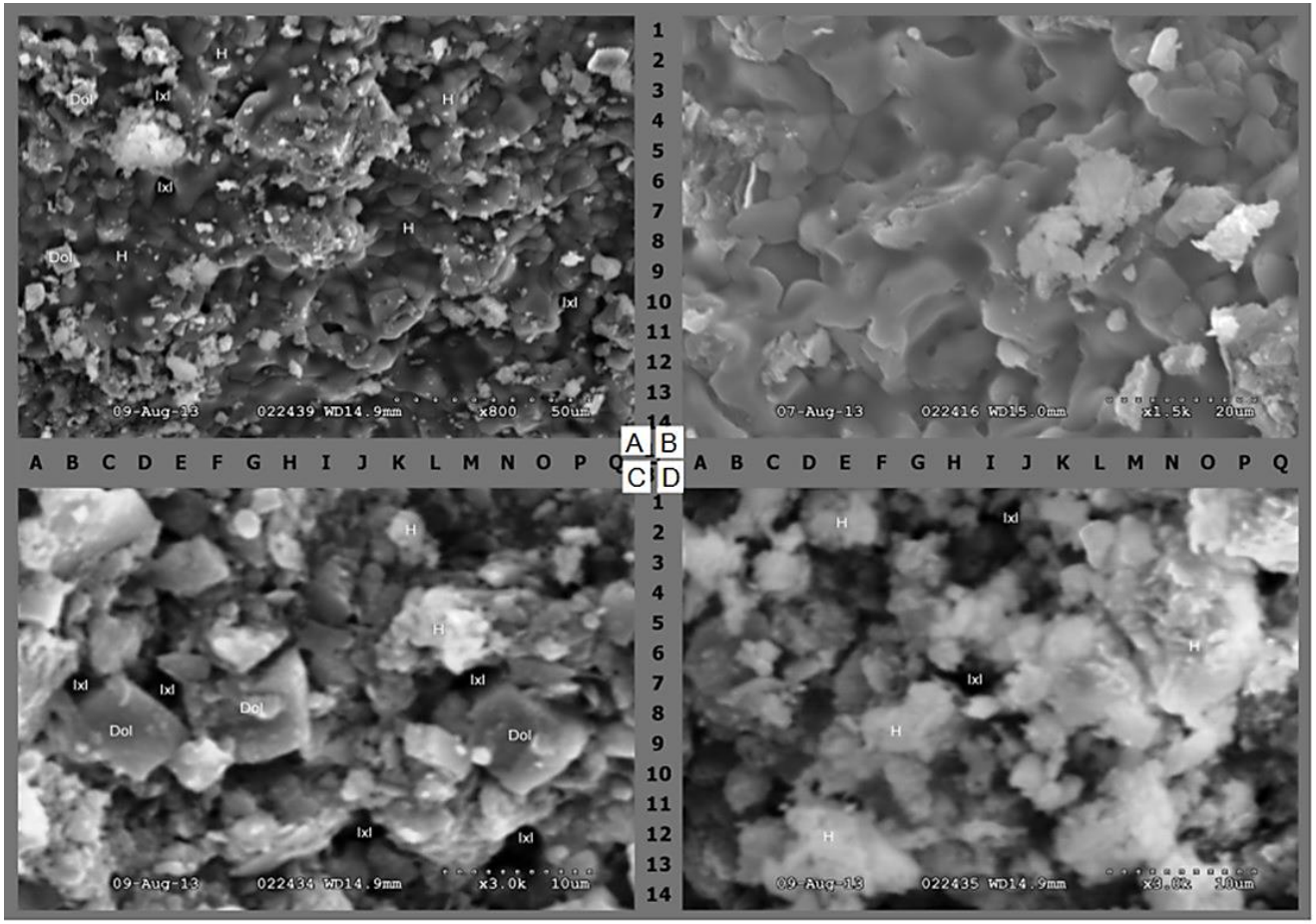

Figure 8-8: SEM Images of Lithofacies 3.Highlighting very fine to medium crystalline dolomite rhombs (A,C: Dol) and small, round or disc shaped coarsely crystalline authigenic hematite (H) coatings on dolomite rhombs and detrital quartz grains. In A to D, scattered hematite inclusions within dolomite rhombs. In B, coarsely crystalline hematite occurs as platy, hexagonal crystals. The intercrystalline (A,C,D: Ixl) porosity is mainly obstructed by the precipitation of anhedral to subhedral dolomite rhombs and subordinately by hematite cements. (x800, x2500, x3000, x3000)

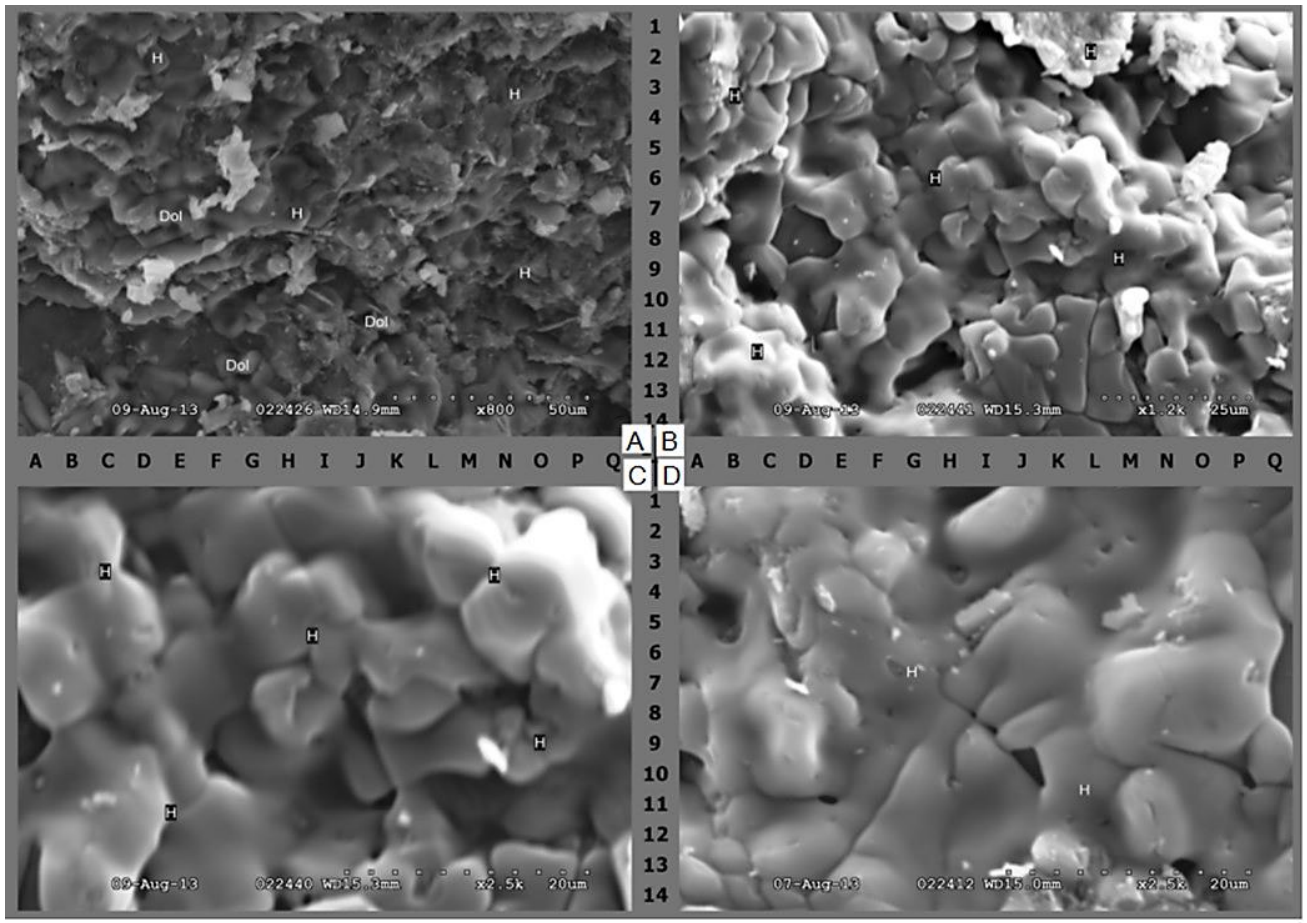

Figure 8-9: SEM Images of Lithofacies 4. This consists of very fine to medium crystalline dolomite rhombs (A: Dol) and surrounded by deep red small, round or disc shaped coarsely crystalline authigenic hematite (H). However, in all views the coarsely crystalline hematite occurs as platy, hexagonal crystals and is dark red to black in reflected light. The intercrystalline (A,B,C: Ixl) porosity is mainly obstructed by the precipitation of anhedral to subhedral dolomite rhombs, plus hematite cements. (x800, x1200, x2500, x2500)

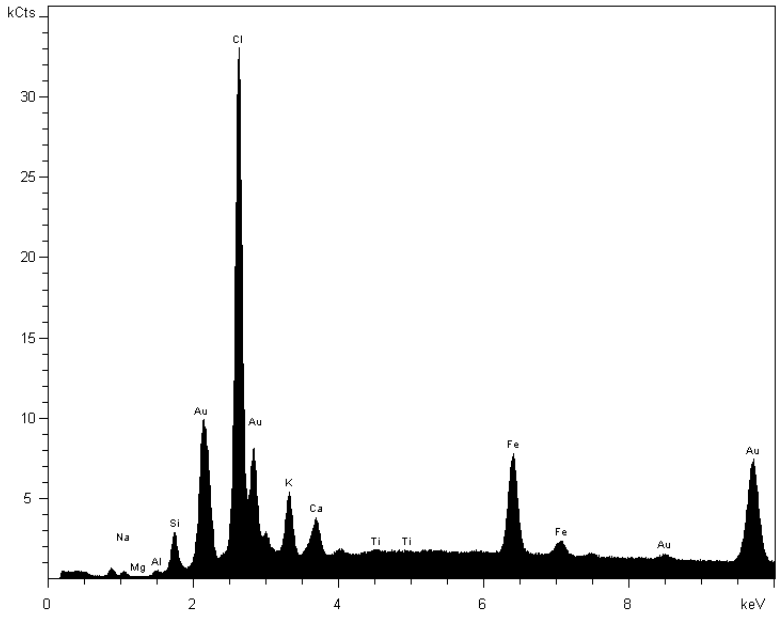

Figure 8-10: EDX Spectra of Lithofacies 4 Illustrating dolomite and hematite cements in Figure 8-9C. The iron (III) oxide cement is responsible for the reddish-brown coloration of the facies (see thin section photomicrographs at Figure 8-6. EDX spectra showing the major elements of hematite primarily iron (Fe) and of dolomite (Ca, Mg).

8.4 Diagenetic History

A generalized paragenetic sequence of the Three Forks minerals is given in Figure 8-11. Diagenetic features, in a paragenetic sequence, include: onset of compaction, precipitation of calcite and pyrite, dolomitization or dolomite cement in pores, and hematite precipitation. Compaction of the sediment sets in immediately after deposition and increases during burial due to rising lithostatic stress. Early stage of compaction reduces volume and porosity of sediment by expelling interstitial waters and framework becomes slightly compacted. Precipitation of pyrite occurs in two stages. The relatively early stage pyrite precipitates in early reducing condition and occludes pores, plus replaces matrix clays. Later stage pyrite is locally precipitated into the dolomite rhombs.

It is my hypothesis that pervasive dolomitization, caused by the influx of magnesium rich fluids took place shortly after deposition. The dolomite 1 mimics the original fine-grained limestone (micrite?) during replacement resulting in a very fine to finely crystalline texture. Euhedral dolomite cement is present mainly as finely to medium crystalline rhombs that fringes interparticle pores and micro-vugs at a later stage of diagenesis. Local ferroan dolomite precipitation occurs at the same time as the euhedral dolomite rhombs. Zonation and overgrowths of dolomite rhombs are rare. Primary porosity is significantly reduced by dolomite cement. Hematite or iron rich oxidized mineral is the weathering and oxidation product of earlier formed pyrite and siderite i.e. the last diagenetic step.

The following schematic paragenetic sequence summarizes the diagenetic events and porosity development of the Three Forks facies.

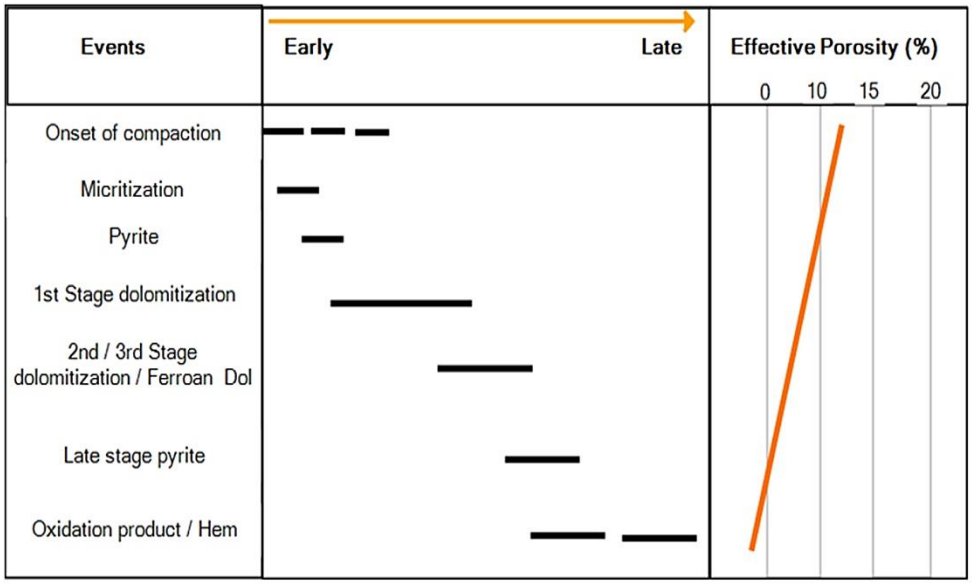

Figure 8-11: Paragenetic Sequence of Diagenetic Events for the Three Forks Formation Based on Three Lithofacies from Wells 19915 and 19918.

CHAPTER 9

PROPOSED DEPOSITIONAL ENVIRONMENTS

A sedimentary environment can be defined as a "part of the earth's surface which is physically, chemically, and biologically distinct from adjacent areas" (Selley, 2011). Quantitative rock components and qualitative interpretation of sedimentary structures are integrated to interpret the sediment source, their provenance, depositional processes, and subsequent modeling of paleo-environmental conditions by invoking Walther's principle of vertical and horizontal facies match, and the principle of uniformitarianism. The importance of evaporites in interpreting the environmental framework cannot be underestimated.

Some limitations to the data used in this work include the fact that 7.6 cm (3 in) diameter cores do not allow assessment of the lateral continuity of sedimentary structures which are particularly important in the interpretation of evaporitic rocks. Macroscopic three-dimensional features are likely the most crucial means of records of the processes occurring during deposition or between deposition and lithification especially when coupled with information from identified lithofacies.

Carbonate sediments are intrabasinal and primarily marine in origin although considerable volumes are deposited in marginal and nonmarine environments. Marine environments can loosely be defined as possessing anywhere between 14 to 50 parts per

thousand in salinity (Martin et al., 2000; Heckel, 1972b). Shallow marine environments occur both as epicontinental (epeiric) seas that lie upon the continents or as marginal seas (pericontinental) occupying shelf areas around the continents (Heckel, 1972b).

The continental shelf is the relatively shallow submarine terrace of continental crust extending from the low-water mark to the continental shelf margin which is about 200 m (600 ft) deep (Selley, 2000). Lime mud is polygenetic in origin involving several sedimentary processes that disaggregate organic debris into their constituent crystals or as cryptocrystalline cement in certain circumstances (Walsh, 1987). Such processes affecting continental shelves include storms, tidal currents, wave action, wave-generated currents, constantly scouring the seabed, or depositing sediments, resulting in bedforms of different geometries. The different carbonate grains result from different processes operating in different environments. Thus a carbonate composed of a single grain type indicates genesis from a single process, one with two grain types reflects those with two processes, and so forth (Smosna, 1987).

Ahr (1973) introduced the carbonate *ramp* and *rimmed* models in an attempt to distinguish gently sloping carbonate platforms that lack a slope-break from carbonate platforms that drop sharply off from shallow to deep water or isolated buildups. Carbonate ramps have very low gradient depositional slopes (<1°) from the shoreline or lagoon to the basin floor. Thus, carbonate ramps describes a depositional surface attached to a shoreline on one end and to the correlative basinal beds on the other (Read, 1985; Burchette and Wright, 1992; and Ahr, 1998;).

A reasonable depositional model for the Three Forks Formation can be inferred from the general theory of sedimentation for a marine system that is not under the influence of terrigenous clastics suggested by Irwin (1965). Irwin's X-Y-Z model for the hydraulic energy distribution that controls sedimentation in marine environments has proven to have unlimited applications in its ability to group all primary marine carbonates into three classes of sands and muds, based solely on their compositional constituent (bioclastics, pelletal, and litho-clastics) and the energy regimes controlling their formation.

Zone X is a low-energy environment in which marine currents control the hydraulic energy that acts upon the sea bottom and provides accommodation space for fine grained detritus gained primarily from Zone Y. Lower temperatures, insufficient sunlight and less water agitation with depth preclude inorganic precipitation and oxidizing conditions. Zone Y, represents the high-energy domain characterized by wave action and strong tidal currents. It is the belt in which winnowed sands form and is characterized by sediments which are essentially biogenic. Zone Z is an extremely shallow, low-energy zone, in which there is little circulation of water, where tides are essentially wanting and in which the only wave action is that produced by local storms. As a consequence, zone Z it represents a site for the deposition of sediments which are basically of chemical origin.

Comparable to the X-Y-Z zone model, ramps contain three major zones with different energy regimes that control facies distribution (Burchette and Wright, 1992). These subdivisions are:

9.1 Inner Ramp

The inner ramp is the shallow zone above the fair-weather wave base (FWWB) that is storm-dominated with very little tidal influence characterized by barrier and back-barrier deposits such as evaporites and calcareous mudstones. It occupies the most landward marine extent of the platform. Usually, the inner ramp is characterized by coarser deposits in channels and carbonate muds on tidal flats. The lower members of the Three Forks Formation contain abundant intrasediment anhydrite which only forms in environments where evaporation losses exceed precipitation and only accumulate in settings where concentrated brines are prevented from diluted by influx of less saline waters (Reading, 1996). Such environments will include, with the exception of "saline giants," shallow-water, subaqueous environments and sabkha-like settings (Fig. 9-1).

Anhydrite forms a major component of Member 1 and Member 2. The main types are of bedded and distorted nodular varieties that represent sabkha to supratidal environments. Very often, the development of nodular (chicken-wire) anhydrites is attributed to the replacement of an earlier gypsum crystal mush in a saline mudflat sabkha environment where additional nodules and nodule layers can develop within supratidal sediment above the main replacement zone as in members 1 and 2. These processes may or may not retain the morphology of the original gypsum (Withington,1961; Masson,1955; Murray,1964).

The source of calcium sulfate to account for the anhydrite within the Three Forks might be from upward migration of ground water as a result of evaporation in an arid supratidal environment or upward, downward, or lateral migration of denser, more saline water in

subaqueous environments (Dean et al., 1975). The mudstone, wackestone restricted biota nature of lithofacies 2 and 3 is indicative of lagoonal deposits above the fair-weather wave base (FWWB).

9.2 Middle ramp

The middle ramp is between FWWB and the storm wave base (SWB) and therefore dominated by very shallow subtidal to intertidal settings. Mid-ramp deposits reflect varying degrees of storm influence depending on the water depth and the depth of wave base. Small scale climbing ripples, trough cross-lamination, isolated small-scale current ripple marks (lunate), lenticular to wavy beddings and soft sediment deformation which are typical of members 3 and 4 may form in various depositional settings although their combination and abundance is very suggestive of tidal processes (Archer, 1993).

Mud predominates in the supratidal and upper intertidal zones. Mixed mud and sand characterized the middle part of intertidal zone while sand dominates the lower intertidal and shallow subtidal zones (Boggs, 2000). Fenestral structures, observed in dolomitic mudstones of members 2 and 4 are deposited in supratidal to arid upper intertidal environments (Parham et al., 2010). Fine laminations, in addition to lightly burrowed to brecciated dolomitize mudstones are characteristics of supratidal to intertidal environments. Member 3 is interpreted as mud- rich coastal deposits that probably represent the transition from intertidal to lower supratidal while Member 4 is thus a change from supratidal to upper or mid-intertidal environments that underwent a very rapid sedimentation as indicated by its lack of burrowing (Allen, 1972). The lack of burrowing is also indicative or suggestive of an inhospitable environment during or soon after deposition.

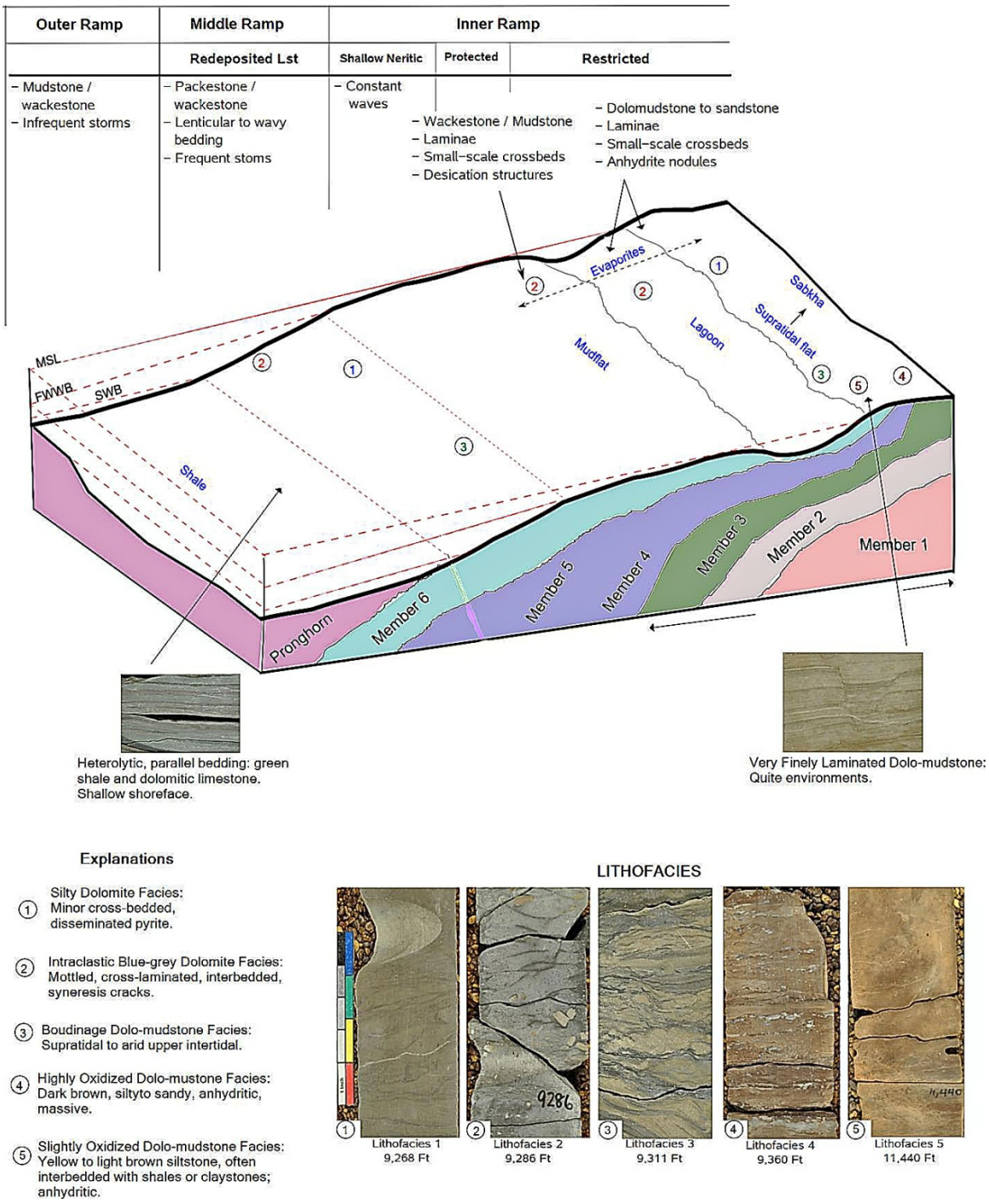

Figure 9-1: Schematic Ramp Illustration of the Depositional Facies Relationship of the Three Forks Formation, North Dakota using Spring and Hansen's (1998) Scheme

9.3 Outer Ramp

The outer ramp extends from the depth-limit to which most storms influence the sea floor down to the basin plain (Fig. 9-1). The outer ramp deposits are principally redeposited argillaceous carbonate mud and wackestone from suspension often with the characteristics of turbidites (consisting of a sequence of strata in which the bottom sediments contain the coarsest grains and the upper sediments the finest).

The brecciated nature of Member 5, largely similar to that of Member 4 reflects wave action that formed the breccias. This is probably a consequence of shoaling of the epicontinental sea because of a decrease in the rate of subsidence. Most of Member 5 constitutes strata lacking internal cross-stratification of any kind or cross-stratification makes up part of the layering but is, typically, a subordinate component. In addition, the presence of disseminated pyrite within Member 5 proves that chemically reducing conditions prevailed at some time during deposition. Such anaerobic conditions occur in subtidal and intertidal sediments where oxygen is depleted just a few millimeters below the sediment surface.

Lenticular to flaser bedding are critical examples of lower shoreface, tidal deposits. Member 5 can therefore be placed between intertidal and mid-supratidal. Also, parallel stratification and scarcity of reef organisms are evidence for a low-energy environment. Given that the upper portion of Member 6 is deformed by bioturbation, the interpretation is a progressive shift from the upper shoreface to subtidal environments from the top of Member 5 to the start of the lower Bakken member; with a marked depositional break in-between.

9.4 Dolomitization Model

Dolomite is a complex mineral not only in terms of Ca:Mg ratios and degree of order, but also in terms of other elements, notably iron (Braithwaite et al., 2004). Dolomite can precipitate from various kinds of water containing Mg^{2+}, Ca^{2+} and CO_3^{2-} ions and under many different environmental conditions and is the main process by which primary and pore-filling dolomites are produced. However, most dolomites have a secondary origin or formed through the replacement of $CaCO_3$ by $CaMg(CO_3)_2$.

Dolomitization refers to the process by which the Ca^{2+} ions in precursor limestones or calcareous muds, consisting chiefly of unstable calcite or aragonite are replaced by Mg^{2+} ions in the presence of Mg^{2+}-rich fluids to form a more stable magnesium calcium carbonate rock. Dolomitization does not include dolomite cementation or situations that involve recrystallization of pre-existing dolomites by hydrothermal processes (Al-Awadi et al., 2009). In view of the highly variable composition of the mineral, it is clear that its origins will never be explained in terms of one unique dolomitising model (Purser et al., 1994).

More often, dolomite is associated with ancient tidal flat deposits. Although the exact mechanism for magnesium enrichment and subsequent dolomitization is unknown, several models have been proposed. All theories must provide explanations for:

1. The source to supply enough Mg^{2+} ions to complete the dolomitising process,
2. The mode of transport into and distributing the Mg^{2+} ions through the host limestone, and
3. A chemically favorable environment in which at least 50% of the Ca^{2+} ions can be

replaced by Mg^{2+} and also removing the displaced Ca^{2+}; this favors settings with an active and long-lasting hydrologic drive.

The anhydrite-dolomitic relationship i.e. the occurrence of anhydrite in dolomitic sediments becomes less abundant and absent towards the outer ramp where silty/sandy lithologies become more prominent. Also, the thickness of the anhydrite-dolomitic cycles decreases upwards, towards the top of the formation. These anhydrite-dolomite cycles are interpreted as deposits of restricted inner ramp environments with occasional seawater recharge. Most bedded dolomites originate from post-depositional alteration of limestones in intensely evaporated environments (Adams and Rhodes, 1960). From results of petrographical analysis such as very fine to fine, unimodal, anhedral crystals of dolomite and features like fenestral fabrics, anhydrite nodules and mud cracks, it is concluded that the origin of this dolomite is closely related to supratidal to arid upper intertidal environments in which the host limestone was being replaced. Based on these indicators the sabkha dolomitization model is suggested for the Three Forks Formation.

It is suggested that dolomitization took place within the intertidal zone and sabkha-like environments where evaporation was severe. It is an interpretation that occasional seawater was brought over the peritidal zone and evaporative flat where very dense, hypersaline brines form as a result of capillary evaporation. This created a gravitationally unstable density gradient which promotes the free convection of the dense brines into the sediments and subsurface as the brine refluxes back into the sea (Garcia-Fresca and Lucia, 2006).

In arid climates, as the brine concentration increases, aragonite, and gypsum (anhydrite) minerals precipitate. This promotes the formation of a high Mg/Ca brine that favors dolomite precipitation or dolomitization as the brine filters through the pores of the underlying rock.

CHAPTER 10

PETROLEUM POTENTIAL

This chapter presents a methodology and results of a reservoir characterization study of the Three Forks as a potential for hydrocarbon exploration. The principal objective is to evaluate the Three Forks Formation's potential for future development. A petrophysical analysis is applied to over 128 well logs from 32 wells within the study area (Fig. 10-1). Log-derived porosities and water saturations agree with core data. Also, results of the Archie, Simandoux, Modified Simandoux, Indonesia and Dual-Water models are quantitatively compared.

Finally, net-to-gross ratios of both potential reservoir rocks and pay zones are estimated for the different members and areas with high reservoir quality and potential pay zones are highlighted. The investigations revealed petroleum accumulations which necessitated the need to reassess the Three Forks Formation.

10.1 Approach

The log data from 32 wells existed as scanned files (TIFF) and had to be digitized in *Neuralog* software, converted to LAS files before any analytical step could be performed. The LAS files were imported into IP where the following analytical steps were performed to calculate the petrophysical parameters. The available logs were resistivity (laterolog and induction) logs, porosity logs (formation density, sonic and compensated neutron),

natural gamma ray, and caliper logs. The caliper log (which measures borehole size) is used to identify where readings are inconsistent as a result

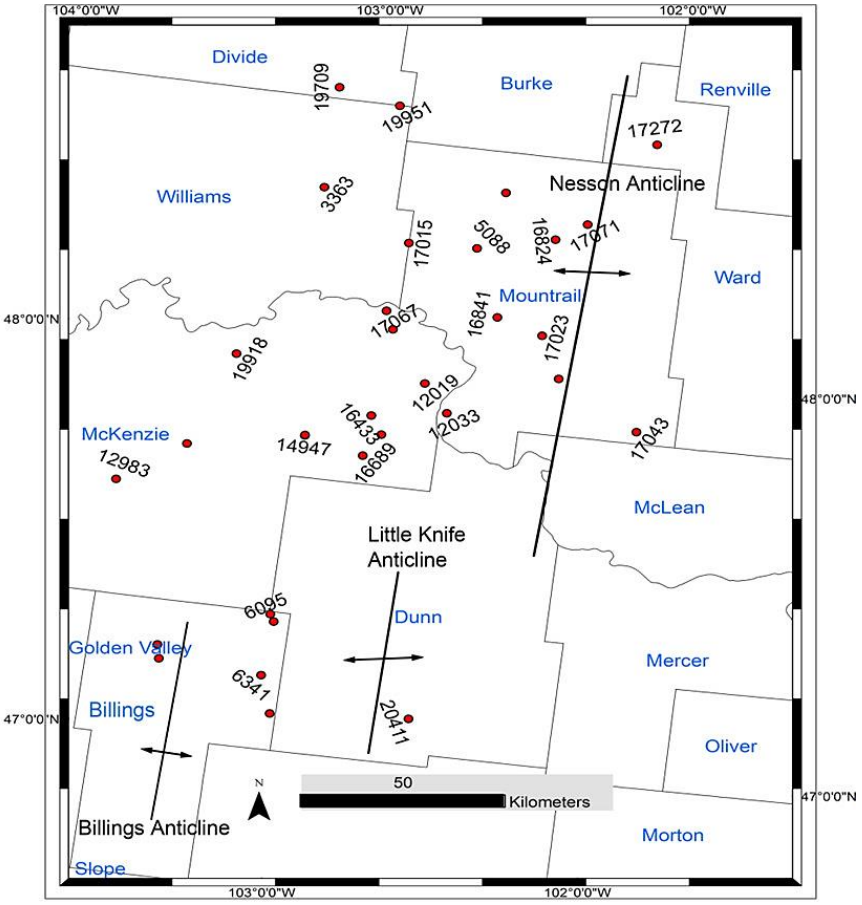

Figure 10-1: Selected Wells for Petrophysical Evaluation.

of borehole cavings. The gamma ray log is used to distinguish clean versus shaly lithologies, while the resistivity and induction logs are used for water saturation volume computations with subsequent determination of hydrocarbon bearing zones in each well.

Measurements of the volume of clay (Vcl), porosity (ϕ), permeability (K) water saturation (Sw) and oil saturation (So) are derived from 4 wells (17271,19709, 19918, 19951)

that penetrate the Three Forks Formation and cored with oil-base mud (OBM). The Vcl is calculated from wells logs and used to calculate log-porosities which are then compared with core derived values. Core-derived values for ϕ, K, Sw, and So are obtained from 770 core plugs from all four wells.

10.2 Clay volume (Vcl)

Figure 10-2 shows that the Three Forks should be classified as a shaly formation with a mean clay volume of 35% (Hilchie, 1978; Ghorab et al., 2008).

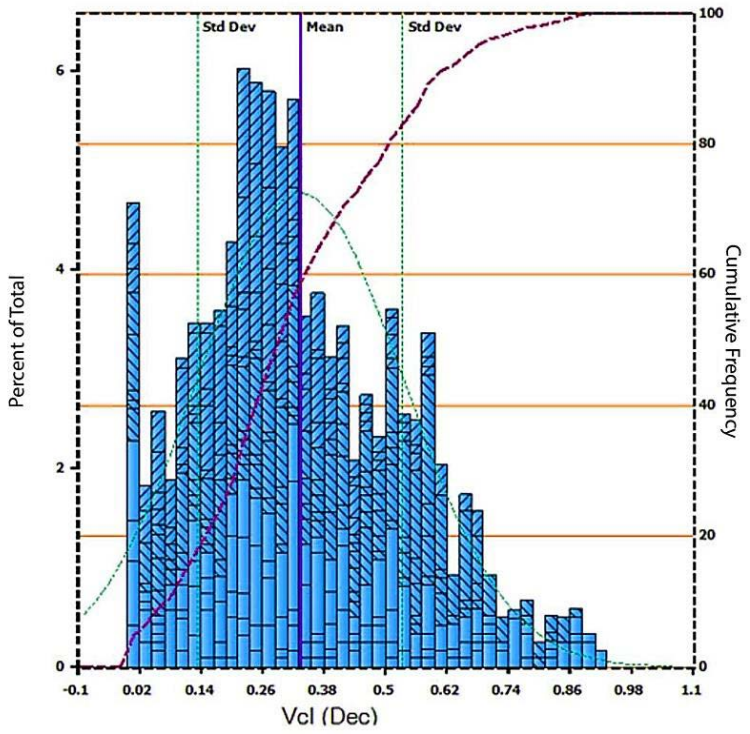

Figure 10-2: Clay Volume Histogram of the Three Forks Formation Based on 32 Wells. The mean clay volume is 35%.

10.3 Porosity– Permeability Relationship

Routing core analysis of samples at net effective overburden stresses of 4000 psi showed that rocks of the Three Forks have very low porosities with a mean value of about 8% (Fig. 10-3A). The distribution of effective porosities within the study area is shown in Figure 10-4. The log-derived porosity agrees quite well with cores value (Tab. 10-1, Fig. 10-5).

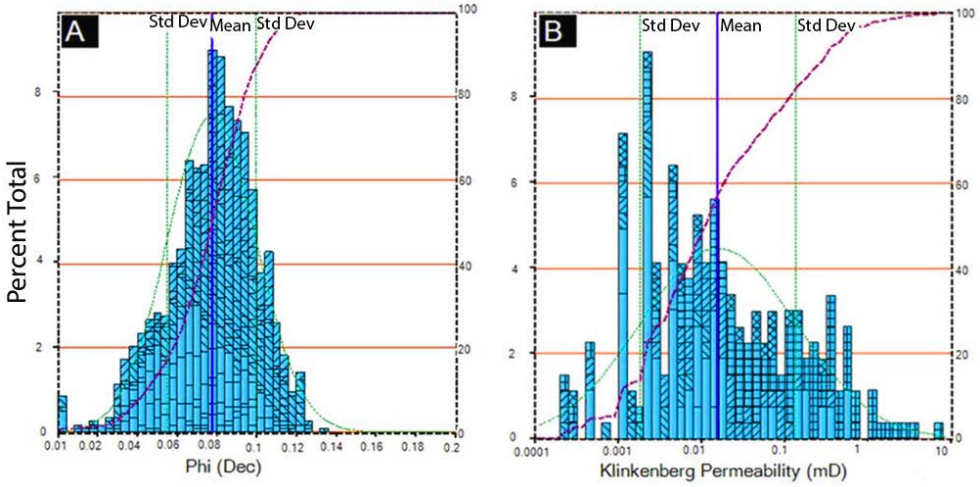

Figure 10-3: Reservoir Quality of the Three Forks. (A) Core derived porosities and (B) log-normal distribution of Klinkenberg permeability. Data from 32 wells, the average porosity of 8% while the average permeability is 0.02 mD.

Permeability corrections to in-situ reservoir conditions were done during lab analysis. The average Klinkenberg permeability of the Three Forks is 0.016 mD (Fig. 10-3B). Permeability values greater than 1 mD accounts for less than 1% of the total permeability in this case. The optimum permeability is between 0.001 and 1.00 mD. Core analysis showed that the grain densities within the Three Forks Formation range from 2.73 gm/cc to 2.95 gm/cc with a mean value of 2.79 gm/cc. As an example, a summary of the petro-physical properties of the Three Forks in well 19709 is presented as Figure 10-5.

Table 10-1: Summarized Core and Log Porosities of the Three Forks Formation.

	Core ϕ (%)	Number of Samples (n)	Log Derived Φ_T	Φ_e(%)
Member 6	7.9	73	8.6	5.6
Member 5	7.3	89	10.2	6.2
Member 4	7.5	256	8.6	6.2
Member 3	5.6	158	9.3	6.64
Member 2	9.1	112	8.1	6.39
Member 1	6.6	112	7.8	4.74

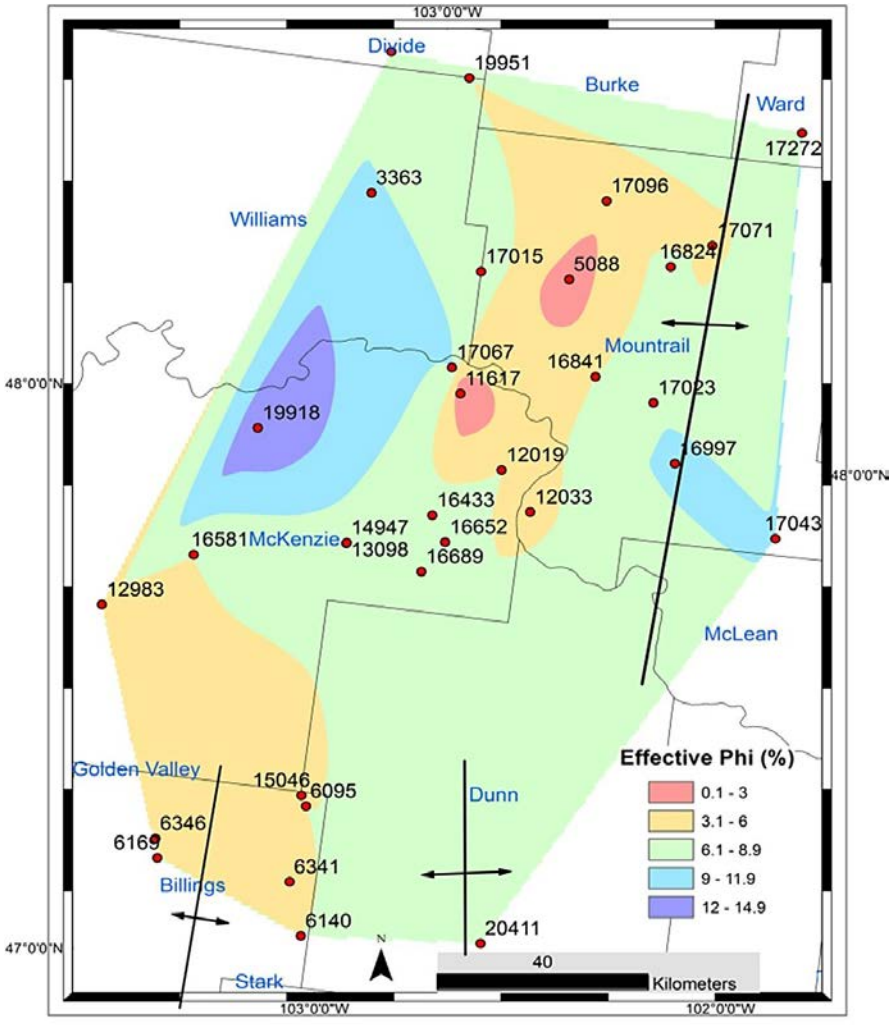

Figure 10-4: Distribution of Effective Porosity within the Study Area.

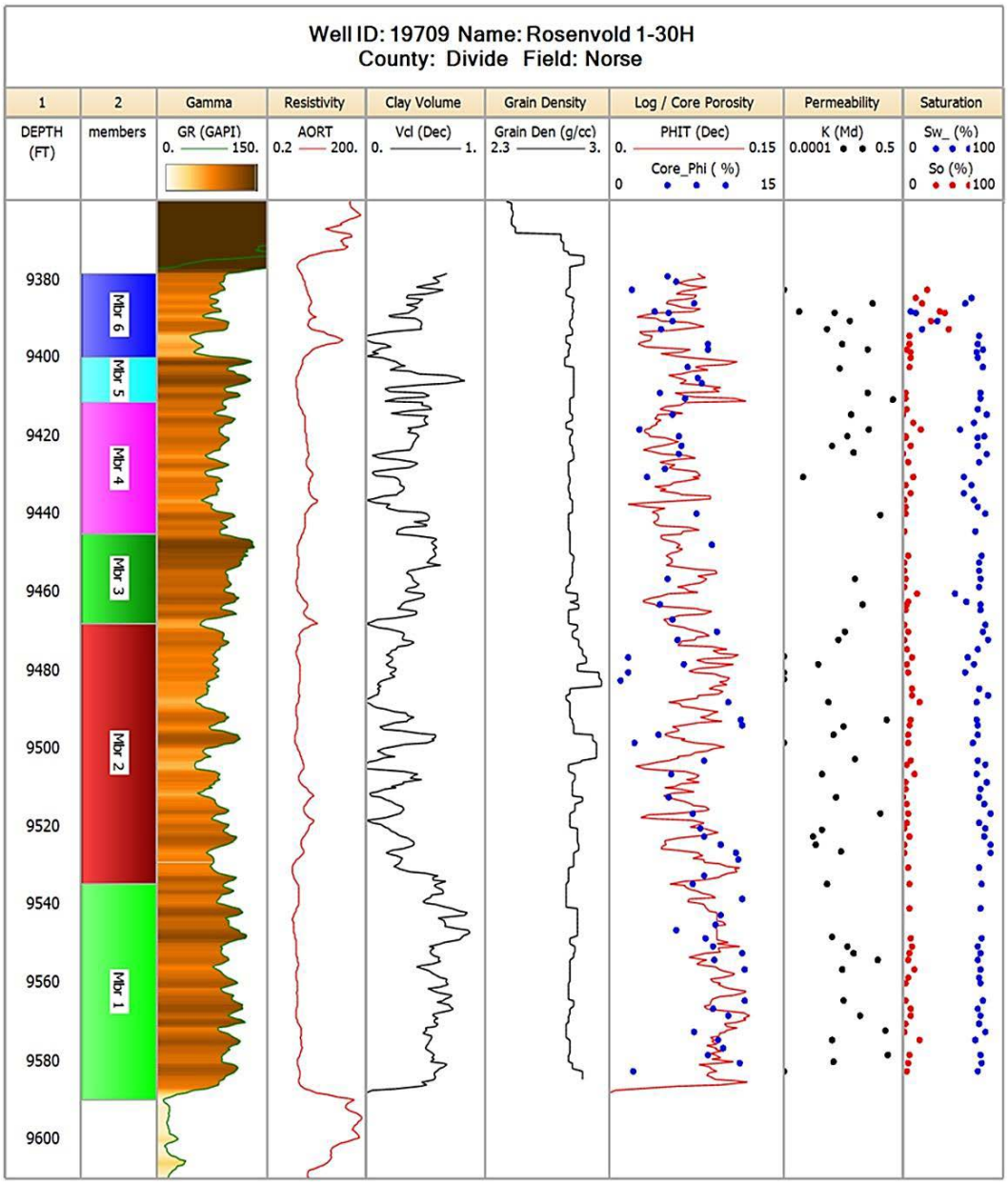

Figure 10-5: Stratigraphic Distribution of the Volume of Clay, Grain Density, Log and Core Porosity, Permeability, Water Saturation and Oil Saturation for the Different Members of the Three Forks Formation in Well 19709.

A crossplot of porosity and permeability for this set of wells is presented in Figure 10-6. The porosity-permeability relationship with a correlation coefficient r^2 of 0.34 (< 1)

confirms the fact that the permeability of the Three Forks Formation is not exclusively governed by its porosity distribution. This is evident from the dispersed arrangement of the data points which give evidence of other factors affecting the permeability for this formation. Also, the high porosity-low permeability zones observed may results from unconnected vugs or intra-clast porosities which may be poorly connected through very small pores. However, a petrographical analysis is necessary to prove this. This relationship is described by the following equation:

$$Log(K) = -3.4399 + \ 0.2251 * \phi(\%) \ldots . (25)$$

From Equation25, the average in-situ permeability at1% porosity is 0.04 mD.

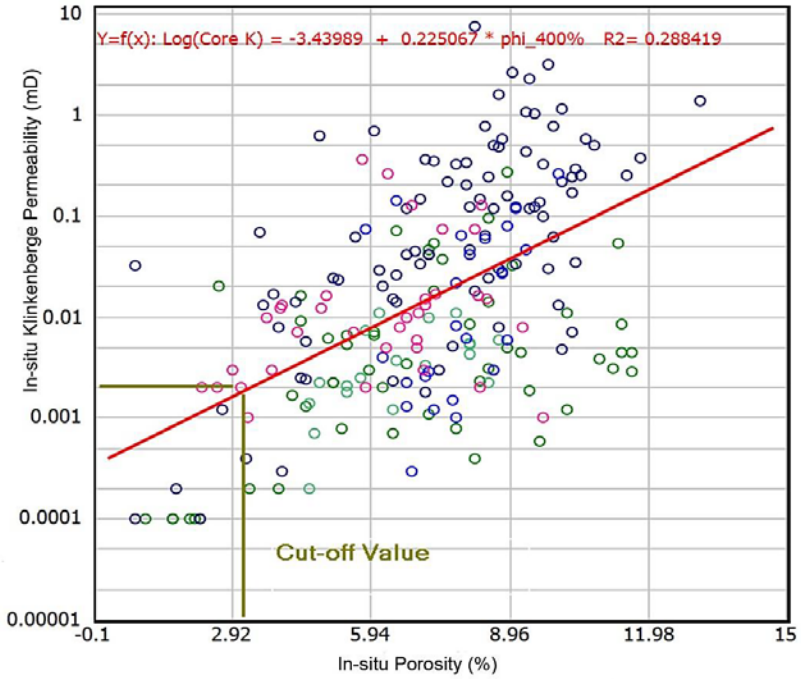

Figure 10-6: Crossplot of Klinkenberg Permeability (mD) and Porosity (%).

10.4 Water and Oil Saturations

Both core and log data sets verify the very low and the medium range saturations. Comparing the different *Sw* models showed that they all behave consistently in the different zones that have varying amounts of clay (Fig. 10-7).Also, these models identify more with the core measured *Sw* when used as total porosity models as opposed to effective porosity models (*SwT* comparison track). The Archie total model (SwArchT) is the least favorite in this group as it greatly underestimates *Sw*. The other models; Dual water, Indonesia, Simandoux and Modified Simandoux provide fairly good results in this particular case considering the fact that no SCAL data on the Archie components are available (Appx.7). The average water and oil saturation from core and log analysis is summarized in Table 10-2.

Tab. 10-2: Summary of Fluid Saturations from Core and Log Analysis (%).

	Cal. Sw	**Core Sw**	**So**	**Total**
Member 6	48	50	20	70
Member 5	75	81	9	90
Member 4	68	76	7	83
Member 3	62	77	7	84
Member 2	81	80	9	89
Member 1	58	76	7	83

A crossplot of ϕ and *Sw* (Fig. 10-9) show a complete scatter (overall) in the log calculations and in routine core analyses. The lack of a consistent pattern indicates that most of the Three Forks is in the transition zone (between irreducible water saturation and 100% *Sw*) and should produce water, with or without oil (Morris and Biggs, 1967). It would therefore be necessary to compare these results with production data, which is unavaila-

ble at this time.

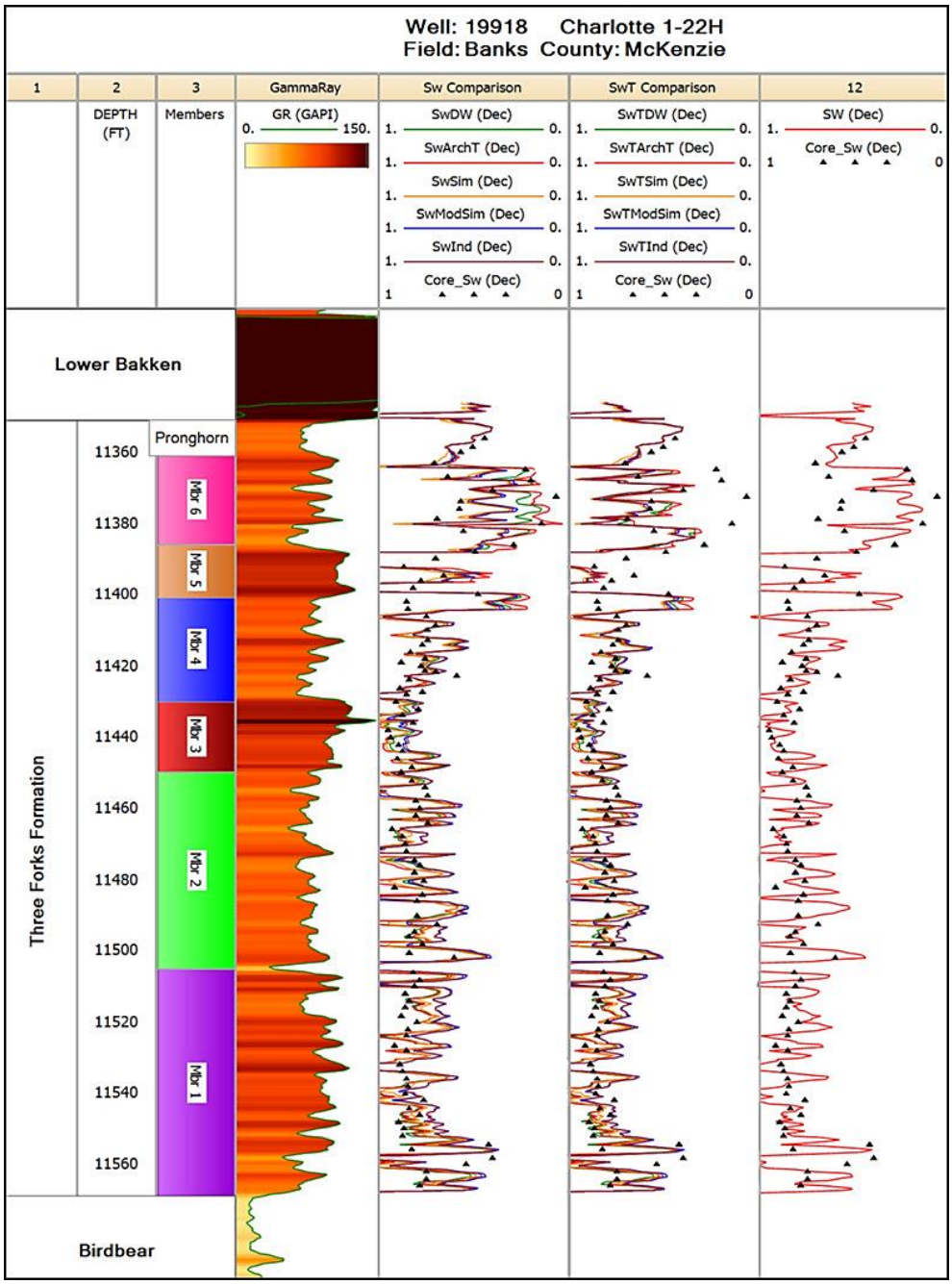

Figure 10-7: A Comparison of Results from Five *Sw* Models Applied to the Three Forks Formation. All models behave consistently within the formation although their predictions vary slightly.

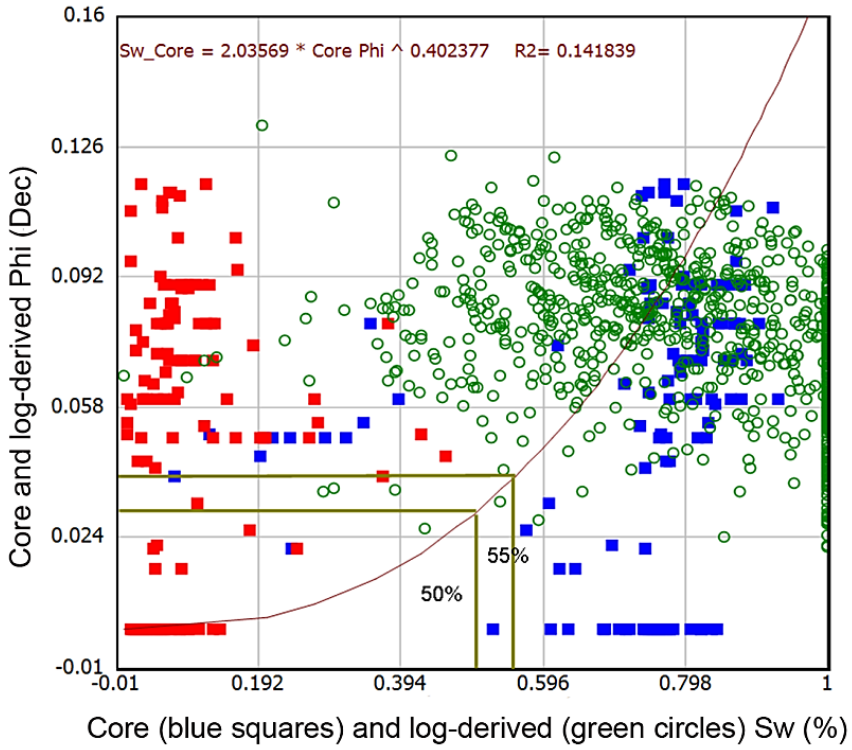

Figure 10-8: Porosity – Water Saturation Crossplot of the Three Forks Formation. Red squares are core *So*, blue squares are core *Sw* and circles represent log derived *Sw*.

10.5 Cut-off and Summations

Cut-off is a measure to discriminate non-reservoir rock (e.g. shale) from reservoir rock (sand and carbonates). The *gross thickness* defines the interval from top to bottom of the reservoir including all non-reservoir rocks. The *gross sand* refers to the portion of the reservoir which excludes the non-reservoir rock. *Net potential reservoir* defined herein as intervals containing rocks that have been identified as having the capability to store fluids and allow them to flow. Net pay constitutes net potential reservoir rocks containing significant volumes of hydrocarbons in place. Net-to-gross (N/G) therefore defines the ratio of net thickness of the reservoir/pay zone to the gross thickness.

10.6 Net Potential Reservoir and PAY Determination

The absence of a true porosity – permeability relationship from the core data makes if quite difficult to select representative cut-off values for the Three Forks Formation. In this study, the quality of the Three Forks Formation was summed over the different members using a density-neutron total porosity, clay volume and water saturation. A *Vcl* = 50 % is chosen, as a cut-off for gross sand (to cleanly separate potential reservoir rocks from shaly non reservoir rocks).

A porosity cut-off should eliminate portions of the formation with porosities (permeabilities) lower than the given value and therefore should be non-productive or would not produce the required flow. From Equation 25, a ϕ cut-off = 3% corresponds with a *K* cut-off ≈ 0.0017 mD (Fig. 10-6) and 50% water saturation (Fig. 10-8). However, the greater proportion of fluid saturation belongs to the upper 40%, a ϕ cut-off = 4% is reasonably assigned to conservatively eliminate 55% of the large volume of water contained in pore spaces without compromising permeability. The resulting *K* cut-off at ϕ = 4% ≈ 0.0028 mD. Based on these criteria, a ϕ cut-off = 4% and *Vcl* cut-off = 50% is used to determine net potential reservoir zones while a ϕ cut-off = 4%, *Vcl* cut-off = 50% and *Sw* cut-off = 55% is used for net pay. Examining Figures 10-6 and 10-8, this criterion does not significantly leave out most of the potential reservoir.

10.7 Summations

The average net potential reservoir thickness is 34 m (110 ft) compared to 9 m (29 ft) for average net pay thickness (Tabs. 10-3 and 10-4). Also, the average porosity of net pay is slightly higher (8.3%) than the average porosity for net potential reservoir (7.2%). This is

simple because the low porosity values had been taking off during the net reservoir calculations. Obviously, porosity does not play a key role in separating the very wet zones from wet zones. The average *Sw* for net pay is much smaller compared to net potential reservoir (35% and 73%). The reason could be that the high water saturation and low porosity portions have been removed, leading to a higher average *Sw* for net pay. Finally, the average *Vcl* does not change much for net reservoir and net pay, ≈ 24% (Figs. 10-9, 10-10).

Table 10-3: Reservoir Summary (Average Reservoir Values).
Cuttoffs used Phi >= 4%, Vcl <=50%, 27 wells considered.

Unit	Gross **ft**	Net **ft**	N/G **%**	Av Phi **%**	Av Sw **%**	Av Vcl **Ari %**	Phi*H **ft**	PhiSo*H **ft**
Member 6	25	14	57	7	50	25	0.9	0.5
Member 5	15	7	47	8	62	29	0.6	0.2
Member 4	31	22	71	7	67	21	1.6	0.5
Member 3	58	39	68	8	75	25	3.0	0.8
Member 2	39	25	63	8	73	21	1.9	0.5
Member 1	45	19	42	7	65	28	1.3	0.5
All	183	110	60	8	70	24	8.3	2.5

Table 10-4: Pay Summary. Cuttoffs used Phi >= 4%, Vcl <=50%, Sw <= 0.55.

Unit	**Gross ft**	**Net ft**	**N/G %**	**Av Phi %**	**Av Sw %**	**Av Vcl Ari %**	**Phi*H ft**	**PhiSo*H ft**
Member 6	31	7	21	8	37	21	0.5	0.3
Member 5	58	8	14	8	41	26	0.7	0.4
Member 4	39	5	12	12	39	18	0.5	0.3
Member 3	45	7	15	8	36	28	0.6	0.4
Member 2	25	7	27	7	22	29	0.5	0.4
Member 1	15	2	16	8	36	32	0.2	0.1
All	183	29	16	9	37	24	2.5	1.6

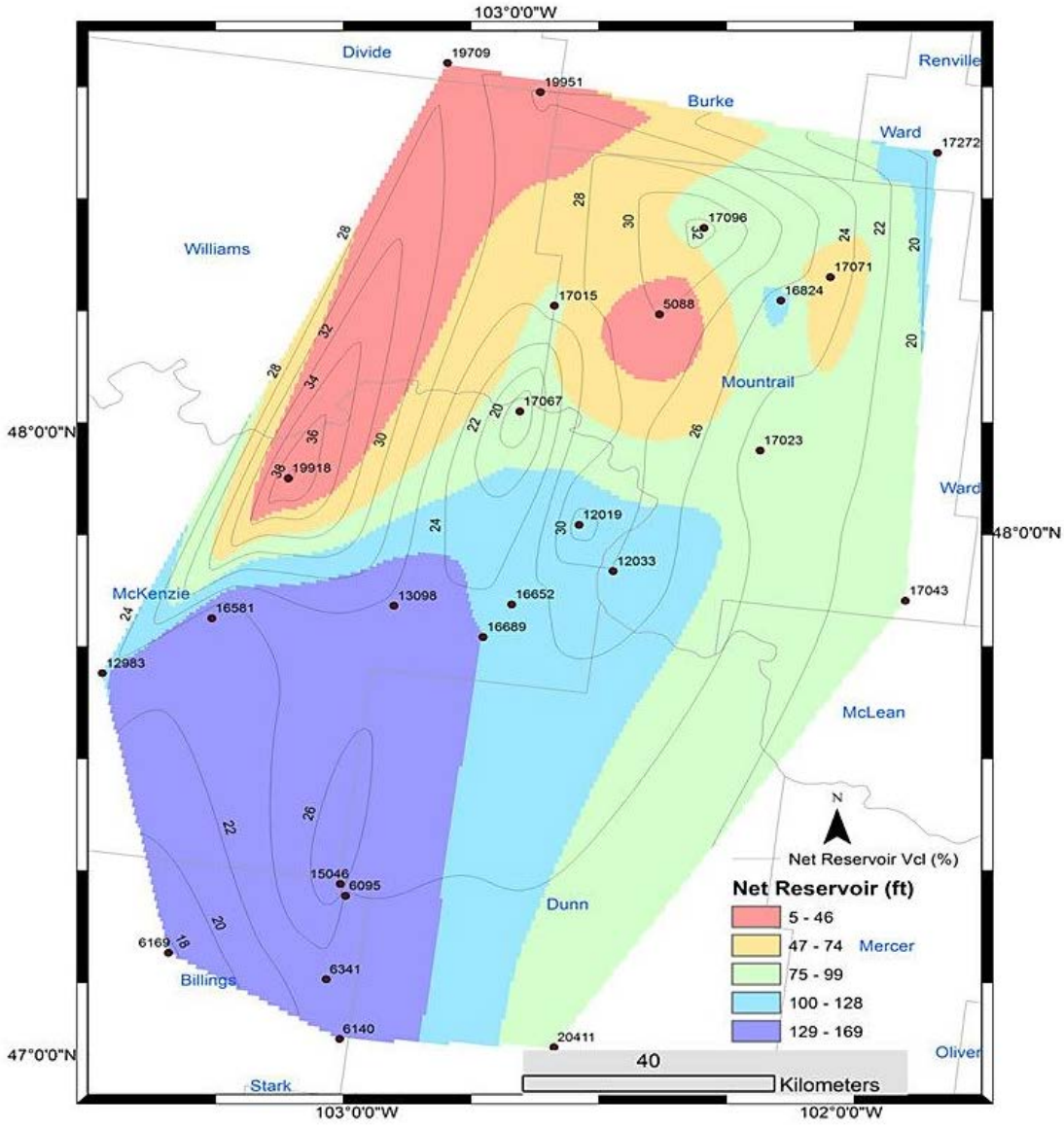

Figure 10-9: Net Reservoir Zonation for the Study Area. Contours represent net reservoir *Vcl.*

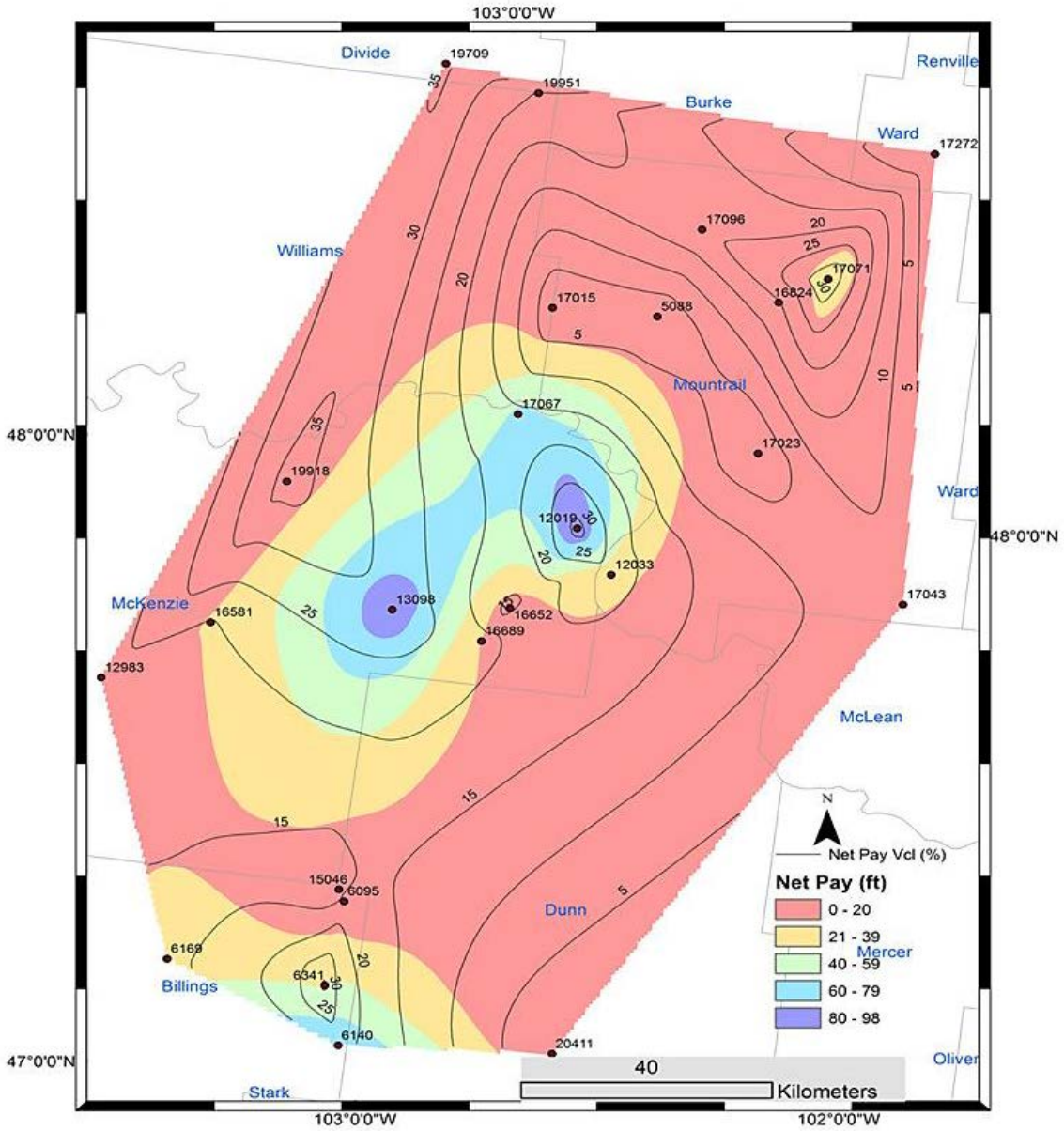

Figure 10-10: Net Pay Zonation for the Study Area. Contours represent net pay *Vcl*.

CHAPTER 11

SOURCE POTENTIAL AND THERMAL MATURITY

Laboratory analyses of the organic compounds contained in the rock are necessary in other to know if a sedimentary rock has any petroleum potential. Two samples from each lithofacies (Fig. 6-11) are analyzed to determine their TOC percent and kerogen characteristics. Within the subsurface, petroleum is generated over long periods through thermal alteration of organic matter at temperatures between 50º and 175º C. Tissot and Welte (1978) define a source rock as that which had generated or is capable of generating petroleum or simply has the potential to generate and expel oil, and considered a 0.4 % TOC as the minimum values for establishing source rock potential in carbonate rocks. Following this definition, the concept of effective source rock was introduced and is generally regarded as rocks with TOC values of approximately 1 wt. percent or organic carbon or more and generation potentials of 6 mg HC/g rock (Momper, 1978; Bissada, 1982; Jones 1984).

11.1 Results and Interpretations

By subjecting sediments containing organic matter to unnaturally high temperatures during pyrolysis, hydrocarbons can produced over practical periods of time under conditions comparable to the natural process of catagenesis (Harwood, 1982). However, if no OM is present or what was present had already been converted to hydrocarbons and

the rock has already undergone high temperatures only carbon-rich compounds (e.g. condensed residues and graphite) will show up in the rock, and no further hydrocarbons will be produced (Tissot et al., 1971).

11.2 Organic Richness, Potential Hydrocarbon, OM Type

TOC measurements represent the sum of kerogen and bitumen within the formation and provide both quantitative assessment of organic richness and an indication of the generative potential of the formation (Jarvie, 1991). Table 11-1 and Fig. 11-1A show that the results of TOC analyses from all five lithofacies range from 0.10 to 0.24 Wt. % HC. Generally, sediments with less than 0.5 Wt. % HC are consistent with rocks that have poor petroleum potential (Peters and Cassa, 1994).

These results are confirmed by the plot of the oil or remaining potential versus depth which clearly shows that the Three Forks Formation has poor source rock potentials with S2 values less than 2.5mg HC/g of rock (Fig. 11-1B). Even so, assessing the petroleum potential of a formation solely by TOC values is not reliable due to the fact that the measured TOC may include inert carbon with little or no generating potential. Roughly, the source rock potential of the Three Forks, in terms of its TOC and S2 increases with depth. Original and present HI values, which are used to interpret the conversion of kerogen to petroleum, indicate that where the Three Forks is shallow the rocks are most likely to produce gas while in areas where the Three Forks is deepest, the rocks can produce a mixture of oil type II and gas type III (Fig. 11-1C).

Table 11-1: Summary of Rock-Eval/TOC Data from Core Samples.

Well #	ID	Depth (Ft)	TOC Wt. % HC	S1 (mg HC/g)	S2 (mg HC/g)	S3 (mg CO2/g)	Tmax ^{0}C	Hydrogen Index (S2/TOC)*100	Oxygen Index (S3/TOC)*100	Production Index S1/(S1+S2)
19951	Facies 1	9,264	0.13	0.21	0.17	0.45	357	130	344	0.55
		9,268	0.15	0.23	0.19	0.45	355	131	310	0.55
	Facies 2	9,279	0.13	0.47	0.21	0.40	420	165	315	0.69
		9,286	0.14	0.46	0.22	0.41	418	159	297	0.68
	Facies 3	9,311	0.10	0.44	0.16	0.38	418	166	393	0.73
		9,321	0.12	0.44	0.17	0.38	417	139	311	0.72
	Facies 4	9,350	0.10	0.24	0.30	0.28	348	306	286	0.44
		9,360	0.10	0.24	0.29	0.28	349	293	283	0.55
19918	Facies 5	11,440	0.24	1.58	0.50	0.17	430	207	70	0.76
		11,469	0.24	1.59	0.51	0.16	430	211	66	0.76

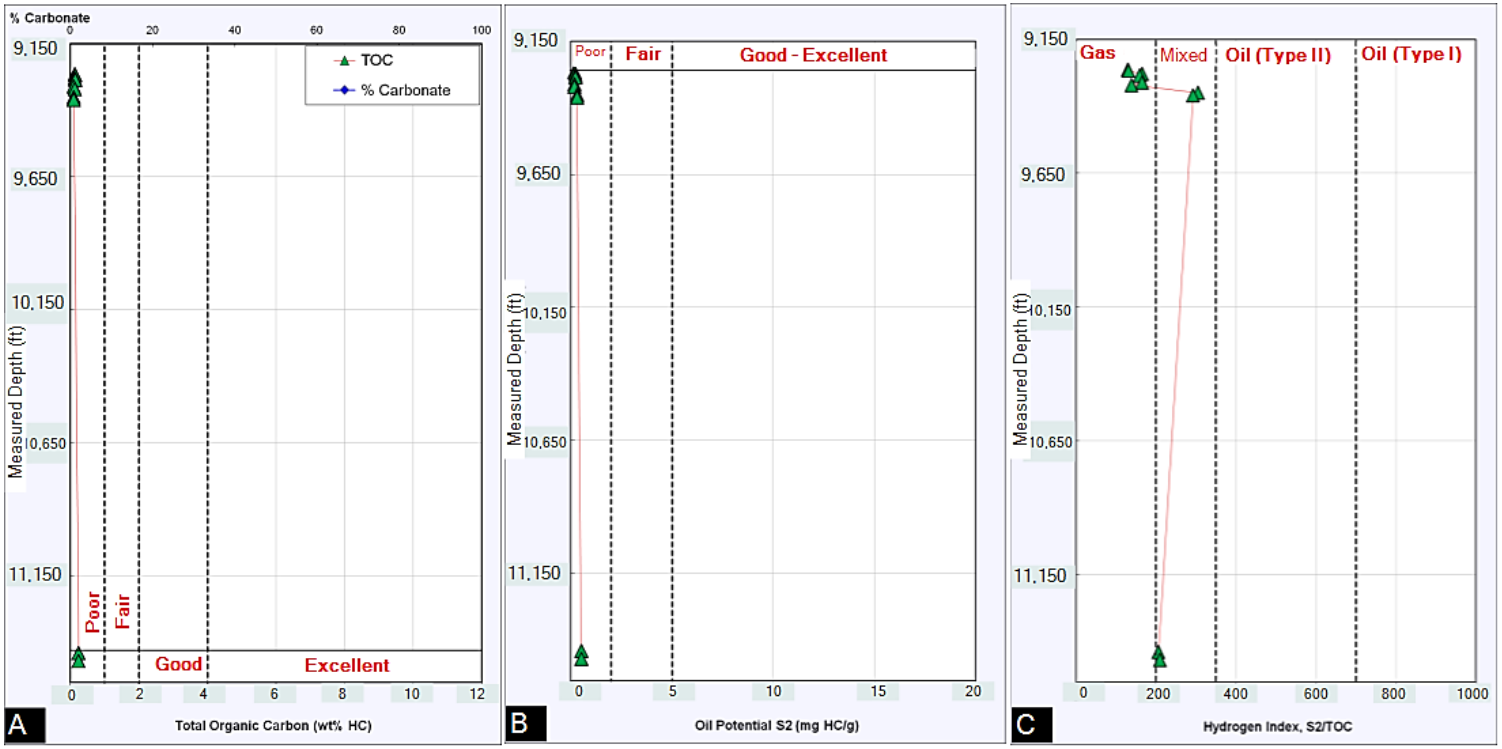

Figure 11-1. Geochemical Source Potential Logs: (A) organic richness – TOC weight% versus depth; (B) hydrocarbon or remaining potential – HC potential versus depth (S2); (C) organic matter type – Hydrogen Index (S2/TOC) versus depth.

11.3 Hydrocarbon Indicators and Maturity

11.3.1 Normalized Oil Content

Figure 11-2A shows the normalized petroleum ratio (S1/TOC) versus depth profile which is indicative of indigenous/migrated petroleum content of the formation. The anomalously high normalized oil contents (Tab. 11-2) (greater than 100) indicate productive oil or gas reservoir intervals that are probably the result of migrated oil.

Table 11-2: H Hydrocarbon Indication and Maturity Parameters: Calculated Vitrinite Reflectance, S2/S3, and Normative Oil Content for the Three Forks Formation.

Well #	ID	Depth (Ft)	Calculated %Ro	S2/S3 Conc. (mg HC/mg CO2)	Norm. Oil Content S1/TOC
19951	Facies 1	9,264	-	0.38	160
		9,268	-	0.42	159
	Facies 2	9,279	0.40	0.53	370
		9,286	0.36	0.54	333
	Facies 3	9,311	0.36	0.42	455
		9,321	0.35	0.45	361
	Facies 4	9,350	-	1.07	245
		9,360	-	1.04	242
19918	Facies 5	11,440	0.58	2.94	653
		11,469	0.58	3.00	657

11.3.2 Production Index (PI)

The PI is used as an indicator of the extent to which kerogen has been transformed into oil or gas. In addition, the PI depends on the type and thermal maturity of organic matter; therefore the PI is not the same for different types of organic matter (Tissot and Welte, 1984; Peters and Cassa, 1994). It can therefore be related to the level of thermal maturation or source of hydrocarbon in a formation. A PI value of 0.1 indicates the beginning of

oil generation and 0.4 indicates the termination of oil generation and start of gas generation (Hunt, 1996). Accordingly, low ratios would indicate either immaturity or extreme postmature organic matter while anomalous values correspond to accumulation or drainage of hydrocarbons or contamination by migrated hydrocarbons or drilling additives.

Hence, the cut-off values used to the data are as follows; PI $\leq$ 0.1 for immature (%Ro $\leq$ 0.5 %), 0.1 > PI $\leq$ 0.25 for early mature (0.5 > %R $\leq$ 0.8 %), and 0.25 > PI $\leq$ 0.4 for mature (0.8 > %R $\leq$ 1.2 %) sediments., The PI values for the Three Forks are anomalously high (Tab. 11-1), and are excluded from the evaluation process of the source rock potential of the Three Forks. Generally, the PI increases with depth (Fig. 11-2B).

11.3.3 Tmax and Vitrinite Reflectance

The level of maturation of the OM is estimated by from the Tmax Range. The hydrocarbons produced by pyrolysis depends on the amount of hydrogen the rock still contains as well as its level of maturation since the more mature the rock is, the lower amount of hydrogen it contains and the more energy it needs to liberate hydrocarbons. Based on interpretations of Peters and Cassa (1994), all five lithofacies are immature since their samples produced S2 peaks with Tmax values less than 435^{o}C. However, Tmax values around 435^{o}C suggest early maturity with respect to oil generation (Appx. 6). Generally, Tmax increases with depth in the Three Forks (Fig. 11-2C).

Vitrinite includes OM derived from vascular plants whose reflectance (Ro) of light increases with maturity. For this reason, vitrinite reflectance can be used as an optical

method for measuring the source rock maturity. Since Tmax obtained indicates the level of thermal maturity, it is possible to convert it to Ro using a mathematical expression (Eq. 26) that is applicable for type II and type III kerogens as proposed by Peters et al., (2005a).

$$Ro\ (calculated) = 0.018\ Tmax - 7.16 \ldots (Eq.\ 26)$$

The calculated vitrinite reflectances of samples from all five lithofacies (Tab. 11-2) supports a claim that reasonable Ro for the Three Forks can only be obtain when Tmax > 400°C.

11.4 Quality of Organic Matter

Kerogen is a mixture of macerals and restructured degradation outcomes of OM and constitute the particulate fraction of OM remaining after extraction of pulverized rock with organic solvents or inorganic acids such as HCl and HF (Durand, 1980). Bitumen refers to the fraction of the organic matter that is soluble in organic solvents which may develop from lipid components in once-living organisms, but mostly by the thermal dissociation of the kerogen.

The type of OM plays a crucial role in qualifying source rocks. It is common for kerogen to be grouped into four classes, based upon provenance, as indicated by their hydrogen, carbon and oxygen content (Demaison et al., 1983; Jacobson, 1991; Peters and Cassa, 1994). Both the pseudo Van Krevelen diagram (Fig. 11-3) and the kerogen quality plot (Fig. 11-4) suggests that these samples are a mixture of oil prone Type II and gas prone Type III as classified in Appendix 6, indicating that the Three Forks has some potential to generate hydrocarbon with lithofacies 4 and 5 having the greatest potentiality.

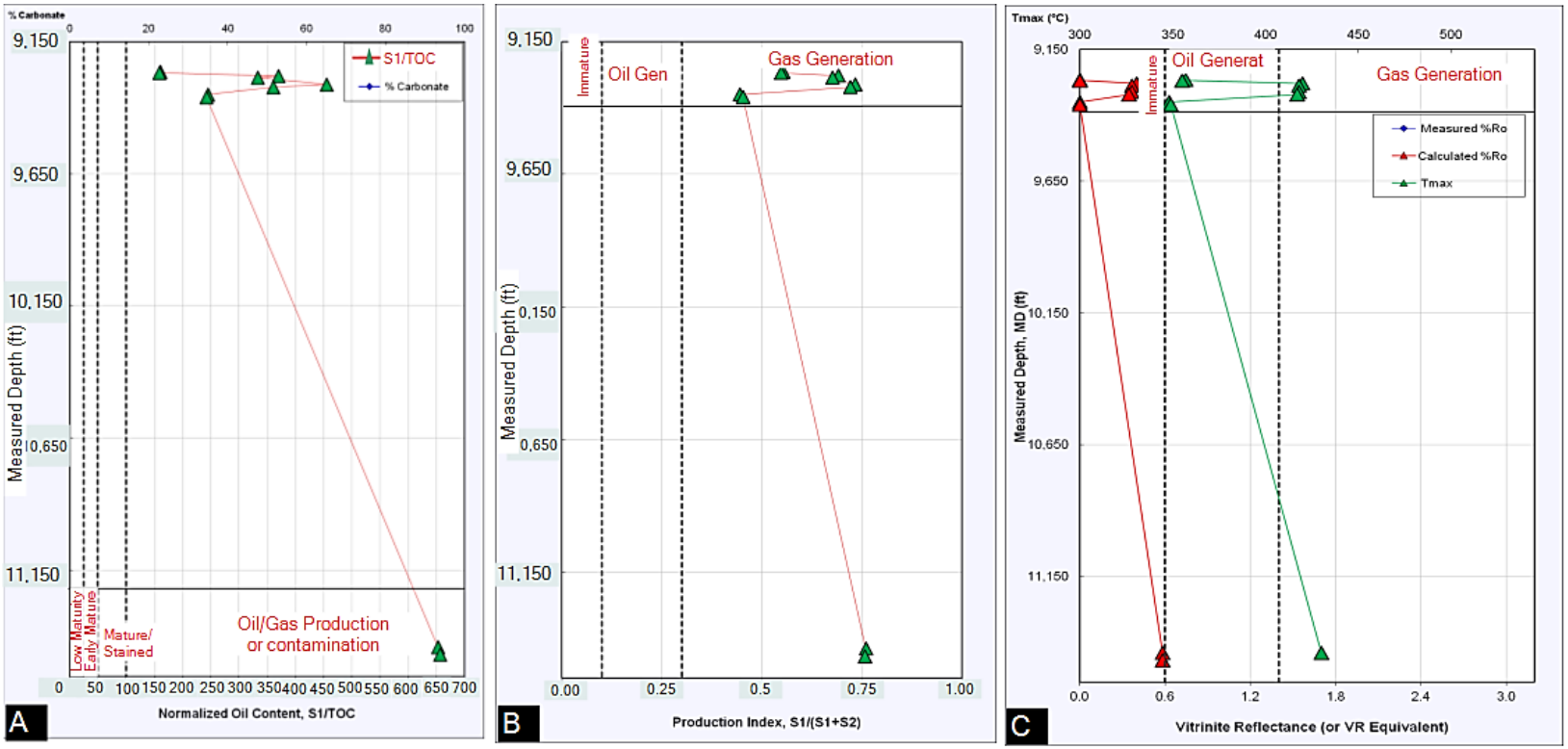

Figure 11-2: Hydrocarbon Logs of the Three Forks Formation. (A) Normalized oil content (S1/TOC) versus depth, (B) Production Index versus depth (S1/S1+S2), (C) calculated vitrinite reflectance and Tmax versus depth.

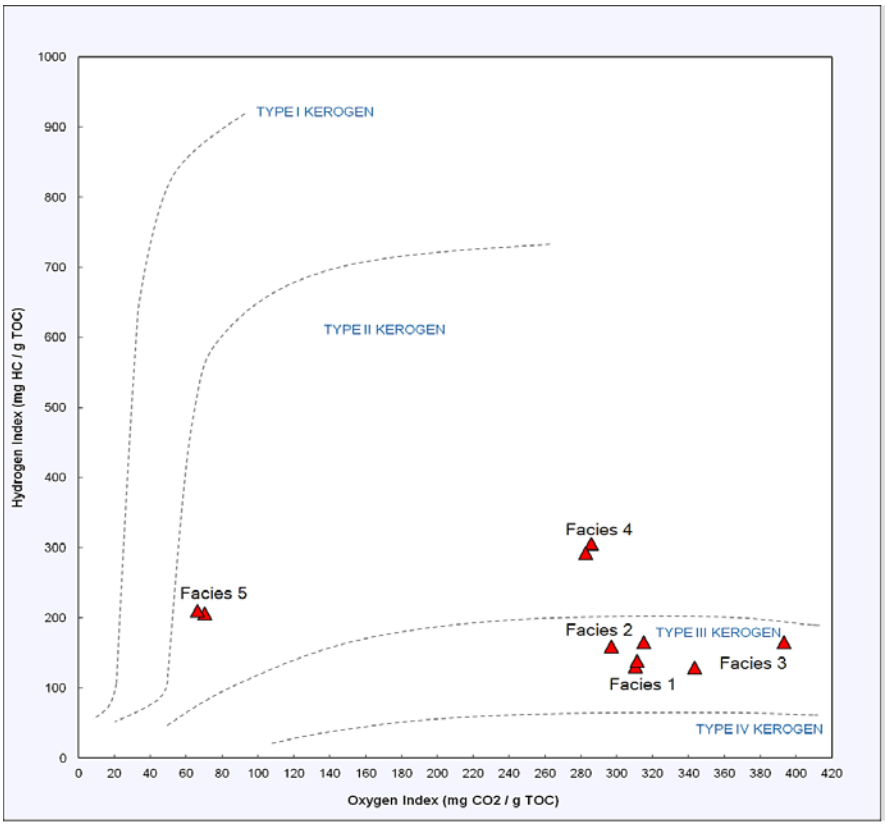

Figure 11-3: Pseudo Van Krevelen Plot of the Three Forks Fomation. Kerogen type (dashed lines) and sample results (red triangles). (After: Hunt, 1996).

In general, higher HI values correspond with higher oil-generative potential hence, the type of hydrocarbons (oil/gas) generated would depend on the hydrogen content of the OM (Snowdon et al., 1998). Organic matter containing Type II–III mixtures may arise from mixtures of terrigenous and marine organic matter with varying oil and gas generation potential or from partially oxidized marine Type II resulting from incomplete preservation during deposition (Alizadeh et al., 2012).

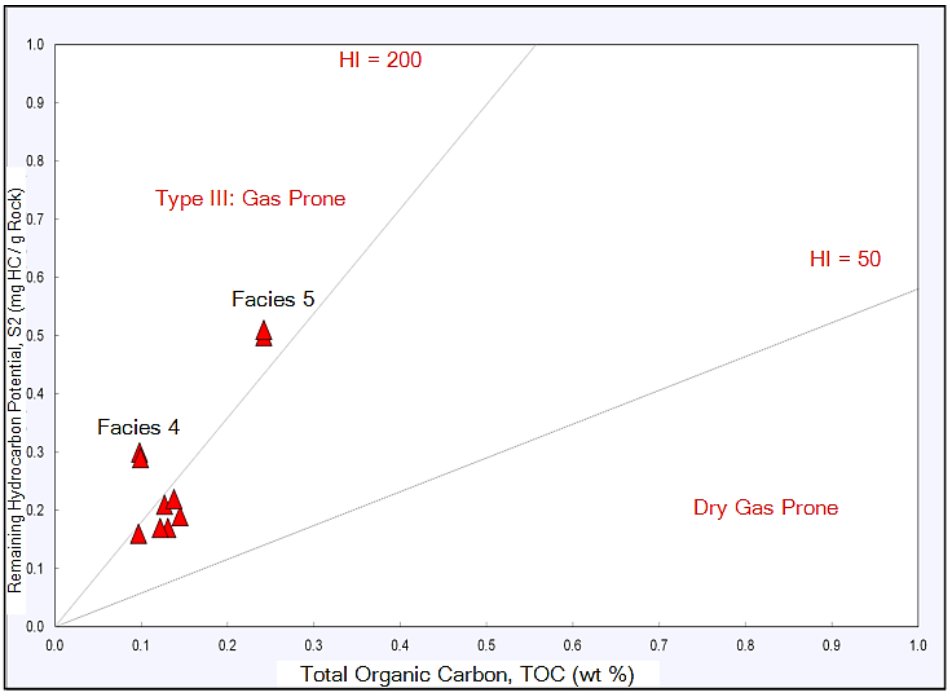

Figure 11-4: Kerogen Quality Plot of TOC versus Remaining Hydrocarbon Potential (S2) for Lithofacies 1 through 5.

11.4.1 Generative Potential (GP)

The GP of a rock can be defined in terms of its genetic potential which is the sum of the quantity of hydrocarbons that the rock has already generated (S1) and those that the rock could still produce if maturation continues (S2) in mg/g of rock (Tissot and Welte, 1978; Hunt, 1996). Therefore, the GP represents the maximum quantity of hydrocarbons that a sufficiently matured source rock might generate. The observed S2 measurements of less than 2 mg HC/g of rock is evidence that all five lithofacies have poor to fair generative potential averaging 0.86 mg/g (Ibrahimbas and Riediger, 2002) (Fig. 11-5).

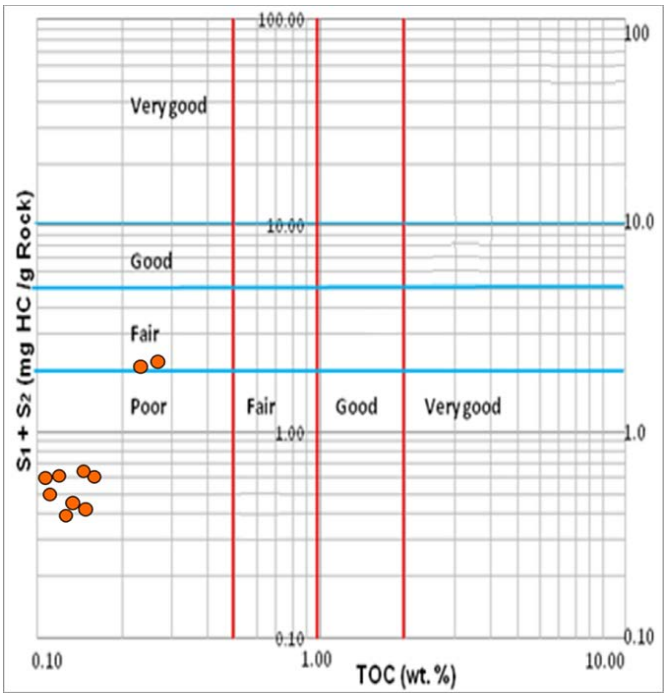

Figure 11-5: Classification of the Generative Potential of the Three Forks Formation using Dembicki's Scheme (2009).

11.4.2 Level of Maturity

Thermal maturity refers to the relative degree of temperature-time progressive alteration of OM to oil, wet gas, and eventually to dry gas and pyrobitumen (thermally-altered, solidified bitumen that is insoluble in organic solvents) (Hunt, 1979; Tissot and Welte, 1984). A thermally immature rock has not been subjected to enough heat to initiate the process of converting kerogen to oil and/or gas while a thermally overmature rock has been under enough heat to modify the OM to graphite. Thermally mature rocks are within the oil window with several intermediate stages (Appx.6).

11.4.3 HI versus Tmax

The HI versus Tmax diagram is the most commonly used method to interpret the type

and maturity of OM in sediments. Figure 11-6 shows that all samples from the Three Forks Formation are immature although the degree of maturity of the OM increases with depth. Lithofacies 5 with a *Ro* value of 0.6% show that the formation is in the immature to early mature stage with respect to oil generation.

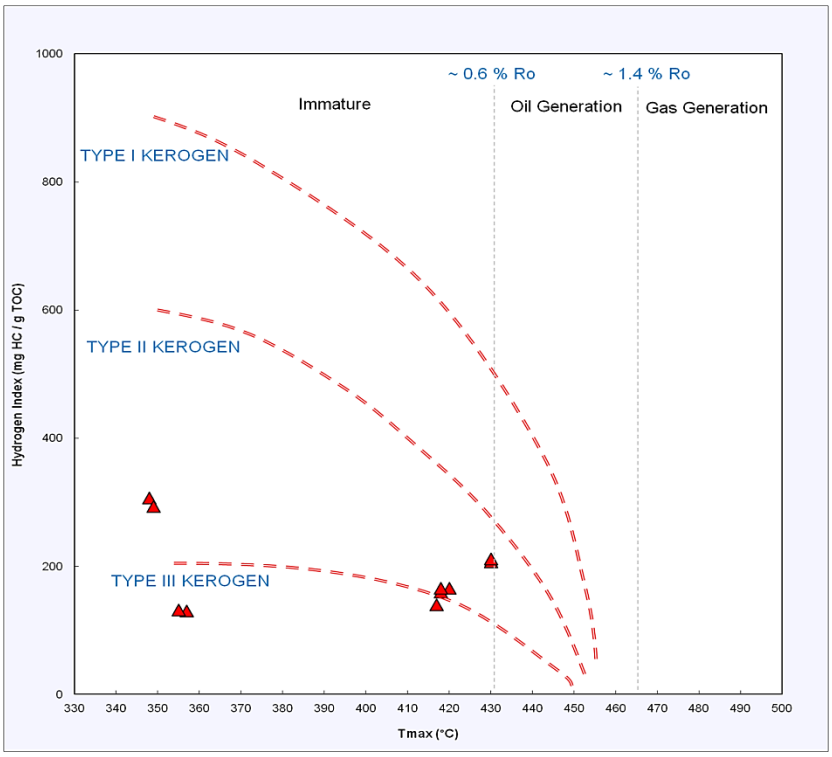

Figure 11-6: Relationship between HI and Tmax. Thermal alteration pathways Types I, II, and III are indicated by dashed lines. Dotted lines indicate approximate vitrinite reflectance values.

11.5 Source of Hydrocarbon

TOC and HI values are influenced by maturation and contamination (Alizadeh et al., 2012).The origin of the hydrocarbon produced, i.e., indigenous or non-indigenous may be verified by cross-plotting PI and Tmax or S1 and TOC (Fig. 11-7). Generally immature OM has Tmax and PI values less than 435°C and 0.10 respectively. This marks the onset of oil generation with PI increasing from approximately 0.1 to 0.4 through the oil window

(Espitalie et al. 1985/1986). Nordeng (2012) discouraged the use of PI within the Williston Basin because of the prevalent use of oil-based drilling mud (OBM) which masks the true oil content of potential source rocks. The observed PI values range from 0.55 to 0.76 while Tmax range from 348 to 430 °C.

As a general guide, a plot of S1 versus TOC is used to discriminate between non-indigenous and indigenous hydrocarbons (Hunt, 1996). The dividing line (Fig. 11-7) is equivalent to the ratio S1/TOC =1.5 where indigenous hydrocarbons plot below while migrated hydrocarbons plot above. Thus all samples from these lithofacies indicate some contribution from non-indigenous (expelled) hydrocarbons suggesting that the migrated hydrocarbon were not generated in situ but were generated by older, deeper source rocks, possibly the Birdbear Formation.

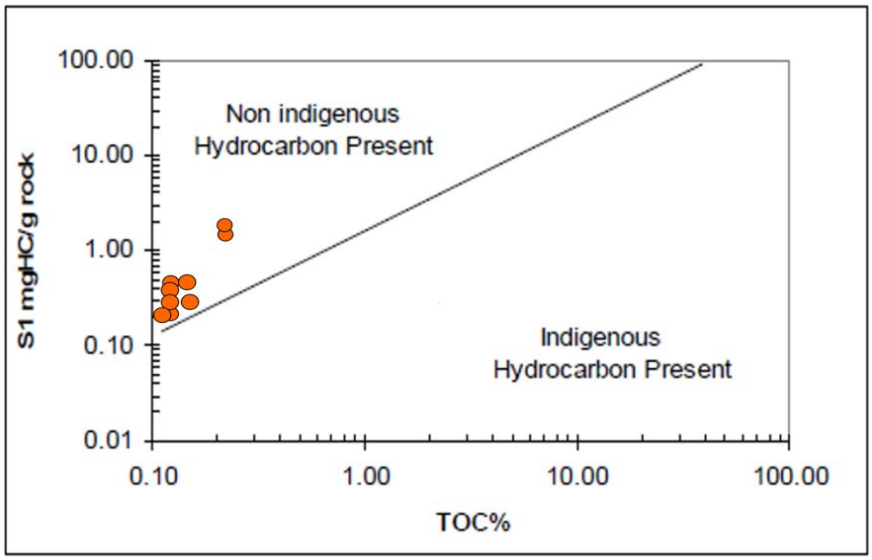

Figure 11-7: Plot of S1 versus TOC Suggesting Non-indigenous Hydrocarbons of the Three Forks Formation.

CHAPTER 12

RESERVOIR QUALITY

The Three Forks Formation is characterized by low porosities and very low permeabilities with very little correlation between them. Data from core analysis suggests average porosity values of 8% and permeability of 0.016 mD. Poor amounts of intercrystalline (trace to 2%) and microvuggy (1%; Facies 1 only) porosities, plus microporosity are the only visible pore types. Microporosity may be associated with the dolo-micrite and other matrix material. The intercrystalline pores are mostly isolated and are poor to moderately inter-connected. The interconnection of the pore system in these facies is limited mostly by the abundance and distribution of dolomite and hematite cements.

Furthermore, trace pyrite cement is irregularly distributed and occlude pores, plus limit the interconnectivity. Scattered disrupted lamina in portions of Facies 1 and Facies 3 make the heterogeneous distribution of pores and causes local isolation of intercrystalline pores. In places, the moderately connected intercrystalline pores are separated or bounded by tight dolo-micrite rich laminae (Figs. 8-4C; 8-5A to C). Moreover, Figures 8-4, plus 8-5B to D displays the intercrystalline and microvuggy pores, which are locally interconnected in certain portions of the facies. The small pore throats and poor interconnectivity of these pores will experience high capillary pressure and are therefore ultimately responsible for the low permeability values obtained by routine core analysis.

The reservoir quality assessment took into consideration the results from petrographical thin section and SEM examinations, plus XRD data. Overall the reservoir quality is controlled by both diagenetic (dolomitization and precipitation of hematite) and the depositional events (matrix, grain sizes or scattered clasts). Based on the visible porosities and the interconnectivity among pores the reservoir quality for the studied facies can be assessed as poor to moderate for Facies 1 and Facies 3, while poor for Facies 4. The following table summarizes the reservoir quality and the porosity controlling factors (major and minor) for the three Three Forks Formation facies:

Table12-1: Summary of Reservoir Quality and Porosity Controlling Factors for the 3 Facies of the Three Forks Formation.

Sample ID	Location	Pore Types	Thin Section Porosity (%)	Main ϕ Controls	Minor ϕ Controls	RQ
Facies 1	Top	Ix1, mV, mP	3	Comp, Dol, Hem	Cal, Clasts, Py	P-M
Facies 3	Middle	Ix1, mP	2	Comp, Dol, Hem	Cal, Clasts, Py	P-M
Facies 4	Lower	Ix1, mP	Trace	Hem, Comp, Dol	Clasts, Py	P

Legend

Pore Types: Ix1– Intercrystalline; mP– micro-porosity; mV– micro-vuggy
Reservoir Quality (RQ): P– poor; M– moderate; G– good
Porosity Controls: Dol– dolomitization; Py– pyrite; Cal– calcite; Hem– hematite
Clast– clay or dolomicrites rich clast
Comp. – mechanical compaction

12.1 Potential Reservoir Problems and Implications

Potential reservoir problems include:

1. Heterogeneous distribution of the pore system. Considering the generally heterogeneous and locally poor pore system, fracture stimulation could be considered to create an overall more homogeneous production environment, improve interconnection of locally isolated pores and increase flow rates. After fracturing production rate should be held under a "critical velocity" flow rate to avoid migration of formation fines that were created during the fracturing process.

2. Sensitivity of dolomite and hematite to hydrofluoric (HF) acid in regards to precipitation of calcium fluoride scales and precipitation of iron hydroxide gels. Potential sensitivity of ferroan dolomite, chlorite, siderite and pyrite to hydrochloric (HCl) or HF acids with respect to the formation of precipitates that may block pore throats. This precipitate problem is usually avoided if an oxygen scavenger and an iron chelating or sequestering agent is added to the HCl acid. These agents can be effective in preventing iron hydroxide gel precipitation, forming a stable complex with dissolved iron and keeping it in solution. It is important to determine the optimum concentration of sequestrating agents; overuse may results in severe gel precipitation.

3. Obstruction of the intercrystalline and micro-vuggy pore systems by abundant authigenic cements (dolomite and hematite).

4. Migration of remnant carbonate fines after any hydrochloric (HCl) acid treatments. Too much use of HCl could cause fabric collapse and migration of carbonate fines, which would be detrimental to production.

5. Migration of formation fines (carbonates, illite and kaolinite clays plus organics) to pore throat-blocking positions. If possible the production rate should be held under a "critical velocity" flow rate to avoid migration of significant amounts of fines.

CHAPTER 13

DISCUSSION

The absence of SCAL data puts a lot of constraint in the analysis of the Three Forks Formation especially with the lack of laboratory clay densities and water resistivities. For modeling, wet-clay densities from Pickett plots and a dry clay density of 2.71 g/cc are used. To understand the causes of observed heterogeneities, a critical examination of the geological controls of the reservoir quality is recommended.

Lithologically, the Three Forks in North Dakota consists of interbedded shale, dolo-mudstone/sandstones and minor anhydrite with a typical oxidized color at its base, and becomes greenish grey to bluish green towards the top of the Formation. Brecciation within the formation is common. The breccia is mostly sand-sized tan to medium brown dolomite and white anhydrite embedded in grey-green shales or dark brown mudstones. Patterns very similar to the predicted sedimentary environments in this study can be observed in modern carbonate epicontinental seas such as the Persian Gulf.

The measured TOC (wt. %) revealed that the Three Forks Formation has poor to fair source rock potentiality. Plotting of TOC against the generation potential (S1+ S2) confirms this conclusion (Fig. 11-5). The kerogen is a mixture of oil-prone type II and gas-prone type III as illustrated on the Pseudo Van Krevelen plot diagram (Fig. 11-3). The same result can be inferred from Tmax against HI. The very high values of PI and

the plot of S1versus TOC indicate non-indigenous hydrocarbons with contamination probably increasing with depth. The plot of Tmax versus HI also indicates immature to near mature organic matter within the studied lithofacies (Fig. 11-6). The overall maturity trend shows that the maturity and petroleum potential of the Three Formation units increases with depth. Finally, the determination of TOC and OI may provide clues concerning the "richness" of a formation but the more important question that needs to be answered has to do with the history of oil generation (Nordeng, 2012).

The proposed depositional model is that dolomitization probably took place on a protected ramp setting possibly a barrier reef environment that prevented the free refluxion of waters from a lagoon or an epicontinental depression. The restricted circulation of sea water within the peritidal zones actively encouraged the formation of a gypsum mush which further accelerated the accumulation of a hypersaline brine. As the brine displaced the surrounding less dense waters, it slowly seeped through the slightly permeable precursor calcite and metastable carbonates of the lagoon floor. During this process, calcium was progressively replaced by magnesium and dolomites recrystallized.

CHAPTER 14

CONCLUSIONS

The lithology of the Three Forks Formation in North Dakota has been studied in detail to provide answers that fit the study objectives using both field and laboratory techniques. Data were gathered from well logs through petrophysical analysis, detailed core description, geochemical analysis, and petrographical investigations, and information on the stratigraphic geometry, depositional environments, and petroleum potential of the Three Forks was provided. Through core description and computer modeling, the lithology of the Three Forks is found to be unusual and heterogeneous, consisting of different textures of dolomitic mudstones, shales, and various forms of anhydrite. Evidently, nodular and bedded anhydrites occur together within the lower units, associated with oxidized dolomudtones with probable origin tied to a sabkha-like environment. Currents were mild to moderate, and the sea floor was predominantly lime mud and/or clay throughout the study area. Also, the environmental conditions changed from more oxygenated and of abnormal salinity waters to a more reducing environment from bottom to top of the formation. Soft sediment deformation and unloading fractures are common and may provide preferential flow within the formation.

Five lithofacies have been identified at the core-scale. These lithofacies correlate closely with electrofacies predicted using a combination of principal component analysis plus

clustering algorithms. The depositional system has been reconstructed based on interpretations of facies characteristics and their lateral and vertical relationships. Facies types and assemblages of this Upper Devonian succession represent a shallow-marine carbonate system of epeiric, ramp-like environment. From the absence of faunas, it is concluded that deposition was rather rapid and/or conditions were inhospitable to organisms after deposition. Large scale juxtaposition of these depositional facies indicates fluctuations in sea-level which resulted in substantial shifts in the position of the paleo-shoreline involving very shallow and subaqueous settings where more supratidal-dominated conditions prevail.

Geophysical data from 32 wells is combined (128 logs) to provide an across-the-board evaluation of the petrophysical characteristics of the Three Forks Formation. The limited data on routing core analysis from 4 wells is used to guide the interpretation of the remaining 28 wells. Overall, the clay volume is high, averaging 35%. Results from log and routine core analysis showed that the Three Forks in the studied wells has average porosities between 6.5 and 10% with a mean value of 8%; the mean permeability is about 0.016 mD. The grain density averages 2.79 g/cc. The expected yields i.e. oil saturation is low (~10%) while water saturation is very high (~ 80%). The use of a dual water model for *Sw* analysis rather than Archie models is recommended.

Geochemical data showed that the Three Forks has poor to fair petroleum potential, consisting of immature organic types II and III kerogens. Also, the petroleum potential

probably increases with depth as indicated by results from TOC and Rock-Eval pyrolysis. The Three Forks Formations has very poor source rock potentiality and the hydrocarbons within the formation are interpreted as non-indigenous, probably from the Birdbear Formation. Even though the lithology of the Three Forks Formation varies quite a lot laterally, the vertical stacking expression of its units do not vary greatly. As a result, the TOC content can be predicted if the different lithofacies can be identified.

Petrological studies of samples from three facies representing the top, middle and lower portions of the Three Forks revealed that the Three Forks is dominated by dolomite, along with substantial hematite, minor monocrystalline quartz and mica flakes, trace feldspar, calcite and pyrite. Dolomitization is pervasive and no original carbonate texture is detectable. In addition, pervasive dolomitization appears to have created all the visible small intercrystalline pores. The dolomite was precipitated in three stages. In places all dolomite types are slightly ferroan. Moderate to abundant hematite appears as micro-blebs and stains dolomite rhombs and clay matrix, plus occurs as intercrystalline and or micro-vuggy pores occluding cement. Rare pyrite also locally replaces dolomite rhombs.

Combined bulk and clay XRD rock composition shows that the clays mainly consist of illite, chlorite, and kaolinite. The illite detected in XRD and SEM is mostly detrital illite with rare portion could being muscovite. Intercrystalline, rare micro-vuggy, plus micro-porosity are the main porosity types. The pores are locally moderately connected or elsewhere are isolated to poorly inter-connected. The reservoir quality, controlled by diagenetic and the depositional events is considered to be poor to moderate. Potential

reservoir problems include: 1) heterogeneity of the pore system due to abundant disrupted laminae, 2) potential acid sensitivity of iron-bearing minerals, 3) the sensitivity of calcium carbonate (both the dolomite and calcite) to hydrofluoric acid, 4) migration of carbonate, organic matter, kaolinite and illite clay fines to pore throat blocking positions.

APPENDICES

APPENDIX 1

Description of the XRD Techniques

In the XRD technique, small portions of each sample were analyzed for bulk and clay mineralogy. The clay fraction (less than 3 μm size) of each sample is separated from the bulk sample by the centrifuging method. In order to fractionate, samples are first treated in an ultrasonic bath using sodium hexametaphosphate as a deflocculating agent that facilitates complete disintegration of the matrix from the grains. The samples are then centrifuged in two phases. In the first phase, the sample is centrifuged at 600 rpm for 5 minutes that enable coarser particles to settle down at the bottom of the tube.

The clay size particles remain in the fluid in suspension, which is decanted to another tube and the clay size particles collected from this fluid after the second phase of centrifuging at 3000 rpm for 20 minutes. The clay fraction is mounted on a glass slide, dried and run and then placed in a glycol vapor bath for 24 hours and then run again in order to identify expandable clays. Weight fractions are measured for both bulk and clay portions of the sample. It should be noted that six XRD samples (two from each facies) are taken from the same position as the thin section samples.

The Bulk and Clay XRD

In identifying crystalline ‘‘fingerprints’’ of unknown samples by XRD technique, the

d-spacings (i.e., the distance between adjacent planes of atoms) is compared with standard reference patterns and measurements (Chen, 1977). The technique has its roots in the examination of the nature of crystal lattices by the diffraction of X-rays through the closely spaced lattice of atoms (Ewald, 1962). X-ray diffraction is a semi-quantitative analytical technique (approx. 10% at best) and identifies only crystalline substances; amorphous (non-crystalline) substances are not detected. Quantification is based on the fact that individual mineral peak intensities are equivalent to their relative amount in the sample.

APPENDIX 2

Rock-Eval Time-Signal Results for the Three Forks Formation.

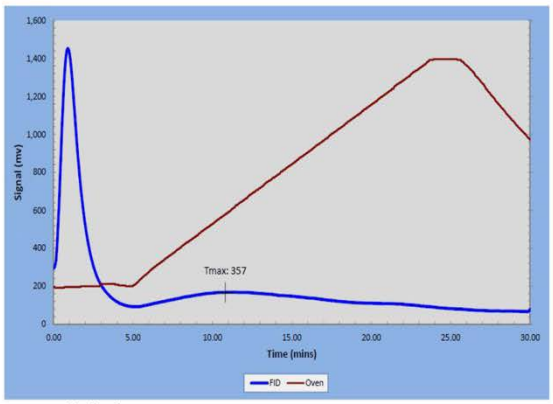

Facies 1

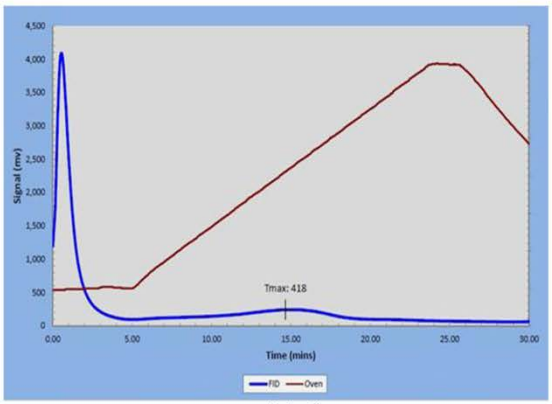

Facies 2

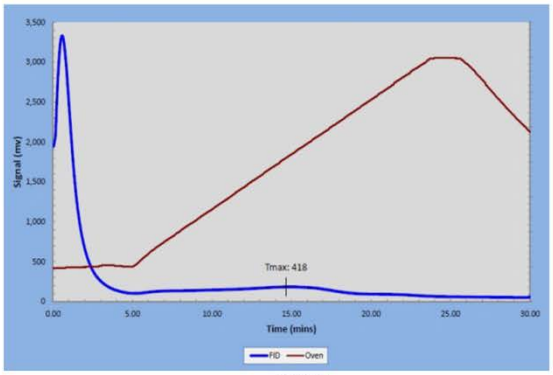

Facies 3

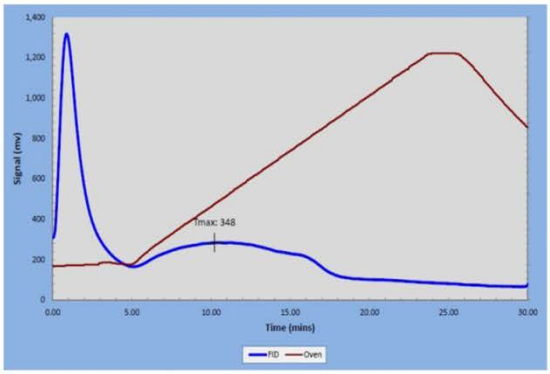

Facies 4

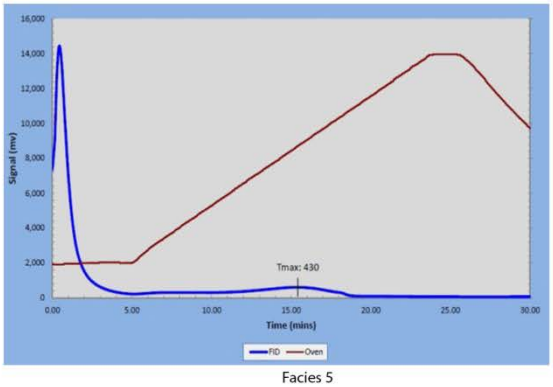

Facies 5

APPENDIX 3

Procedure for Thin Section and SEM Analysis

Thin sections are impregnated with blue epoxy (to identify porosity and preserve textures), polished and mounted onto a glass slide. Next, the samples are ground down to a total thin section thickness of 30μm. Later, the samples are stained with a combined carbonate stain of Alizarin Red-S solution to distinguish calcite from dolomite (Friedman, 1959) and potassium ferricyanide to highlight ferroan carbonate, rich in iron(II) oxide (Dickson, 1965). Finally, a second glass slide is glued on the polished surface. The prepared thin sections are examined petrographically and visual estimates of grains and cements are obtained by point counting (300 points).

In order to perform SEM study, a small piece of each sample is glued on to an aluminum stub and after lightly blowing off loose particles with air the sample is coated with gold to facilitate observations and photography. The gold-coated sample is examined in a SEM to highlight the occurrence, distribution and origin of micropores, plus constituent minerals and their textural features.

APPENDIX 4

Wells Used for Stratigraphic and Petrophysical Modeling and Core Description

Well	ID	API	Name	County	Field
1	6095	33-007-00203	E.E Miller No. 10-1	Billings	Wildcat
2	6140	33-007-00209	BN No. 1-25	Billings	Wildcat
3	6169	33-007-00206	State School Land	Billings	Wildcat
4	6341	33-007-00233	Federal No. 4-33	Billings	Four Eyes
5	6346	33-007-00234	Whitetail Creek Unit No. 15-11	Billings	Wildcat
6	15046	33-007-01431	Zabolotny 8-4	Billings	Little Knife
7	11617	33-053-02076	Pagem 01-13	McKenzie	Wildcat
8	12019	33-053-02163	Rose No. 1	McKenzie	Wildcat
9	12983	33-053-02340	Spring Creek No. 27X-31BN	McKenzie	
10	13098	33-053-02357	Stenehjem ND 27 No. 1	McKenzie	Wildcat
11	14947	33-053-02534	Stenehjem No. 43-27	McKenzie	North Fork
12	16433	33-053-02769	Lars Rothie 32- 29H	McKenzie	Blue Buttes
13	16581	33-053-02794	Curls No. 23-14	McKenzie	Ellsworth North Field
14	16652	33-053-02806	Levang 3-22H	McKenzie	Wildcat
15	16689	33-053-02809	Linseth 4-4H	McKenzie	Wildcat
16	17067	33-053-02858	Sakakawea Federal 13X-35	McKenzie	Charlson
17	5088	33-061-00187		McKenzie	White Earth River
18	12033	33-061-00344	Sun-Marathon-Shobe 01	Mount rail	Wildcat

19	16824	33-061-00577	Rs Nelson 156-91-1423H-1	Mount rail	Wildcat
20	16841	33-061-00581	Deadwood Canyon Ranch	Mount rail	Wildcat
21	16997	33-061-00630	Van Hook 1-13H	Mount rail	Parshall
22	17023	33-061-00641	Braaflat 11-11H	Mount rail	Sanish
23	17043	33-061-00653	St Andes 151-89-2413H-1	Mount rail	Banner
24	17071	33-061-00666	RS State C-157-90-3603H-1	Mount rail	Ross
25	17096	33-061-00680	Farhart 11-11H	Mount rail	Wildcat
26	17272	33-101-00473	IM-Shorty 159-88-0806H-1	Ward	Wildcat
27	3363	33-105-00633	Clarence Pederson # 1	Williams	Wildcat
28	17015	33-105-01667	Nesson State 42X-36	Williams	Manitou
29	19709	33-023-00658	Rosenvold 1-30H	Divide	Norse
30	19918	33-053-03358	Charlotte 1-22H	McKenzie	Banks
31	19951	33-105-02037	Lokken 2-2H	Williams	Sauk
32	20411	33-025-01299	State Jaeger 12116H14294	Dunn	

Cores Described		**Interval (feet)**	
Well	API		
16824	33-061-00577	9292	9330
16841	33-061-00581	10189	10268
17272	33-101-00473	7540	7662
16581	33-053-02794	11033	11096
19918	33-053-03358	11360	11500
19951	33-105-02037	9247	9362
17067	33-053-02858	9871	9900

APPENDIX 5

The Wentworth grain size classification. Note that all particles finer than sand (1/16 − 2.0 mm) are included as mud and all particles coarser than sand are included as gravel. http://www-odp.tamu.edu/publications/200_IR/chap_02/c2_f7.htm

Millimeters (mm)		Micrometers (μm)	Phi (ϕ)	Wentworth size class		Rock type
	4096		-12.0	Boulder	Gravel	Conglomerate/ Breccia
	256		-8.0	Cobble		
	64		-6.0	Pebble		
	4		-2.0	Granule		
	2.00		-1.0	Very coarse sand	Sand	Sandstone
	1.00		0.0	Coarse sand		
1/2	0.50	500	1.0	Medium sand		
1/4	0.25	250	2.0	Fine sand		
1/8	0.125	125	3.0	Very fine sand		
1/16	0.0625	63	4.0	Coarse silt	Silt	Mud
1/32	0.031	31	5.0	Medium silt		
1/64	0.0156	15.6	6.0	Fine silt		
1/128	0.0078	7.8	7.0	Very fine silt		
1/256	0.0039	3.9	8.0			
	0.00006	0.06	14.0	Clay		

APPENDIX 6

Geochemical parameters applied to TOC and Rock-Eval Pyrolysis and vitrinite reflectance in the assessment of the amount, character of expelled products, thermal maturity, and type Kerogen quality. (After, Peters, 1986; Tissot and Welte, 1984; Tissot et al., 1987, Peters and Cassa, 1994).

Measurement		**Index**			
		Quantity	**TOC (wt.%)**	**S1**	**S2**
A	Source Potential	Poor	0.0 -0.5	0.0 -0.5	0.0-2.5
		Fair	0.5-1.0	0.5-1.0	2.5-5.0
		Good	1.0-2.0	1.0-2.0	5.0-10.0
		Very good	>2.0	>2.0	>10
		Type	**HI**		**S2/S3**
B	Type of Hydrocarbon	Gas	0-150		0-3
		Gas/Oil	150-300		3-5
		Oil	>300		>5
			Tmax (°C)	**PI**	**%Ro**
C	Stage of Thermal Maturity	Immature	<435		
		Early Mature	435- 445	0.1	0.5
		Peak	445-450		
		Late	450-470	0.4	>1.1
		Postmature	>470		
			HI	**S2/S3**	**Main Product**	**Petroleum Potential**
D	Kerogen Type	**I**	>600	>15	Oil	High
		II	300-600	10-15	Oil	Poor
		II/III	200-300	5-10	Oil/gas	Poor
		III	50-200	1-5	Mainly gas	Poor
		IV	<50	<1	none	

APPENDIX 7

Comparisons of core-derived *Sw* with log-calculated *Sw* for several shaly-sand models using well 19918. These models seem to either underpredict or overpredict *Sw* and the deviation worsens for lower values of Sw.

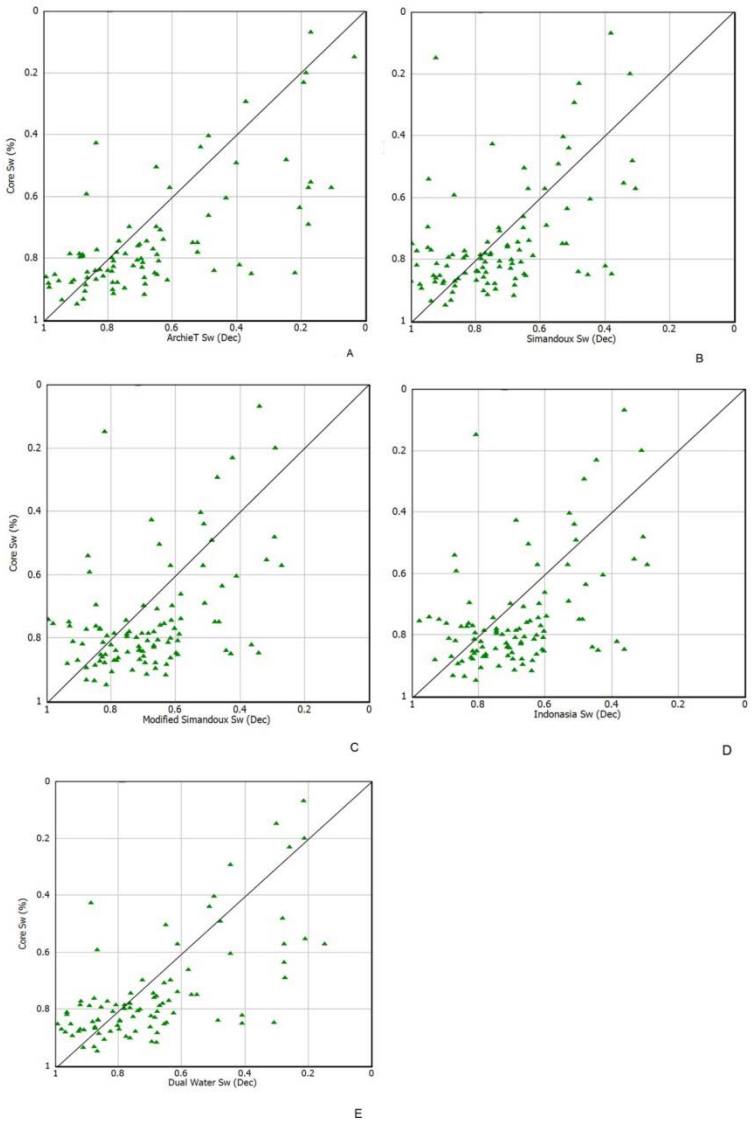

REFERENCES

Adams, J., and Rhodes, M., 1960, Dolomitization by seepage refluxion: American Association of Petroleum Geologist Bulletin, v. 44, no. 12, p. 1912-1920.

Ahr, W.M., 1973, The carbonate ramp: an alternative to the shelf model: Gulf Coast: Association of Geological Societies Transactions Transactions, v. 23, p. 221-225.

Ahr, W.M., 1998, Carbonate ramps, 1973-1996: a historical review; *in* Wright, V.P. and Burchette, T., Carbonate ramps: Geological Society, London, Spec. Pub. v. 149, no. 1, p. 7-14.

Al-Awadi, M., Clark, W., Moore, W., Herron, M., Zhang, T., Zhao, W., et al., 2009, Dolomite: Perspectives on a Perplexing Mineral: Oilfield Review, no. 3, 14 p.

Alizadeh, B., Sarafdokht, H., Rajabi,M., Opera, A., Janbaz, M., 2012, Organic geochemistry and petrography of Kazhdumi (Albian–Cenomanian) and Pabdeh (Paleogene) potential source rocks in southern part of the Dezful Embayment, Iran: Organic Geochemistry, 49, p. 36-46.

Anna, L.O., Pollastro, Richard, and Gaswirth, S.B., 2013, Williston Basin Province—Stratigraphic and structural framework to a geologic assessment of undiscovered oil and gas resources, chap. 2 *of* U.S. Geological Survey Williston Basin Province Assessment Team, Assessment of undiscovered oil and gas resources of the Williston Basin Province of North Dakota, Montana, and South Dakota, 2010 (ver. 1.1, November 2013): U.S. Geological Survey Digital Data Series 69–W, 17 p.

Archie, G. E., 1942, The electrical resistivity log as an aid in determining some reservoir characteristics: Petroleum Transactions of the AIME, v. 146, p. 54-62.

Archer, A.W., 1993, Tidal processes in the fluvio-tidal transition within estuaries, *in* Incised Paleovalleys of the Douglas Group in Northeastern Kansas; Field Guide and Related Contributions, A.W. Archer, H.R. Feldman, and W.P. Lanier, eds.: Kansas Geological Survey, Open-file Report 93-24, section 2, 35 p.

Arps, J.J., 1964, Engineering concepts useful in oil finding: American Association of Petroleum Geologist Bulletin, v. 43, no.2, p.157-165.

Baillie, A.D., 1953, Devonian names and correlations in Williston Basin area: American Association of Petroleum Geologist Bulletin, v. 37, p. 444-452.

Bahremandi, M., Mirshahani, M., Nazarian S.P., and Zamani, Z., 2013, Application of O and C isotopes and trace elements as evidence for original mineralogy in Precambrian dolomite and limestone sediments, Iran: Journal of Scientific Research and Reviews, v. 2, no. 44, p. 056-066.

Bateman, R.M., 1985, Openhole log analysis and formation evaluation, Boston: IHRDC.

Beitsch, R., 2010, Three Forks formation to yield lots of oil in North Dakota, Retrieved Feb.06, 2011: The Bismarck Tribune: http://www.bismarcktribune.com/news/state-and-regional/article_368dcb38-53ef-11df-a6c8-001cc4c03286.html

Benson, A.L., 1966, Devonian stratigraphy of western Wyoming and adjacent areas: American Association of Petroleum Geologist Bulletin, v. 50, p. 2594-2601.

Berner, R.A., 1980, Early diagenesis a theoretical approach: Princeton: Princeton University Press, 241 p.

Berry, G.W., 1943, Stratigraphy and structure at Three Forks, Montana: Geological Society of America, 54, pp. 14-16.

Berwick, B. R., 2008, Depositional environment, mineralogy, and sequence stratigraphy of the Late Devonian Sanish Member (Upper Three Forks Formation), Williston Basin, North Dakota: Master's Thesis, Colorado School of Mines, Golden, Colorado, 263 p.

Bish, D.L., and Post, J.E., 1989, Modern powder diffraction: Mineralogical Society of America, Reviews in Mineralogy, v. 20, 369 p.

Bissada, K.K., 1982, Geochemical constraints on petroleum generation and migration-a review, *in* Proceeding from the Association of South East Asian Nations Council on Petroleum 81, Manila, Philippine, October, 1981, p. 69-87.

Boggs, S.Jr., 2009, Petrology of sedimentary rocks, 2nd ed., New York: Cambridge University Press, 600 p.

Boggs, S. Jr., 2000, Principles of sedimentology and stratigraphy, 4rd. ed.: Prentice-Hall, Upper Saddle River, New Jersey, 726 p.

Borchert, R., Fischer, D., Johnson, R., and Gerhard, L.C., 1990, Glenburn field - U.S.A., Williston Basin, North Dakota: American Association of Petroleum Geologist, TR, Stratigraphic Traps I, p. 91-106.

Bornemann, E., Doveton, J., and St.Clair, P., 1982, Lithofacies analysis of the Viola Limestones, *in* South-central Kansas: Kansas Geological Survey, Petrophysical Series 3, 44 p.

Buatier, M., Chauvet, A., Kanitpanyacharoen, A., Wenk, H., Ritz, J., and Jolivet, M., 2012, Origin and behavior of clay minerals in the Bogd fault gouge, Mongolia: Journal of Structural Geology, v. 34, p. 77-90.

Bucheb, J. A. and Evans, H. B., 1994, Some applications of methods used in electrofacies identification: Log Analyst, v. 35, p. 14-26.

Burchette, T., and Wright, V., 1992, Carbonate ramp depositional systems: Journal of Sedimentary Geology, v. 79, issues 1-4, p. 3-57.

Butler, G., 1970, Holocene gypsum and anhydrite of the Abu Dhabi sabkha, tropical coast: an alternative explanation of origin; in, Rau, J.L., and Delliwig, L.F., proceedings of the third salt symposium, Cleveland: Northern Ohio Geological Society, p. 120-152.

Butler, G, 1969, Modern evaporite deposition an geochemistry of coexisting brines, the sabkha, Trucial coast, Arabian Gulf: Journal of Sedimentary Petrology, v. 39, p. 70-89.

Campbell C.V., 1979, Laminae, laminaset, bed and bedset: Sedimentology, v. 8, p. 7-26

Chen, P., 1997, Table of key lines in X-ray powder diffraction patterns of minerals in clays and associated rocks: Indiana Geological Survey Occasional Paper, v. 21, p. 1-67.

Chilingar, G.V., Bissell, H. J., and Fairbridge, R. W., 1967, Carbonate rocks: Origin, occurrence and classification (developments in sedimentology 9A), Elsevier, 475 p.

Christopher, J.E., 1961, Transitional Devonian-Mississippian formations of southern Saskatchewan: Saskatchewan Department of Mineral Resources Report 66, Regina, Saskatchewan, 103 p.

Braithwaite, J.R., Rizzi, G., and Darke, G., 2004, The geometry and petrogenesis of dolomite hydrocarbon reservoirs: Geological Society of London, Special publication 235, p. 413.

Davies, G., and Ludlam, S., 1973, Origin of laminated and graded sediments, middle Devonian of western Canada: Geological Society of America Bulletin, v. 84, p. 3527-3546.

Dean, W.E., Davies, G.R., and Anderson, R.Y., 1975, Sedimentological significance of nodular and laminated anhydrite: Geology, v. 3, p. 367-372.

Demaison, G.J., Hoick, A.J., Jones, R.W., and Moore, G.T., 1983, Predictive source bed stratigraphy; a guide to regional petroleum occurrence: Proceedings of the 11th World Petroleum Congress, London, v. 2, p. 17-29.

Demicco, R.V., and Hardie, L.A, 1994, Sedimentary structures and early diagenetic features of shallow marine carbonate deposits, Tulsa, Oklahoma: Society for Sedimentary Geology, series 1, 265 p.

Dickson, J.A.D., 1965, A modified staining technique for carbonates in thin section: Nature, v. 205, 587 p.

Dunham, R.J., 1962, Classification of carbonate rocks according to depositional texture, *in* Ham, W.E., ed., Classification of carbonate rocks: American Association of Petroleum Geologists Memoir, p. 108-121.

Durand, B.,1980, Kerogen, insoluble organic matter from sedimentary rocks, Paris: Editions Technip., 519 p.

Ellis, D.V., and Singer, J.M., 2007, Well Logging for Earth Scientists. Elsevier Science, New York, NY: Springer-Verlag, Dordrecht.

Engler, T.W., 2003, Fluid Flow in Porous Media – Notes of Class Petroleum Engineering 524 – Fall.

Enos, P., and Moore, C., 1983, Fore-reef slope environment, *in* Scholle, P.A., Bebout. D.G. and Moore, C.H., eds., carbonate depositional environments: American Association of Petroleum GeologistMemoir33, p. 508- 537.

Espitalié, J., Laporte, L., Madec, M., 1977, Rapid method for source rocks characterization and for determination of petroleum potential and degree of evolution: Revue De L'institut Français Du Pétrole (IFP), v. 32, no. 1, p. 23-42.

Espitalié, J., Deroo, G. and Marquis, F., 1985, La pyrolyse Rock-Eval et ses applications; première partie: Rev. Inst. Fr. Pét., v. 40, p. 563-579.

_1986, La pyrolyse Rock-Eval et ses applications, partie III: Rev. Inst. Fr. Pet, v. 41, p. 73-89.

Ewald, P., 1962, Fifty years of X-ray diffraction: international congress of crystallography, Glassgow, Scotland.

Folk, R.L., 1959, Practical petrographical classification of limestones: American Association of Petroleum Geologist Bulletin, v. 43, p. 1-38.

Folk, R.L., 1987, Detection of organic matter in thin sections of carbonate rocks using a White Card: Journal of Sedimentary Geology, v. 54, p. 193-200.

Friedman, G.M., 1959, Identification of carbonate minerals by staining methods: Journal of Sedimentary Petrology, v. 29, no. 1, p. 89-97.

Friedman, G.M., 1965, Terminology of crystallization textures and fabrics in sedimentary rocks: Journal of Sedimentary Petrology, v. 35, p. 643-655.

Garcia-Fresca, B., and Lucia, F., 2006, Outcrop and subsurface comparison of lithology Distributions in the Permian San Andres Formation-Implications for a dolomitization model: WTGS Fall Symposium 2006 – Final Draft.

Gaswirth, B., and Marra, R., 2014,Bakken, Three Forks largest continuous US oil accumulation: Oil and Gas Journal, http://www.ogj.com/articles/print/volume-112/issue-1/exploration-development/bakken-three-forks-largest-continuous-us.html

Ginsburg, R., 1974, Introduction to comparative sedimentology of carbonates: American Association of Petroleum Geologist Bulletin, v. 58, p. 781-786.

Goss, C.J., 1987, The kinetics and reaction mechanism of the goethite to hematite transformation: Mineralogical Magazine, v.51, p. 437–51.

Gregg, J.M., and Sibley, D.F., 1984, Epigenetic dolomitization and the origin of xenotopic dolomite texture: Journal of Sedimentary Petrology, v. 54,p. 908-931.

Gregg, J.M., and Sibley, D.F., 1986, Epigenetic dolomitization and the origin of xenotopic dolomite texture - reply: Journal of Sedimentary Petrology, v. 56, p. 735-736.

Gregg, J.M., and Sibley, D. F., 1987, Classification of dolomite rock textures: Journal of Sedimentary Petrology, v. 57, p. 967–975.

Haldiki, M., Batistakis, Y., and Vazirgiannis, M., 2002, Cluster validity methods: SIGMOD Record 31, p. 40-45.

Hardie, L., 1977a, Sedimentology of the modern carbonate tidal flats of northwestAndros Islands, Bahamas, Baltimore: John Hopkins University Press, Baltimore, 202 p.

Hardy, R.G., and Tucker, M.E., 1988, X-ray powder diffraction of sediments; *in* M.E. Tucker, ed., Techniques in sedimentology, Blackwell, Oxford, UK, 394 p.

Harwood, R.J., 1982, Oil and gas generation by laboratory pyrolysis of kerogen, *in* Cluff, R.M., and Barrows, M.H., eds., Hydrocarbon generation and source rock evaluation (Origin of Petroleum III): American Association of Petroleum Geologist, Reprint Series, no. 24, p. 78-98.

Heckel, P.H., 1972b, Recognition of ancient shallow marine environment, *in* Rigby, J.K., and Hamblin,W.K., Recognition of ancient sedimentary environments: Society of Economic Paleontologists and Mineralogists, Special Publication, 16, p. 226-286.

Hilchie, D.W., 1978, Applied open hole log interpretation: D.W. Hilchie, Golden CO.

Hilchie, D.W., 1982, Applied openhole log interpretation for geologist and engineers: D.W. Hilchie Inc., Golden, CO.

Hsien-Cheng, C., Kopaska-Merkel, C.D., and Hui-Chuan, C., 2002, Identification of lithofacies using Kohonen self-organizing maps: Computers and Geosciences, v. 28, issue 2, p. 223-229.

Hunt, J.M., 1979, Petroleum Geochemistry and Geology: San Francisco, W.H. Freeman and Company, 617 p.

Hunt, J.M., 1996, Petroleum geochemistry and geology, second edition: New York, W.H. Freeman and Company, 743 p.

Human, H.J., Van Der Eerden, J.P., Jetten, L. A.M.J., and Odekerden J.G.M., 1981, On the roughening transition of biphenyl: transition of faceted to nonfaceted growth of biphenyl for growth from different organic solvents and the melt: Journal of Crystal Growth, v. 51, p. 589-600.

Ibrahimbas, A., Riediger, C., 2002, Hydrocarbon source rock potential as determined by Rock-Eval 6/TOC pyrolysis: http://www.em.gov.bc.ca/Mining/Geoscience/ PublicationsCatalogue/OilGas/OGReports/Documents/2004/OG_Report2004 _ibrahimbas_riediger. Pdf

Interactive Petrophysics (IP), 2011, Senergy Software Ltd., Ternan House, North Deeside Road, Banchory, Kincardineshire AB31 5YR, Scotland:http://www.senergyworld.com

Irwin, M., 1965, General theory of epeiric clear water sedimentation, American Association of Petroleum Geologist Bulletin, v. 49, no. 4, p. 445-459.

Jacobson, S.R., 1991, Petroleum source rocks and organic facies, *in* Merrill, R.K., ed., Source and migration processes and evaluation techniques: American Association of Petroleum Geologists Handbook of Petroleum Geology, p. 1-11.

Jarvie, D.M., 1991, Total organic carbon (TOC) analysis, *in* Merrill, R.K., ed., Source and migration processes and evaluation techniques: American Association of Petroleum Geologists Handbook of Petroleum Geology, p. 113-118.

Jones, R.W., 1984, Comparison of carbonate and shale source rocks, *in* J.G. Palacas, ed., Petroleum geochemistry and source rock potential of carbonate rocks: American Association of Petroleum Geologist Studies in Geology, 18, p. 163-180.

Jetten, L.A., Human, H. J., Bennema, P., and Van Der Eerden, J. P., 1984, On the observation of the roughening transition of organic crystals growing from solution: Journal of Crystal Growth, v. 68, p. 503- 516.

Kamel, H. M., and Mabrouk, M. W. (2003, May 20). Estimation of shale volume using a combination of the three porosity logs, Journal of Petroleum Science and Engineering, v. 13, no.40, p.145– 157.

Katz, B.J., 1983, Limitations of 'Rock-Eval' pyrolysis for typing organic matter: Organic Geochemistry, vol. 4, p. 195-199.

Kendall, C.G., 1969, An environmental re-interpretation of the Permian evaporite/ carbonate shelf sediments of the Guadalupe Mountains: Geological Society of America Bulletin, 80, p. 2503-2526.

Kinsman, D.J., 1966, Gypsum and anhydrite of Recent age,Trucial Coast, Persian Gulf, *in* Rau, J.L., Ed., Proceedings of the second salt symposium: Northern Ohio Geological Society, Cleveland, v. 1, p. 302-326.

Langford, F.F. and Blanc-Valleron, M.M., 1990, Interpreting Rock-Eval pyrolysis data using graphs of pyrolizable hydrocarbons vs. total organic carbon: American Association of Petroleum Geologist Bulletin, vol. 70, no. 6, p. 799-804.

LeFever, J.A., and S. H. Nordeng, 2011, Cyclic sedimentation patterns of the Mississippian-Devonian Bakken Formation, North Dakota: Search and Discovery Article #50371, posted January 7, 2011, Oral presentation at American Association of Petroleum Geologist International Conference and Exhibition, Calgary, Alberta, September 12-15, 2010.

Lewis, B., 1975, Nucleation and growth theory, *in* Pamplin, B.R., ed., Crystal growth: Pergamon Press, New York, p. 12-39.

Mandala, N., Chakraborty, C., Samanta, S. K., 2000, Boudinage in multilayered rocks under layer-normal compression: a theoretical analysis: Journal of Structural Geology, v. 22 p. 373-382.

Maiklem, W., Bebout, D., and Glaister, R., 1969, Classification of anhydrite- a practical approach: Bulletin of Canadian Petroleum Geology, v. 17, no. 2, p. 194-233.

Martin, R.E., Carter, E.G., and Davis, L., 2000, Marine and freshwater products handbook, Lancaster: Technomic Publishing Company, Inc., p. 641-62.

Masson, P.,1955, An occurrence of gypsum in southwest Texas: Journal of Sedimentary Petrology, v. 25, p. 72-79.

Momper, J.A., and Williams, J.A., 1984, Geochemical exploration in the Powder River Basin, *in* Demaison, G., and Murris, R.J., eds., Petroleum geochemistry and basin evaluation: Tulsa, OK., American Association of Petroleum Geologist Memoir 35, p. 181-191.

Monicard, R.P., 1980, Properties of Reservoir Rocks: Core Analysis: Gulf Publishing Co., Houston, TX.

Moore, C.H., 2001, Carbonate reservoirs, porosity evolution and diagenesis in a sequence stratigraphic framework, Developments in Sedimentology 55: Elsevier, Amsterdam, p. 444

Moore, R., 1949, Meaning of facies: Sedimentary facies in geologic time, v. 39, p. 1-34

Moore, D.M., and Reynolds, R.C., Jr., 1997, X-ray diffraction and the identification and analysis of clay minerals, 2nd edition: Oxford University Press, Oxford, p. 378.

Murray, R., 1964, Origin and diagenesis of gypsum and anhydrite: Journal of Sedimentary Petrology, v. 34, p. 512-523.

Nordeng, S.H., 2012, Basic geochemical evaluation of unconventional resource plays: Geows, https://www.dmr.nd.gov/ndgs/newsletter/2012%20January/Basic%20Geochemical%20Evaluation%20of%20Unconventional%20Resource%20Plays.pdf

Parham, S., Kamali, M., and Fayazi, F., 2010, Petrography, geochemistry and reservoir characterization of dolomicrites in the Upper Member of the Dalan Formation, Persian Gulf, Iran: The 1st International Applied Geology Conference, Department of Geology, Islamic Azad University, Mashad Branch, Iran.

Peale, C.A., 1893, The Paleozoic section in the vicinity of Three Forks, Montana: U.S. Geological Survey Bulletin, 110, 56 p.

Peters, K.E, 1986, Guidelines for evaluating petroleum source rock using programmed pyrolysis: American Association of Petroleum Geologist Bulletin, v. 70, no. 3, p. 318-329.

Peters, K.E., and Cassa, M.R., 1994, Applied source rock geochemistry, in Magoon, L.B., and Dow, W.G., eds., The petroleum system—From source to trap: Tulsa, Okla., American Association of Petroleum Geologist Memoir 60, p. 93-117.

Peters, K.E., Walters, C.C., and Moldowan, J.M., 2005a, The biomarker guide, volume II, Biomarkers and isotopes in petroleum exploration and earth history: Cambridge University Press, Cambridge, UK, p. 475-1155.

Pettijohn, F.J., Potter, P.E., and Siever, R., 1987, Sand and Sandstones. Springer, New York, p. 553.

Petrolog, 2012: http://www.petrolog.net/webhelp/Logging_Tools/gr/gr.html

Purser, B., Tucker, M., and Zenger, D., 1994, Problems, progress and future research concerning dolomites and dolomitization, *in* Purser, B., Tucker, M., and Zenger, D., Eds., *Dolomites:* A Volume In Honour of Dolomieu (p. 3-33), Boston: Special publication of the International Association of Sedimentologists, Blackwell Scientific Publications.

Qi, L., and Carr, T.R., 2006, Neural network prediction of carbonate lithofacies from well logs, Big Bow and Sand Arroyo Creek fields, Southwest Kansas: Computers and Geosciences, 32, p.947-964.

Randazzo, A.F. and Zachos, L.G., 1984, Classification and description of dolomitic fabrics and rocks from the Florida aquifer: Journal of Sedimentary Geology, 37, p. 151–162.

Read, J.F.,1985, Carbonate platform facies models: American Association of Petroleum Geologist Bulletin, v. 69, p. 1-21.

Reading, H.G., 1996, Sedimentary environments: processes, facies and stratigraphy, 3rd edition, Malden: Blackwell Science Ltd.

Reyment, R.A., Savazzi, E., and Reyment, R.A, 1999, Aspects of Multivariate Statistical Analysis in Geology: Elsevier Science, 285 p.

Ruan, C.D., and Ward, C.R., 2002, Quantitative X-ray powder diffraction analysis of clay minerals in Australian coals using Rietveld methods: Applied Clay Science, v. 21, p. 227–240.

Saggaf, M.M., and Nebrija, E.L., 2003a, A fuzzy logic approach for the estimation of facies from wire-line logs: American Association of Petroleum Geologist Bulletin, v. 87, no.7, p.1233-1240.

Sandberg, C., and Hammond, C., 1958, Devonian system in williston basin and central montana: American Association of Petroleum Geologist Bulletin, v. 42, no. 10, p. 16-17.

Sandberg, A.C., 1961, Distribution and Thickness of the Devonian rocks in the Williston basin and in Central Montana and North-Central Wyoming: U.S. Geological Survey, Bulletin 1112-D, p.105-127.

Selley, R.C., 1970, Studies of sequence in sediments using a simple mathematical device: Quart. Journal of the Geological Society of London, v. 125, p. 557-558.

Selley, R.C., 1978, Ancient sedimentary environments, 2nd edition: Cornell University Press, Ithaca, NY.

Selley, R.C., 2000, Applied sedimentology, 2nd, Edion: Elsevier Inc, p. 523.

Selley, R.C., 2011, Ancient sedimentary environments: and their sub-surface diagnosis, New York: Routledge.

Serra, O., and Abbott, H., 1982, The contribution of logging data to sedimentology and stratigraphy: Society of Petroleum Engineers Journal, v. 22, no. 1, p. 117-131.

Schmoker, J.W., Krystinic, K.B., Halley, R.B., 1985, Selected characteristics of limestone and dolomite reservoirs in the United States: American Association of Petroleum Geologist Bulletin, v. 69, no. 5, p 733-741

Shukla, V., and Friedman, G.M., 1983, Dolomitization and diagenesis in a shallowing-upward sequence: Journal of Sedimentary Petrology, v. 53, no. 3, p. 703-717.

Slatt, R.M., Singh, P., Borges, G., 2009, Reservoir characterization of unconventional gas shale reservoirs: example from the Barnett Shale, Texas, U.S.A, Oklahoma City Geological Society Shale Shaker, vol. 60, no. 1, p. 15–31.

Sloss, L.L., 1984, Comparative anatomy of cratonic unconformities, *in* Schlee, J.S., ed., Interregional unconformities and hydrocarbon accumulation: American Association of Petroleum Geologist Memoir 36, p. 7-36.

Smosna, R.1987, Compositional maturity of limestones - a review: Journal of Sedimentary Geology, v. 51, 137-146.

Snowdon, L.R., Fowler, M.G., Riediger, and C.L., 1998, Interpretation of organic geochemical data: Short Course Notes, CSPG, November 5-6, 1998, Calgary, Alberta.

Tissot, B.P., and Welte, D.H., 1984, Petroleum formation and occurrence, second edition: Springer, Berlin, 699 p.

Tissot B.P., Pelet, R., and Ungerer, P.H., 1987, Thermal history of sedimentary basins, maturation indices, and kinetics of oil and gas generation: American Association of Petroleum Geologist Bulletin, v. 71, p.1445-1446.

Tissot, B.P., Califet-Debyser, Y., Deroo, G., and Oudin, J.L., 1971, Origin and evolution of hydrocarbons in early Toarcian shales, Paris Basin, France: American Association of Petroleum Geologist Bulletin, 55, P. 2177-2193.

Walsh, J.J., 1987, On the nature of continental shelves, London: Academic Press, p. 274.

Walton, A.G., 1969, Nucleation in liquids and solutions; *in* Zettlemoyer, A.C., ed., Nucleation: Marcel Dekker, New York, p. 225-307.

Wanless, H.R., 1977, Limestone response to stress: pressure solution and dolomitization, Journal of Sedimentary Petrology, vol. 49, no. 2, p. 437-462.

Weeks, J. D., and Gilmer, G. H., 1979, Dynamics of crystal growth, *in* Prigogine, H. J., and Rice, J.H., eds., Advances in chemical physics: New York: Wiley-Interscience Publications, v. 40, p. 157- 228.

Wentworth, C.K., 1922, A scale of grade and class terms for clastic sediments: The Journal of Geology, v. 30, no. 5.
(http://www-odp.tamu.edu/publications/200_IR/chap_02/c2_f7.htm)

Wilson, J., 1975, Carbonate facies in geologic history, New York: Springer-Verlag, p. 471.

Withington, C., 1961, Origin of mottled structure in bedded calcium sulfate: U.S. Geological Survey Professional Paper 424-D, p. 342- 344.

Wyllie, M.J., Gregory, A.R., and Gardner, L.W., 1956, Elastic wave velocities in heterogeneous and porous media: Geophysics, 21, p. 41-70.

Zenger, D.H., 1981, On the formation and occurrence of saddle dolomite: discussion: Journal of Sedimentary Petrology., 51, p. 1350-1352.

Zimmerle, W., 1995, Petroleum sedimentology: Kluwer Academic Publishers, Dordrecht.